

Modeling and Bounded Feedback Stabilization of Centrifugal Compressor Surge

CIP-DATA LIBRARY TECHNISCHE UNIVERSITEIT EINDHOVEN

Willems, Franciscus P.T.

Modeling and Bounded Feedback Stabilization of Centrifugal Compressor Surge

by Franciscus P.T. Willems. – Eindhoven :

Technische Universiteit Eindhoven, 2000. – Proefschrift. –

ISBN 90-386-2931-1

NUGI 841

Trefwoorden: centrifugaal compressoren / stromingsinstabiliteiten / modellering / regelsystemen, experimenteel / active surge control / bounded feedback stabilization

Subject headings: centrifugal compressors / aerodynamic compressor flow instabilities / modeling / control systems, experimental / active surge control / bounded feedback stabilization

This thesis was prepared with the \LaTeX 2_ε documentation system.

Printed by University Press Facilities, Eindhoven, The Netherlands.

This work forms a part of the research program of the Dutch Institute of Systems and Control (DISC).

Modeling and Bounded Feedback Stabilization of Centrifugal Compressor Surge

PROEFSCHRIFT

ter verkrijging van de graad van doctor
aan de Technische Universiteit Eindhoven,
op gezag van de Rector Magnificus, prof.dr. M. Rem,
voor een commissie aangewezen door het College voor Promoties
in het openbaar te verdedigen op
dinsdag 6 juni 2000 om 16.00 uur

door

Franciscus Petrus Thomas Willems

geboren te Heerlen

Dit proefschrift is goedgekeurd door de promotoren:

prof.dr.ir. J.J. Kok

en

prof.dr.ir. A.A. van Steenhoven

Co-promotor:

dr.ir. A.G. de Jager

Contents

Summary	vii
1 Introduction	1
1.1 Axial and centrifugal compressors	1
1.2 Rotating stall and surge	4
1.3 Suppression of rotating stall and surge	8
1.4 Research objectives	12
1.5 What is new?	13
1.6 Scope of the thesis	14
2 Compression System Modeling	15
2.1 Experimental set-up	15
2.2 Greitzer lumped parameter model	18
2.3 Identification of the Greitzer model	24
2.3.1 Compressor and throttle characteristics	24
2.3.2 Greitzer stability parameter	25
2.4 Discussion	30
3 Design of the Surge Control System	33
3.1 Active control of aerodynamic compressor flow instabilities	33
3.2 Experimental active surge control systems	34
3.3 Selection of sensors and actuators	36
3.3.1 Results of selection methods	36
3.3.2 Motivation of the selected sensor and actuator	37
3.3.3 Compression system with surge control system	38
3.4 Control valve specification	40
3.5 Discussion	42
4 Active Surge Control	43
4.1 Effect of nominal control valve position	43
4.2 One-sided surge control	45
4.2.1 Compression system without valve dynamics	47
4.2.2 Compression system with valve dynamics	49
4.3 Simulation results	50
4.3.1 Static output feedback	50
4.3.2 State feedback	56
4.4 Discussion	57

5	Experimental Results	59
5.1	Open-loop behavior	59
5.1.1	Control valve model	59
5.1.2	Control valve capacity c_b	62
5.1.3	Nonlinear flow curve	62
5.1.4	Frequency response measurements	64
5.1.5	Surge avoidance	66
5.2	One-sided surge control	68
5.2.1	Effect of measurement noise	68
5.2.2	Effect of desired plenum pressure ψ_{ref}	69
5.2.3	Band-pass filter	72
5.3	Discussion	76
6	Conclusions and Suggestions for Future Research	79
6.1	Conclusions	79
6.1.1	Modeling of centrifugal compressor surge	79
6.1.2	Design of control system	80
6.1.3	Development of control strategy	80
6.1.4	Realization and experiments	80
6.2	Suggestions for future research	81
6.2.1	Modeling of rotating stall and surge	81
6.2.2	Active stall control	82
	References	83
A	Rotating Stall	89
B	Experimental Set-Up	93
B.1	Gas turbine installation	93
B.2	Dimensionless component characteristics	95
B.2.1	Compressor characteristics	95
B.2.2	Throttle characteristics	96
B.3	Measurement system	97
B.3.1	Mass flow measurement	98
B.4	Surge control system	99
C	Lumped Parameter Modeling	101
C.1	Helmholtz resonator	101
C.2	Greitzer lumped parameter model	102
C.2.1	Conservation equations	103
C.2.2	Dimensionless equations of motion	106
	Samenvatting	107
	Dankwoord	109
	Curriculum Vitae	111

Summary

Stable operation of axial and centrifugal compressors is limited towards low mass flows by the occurrence of two aerodynamic compressor flow instabilities: *rotating stall* and *surge*. These instabilities can lead to severe damage of the machine due to large mechanical and thermal loads in the blading, and restrict its performance and efficiency. One way to cope with these instabilities is *active control*. In this approach, the dynamics of the compression system are modified by feeding back perturbations into the flow field. This results in an extension of the stable operating region, and the performance and efficiency of the compression system can be improved.

This thesis deals with active surge control in an experimental centrifugal compressor system. To describe the behavior of the compression system during fully-developed surge, the *Greitzer lumped parameter model* is used. This model is identified and experimentally validated. For the examined compression system, it reasonably predicts the system behavior in a broad operating range and it is used to guide the design of a surge control system.

Application of methods for the selection of sensors and actuators indicate a *plenum pressure sensor* in combination with a *bleed valve* to give satisfactory results. The Greitzer model is extended with a valve model to incorporate the effect of the valve dynamics on system behavior. Simulations are performed with this nonlinear compression system model to specify the bandwidth and capacity of the bleed valve, which are required for active surge control in the examined installation.

To stabilize surge, a new control strategy is developed: *one-sided control*. In this strategy, the bleed valve is closed in the equilibrium point and, to stabilize the system in this operating point, it can only be operated to one side (opening the valve). As a result, the equilibrium point is reached with zero stationary bleed valve mass flow if persistent disturbances and measurement noise are absent. This control strategy improves the overall efficiency of the compressor system compared to studies which accept stationary bleed or recycle losses. From simulations with the nonlinear compression system model, it is seen that surge can be stabilized using static output feedback based on plenum pressure measurements. The theory of positive feedback stabilization is applied to examine the stability of the one-sided controlled linearized compression system.

The proposed control system is implemented on the experimental set-up. A band-pass filter is applied to overcome practical problems associated with measurement noise and the unknown actual equilibrium point. As a result, we have realized a bounded dynamic output feedback controller. Experiments with this control system show that surge can be suppressed, and that the surge point mass flow can be reduced by 7%. However, active surge control is seen to modify the system dynamics; if surge is suppressed rotating stall seems to be present in the centrifugal compressor.

Chapter 1

Introduction

The topic of this thesis is the modeling and control of rotating stall and surge in compressors. Aerodynamic flow instabilities of this kind can severely damage a compressor and limit the performance and operating region of the machine, so they have to be avoided. The focus is on surge control in centrifugal compressors. In this introduction, first the operation principles of both axial and centrifugal compressors are presented in Section 1.1. The main characteristics of rotating stall and surge are discussed in Section 1.2. Furthermore, this section is concerned with the problems associated with these aerodynamic flow instabilities and how these instabilities can occur. Section 1.3, on the other hand, deals with available techniques to take care of rotating stall and surge. In Section 1.4, the motivation is presented for the research and its objectives are formulated. Finally, the main contributions of this research are summarized and the outline of the thesis is given in Section 1.5 and 1.6, respectively.

1.1 Axial and centrifugal compressors

Compressors are widely used for the pressurization of fluids. Applications involve air compression for use in aircraft engines, in industrial gas turbines, and in turbocharged combustion engines. Other applications are the pressurization and transportation of gas in the process and chemical industries (Badmus *et al.*, 1996; Cohen *et al.*, 1996; Gravdahl and Egeland, 1998).

Principles of operation

Based on the principle of operation, compressors can be categorized as follows (Nisenfeld, 1982):

- **Pressurization by decreasing the volume of the fluid.** Reciprocating as well as rotary compressors operate on this principle; reduction of the volume of a trapped gas results in an increased pressure. After compression, this fluid is discharged and new gas is ingested. In reciprocating compressors, compression is realized by a moving piston in a cylinder with inlet and discharge valves. Rotary compressors, on the other hand, use rotating lobes and screws or sliding vanes. For a detailed discussion of these machines, see, *e.g.*, Bloch (1996) or Brown (1997).
- **Pressurization by momentum transfer.** This approach is realized in axial and centrifugal compressors. In this type of continuous flow machines, the entering fluid is accelerated via the kinetic energy imparted in the rotor (often called impeller in centrifugal compressors), and then converting the kinetic energy into potential energy by decelerating the fluid in diverging

channels. During the first step, the *total pressure* of the fluid increases due to the momentum imparted to the flow by the rotor blades. The second step of the pressurization is the diffusion process in the diffuser (in centrifugal compressors, see Fig. 1.1) or in the stator (in axial compressors). The deceleration of the fluid results in a *static pressure* rise as described by Bernoulli's theorem (Nisenfeld, 1982). Further details about axial and centrifugal compressors can be found in Cohen *et al.* (1996) or Cumpsty (1989).

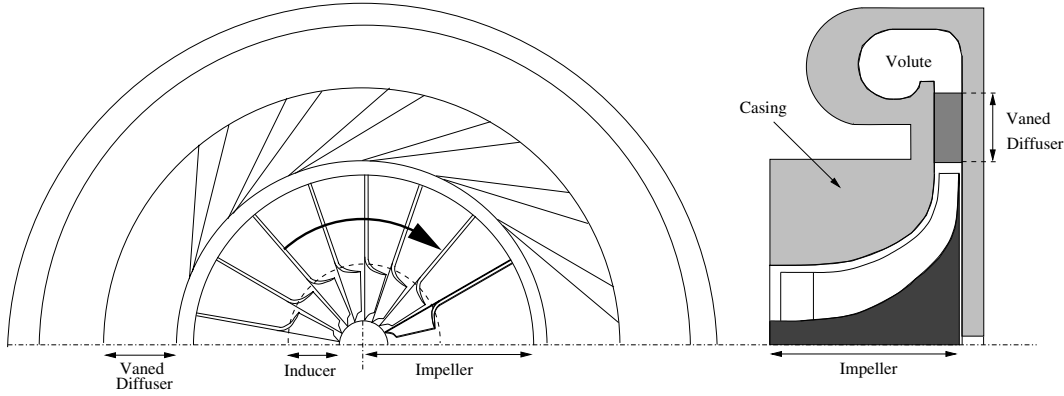


Figure 1.1: Sketch of a centrifugal compressor with a vaned diffuser.

Rotating stall and surge are associated with the two latter types of compressors: (i) the *axial compressor* where the gaseous fluid is processed in a direction parallel to the rotational axis and (ii) the *radial or centrifugal compressor* where the pressurized fluid leaves the compressor in a direction perpendicular to the rotational axis.

Compressor performance

The performance of a compressor is often specified in a compressor map by curves that relate the rotational speed, the pressure rise across the compressor, and the mass flow through the compressor (Cumpsty, 1989; De Sa and Maalouf, 1996), as shown in Fig. 1.2. Steady-state operating points with constant rotational speed are indicated by *speed lines* or *compressor characteristics* and the rotational speed increases in the direction of the arrow. The load or throttle line represents the pressure requirements of the system. Consequently, the steady-state operating point of a compression system is the intersection point of the compressor characteristic and the load line.

Compressor manufacturers generally specify the compressor performance using scaled quantities. To uniquely define the operating point of a compressor, four dimensionless parameters are required (Cohen *et al.*, 1996; Cumpsty, 1989):

- **Pressure rise Ψ :** *e.g.*, dimensionless total-to-static pressure rise $\frac{\Delta p}{\rho U_t^2}$ (with impeller tip speed U_t and density ρ) is quite common for centrifugal compressors. It is a measure of the actual work put into the flow compared to the work available (U_t^2).
- **Mass flow ϕ :** *e.g.*, flow coefficient $\frac{C_x}{U}$ (with axial flow velocity C_x and rotor speed U at mid-radius) is used for axial compressors. This flow coefficient determines the incidence i into the first rotor (as illustrated in Fig. 1.3a), and is an important property in determining the performance of a blade row, see Fig. 1.3b. From this figure, it is seen that the mean total head losses

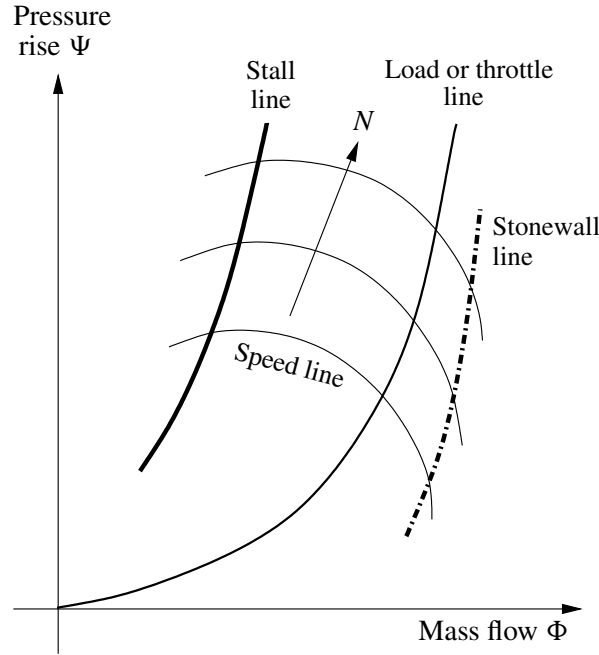


Figure 1.2: A schematic representation of a compressor map.

(with total pressure loss $p_{01} - p_{02}$) are nearly constant over a wide range of incidence, but increase rapidly for large positive and negative values of the incidence.

In centrifugal compressors, the flow coefficient is often defined as $\phi = \frac{\dot{m}}{\rho_0 U_t D^2}$ with mass flow rate \dot{m} , density ρ_0 based on inlet conditions, and impeller diameter D .

- **Compressor speed N :** *e.g.*, blade tip speed expressed in the Mach number $\frac{U_t}{\sqrt{\gamma R T_0}}$ based on inlet conditions.
- Additionally, the **temperature rise** or a related variable like the **efficiency** is needed.

Experiments show that in the normal operating range of compressors the Reynolds number is high, so the flow is turbulent and friction effects are approximately constant. For a compressor with no variable geometry, and where the dependence on the Reynolds number can be neglected, the pressure rise Ψ is only a function of ϕ and N (Batson, 1996; Cumpsty, 1989). Then, a steady-state operating point can be defined by two independent dimensionless variables. Because of the shape of the compressor characteristic, the pair (Ψ, N) does not uniquely define an operating point while (ϕ, N) and (Ψ, ϕ) do. Using an appropriate scaling, the compressor data can be presented independent of the rotational speed (Fink *et al.*, 1992; Staroselsky and Nadin, 1979). For a comprehensive discussion on scaling, the interested reader is referred to Batson (1996) or Cumpsty (1989).

For constant rotational speed, reduction of the compressor mass flow, *e.g.*, due to throttling the flow, will generally result in an increase of the compressor pressure rise, as illustrated in Fig. 1.2. The operating range of a compressor is bounded for high mass flow by the limited capacity of the compressor due to choked flow. This is marked by the *stonewall line*. For low flow regimes, the operating range is limited by the occurrence of *rotating stall* and *surge*. Note that both instabilities are often termed stall. The transfer from stable to unstable operation is demarcated by the *surge*

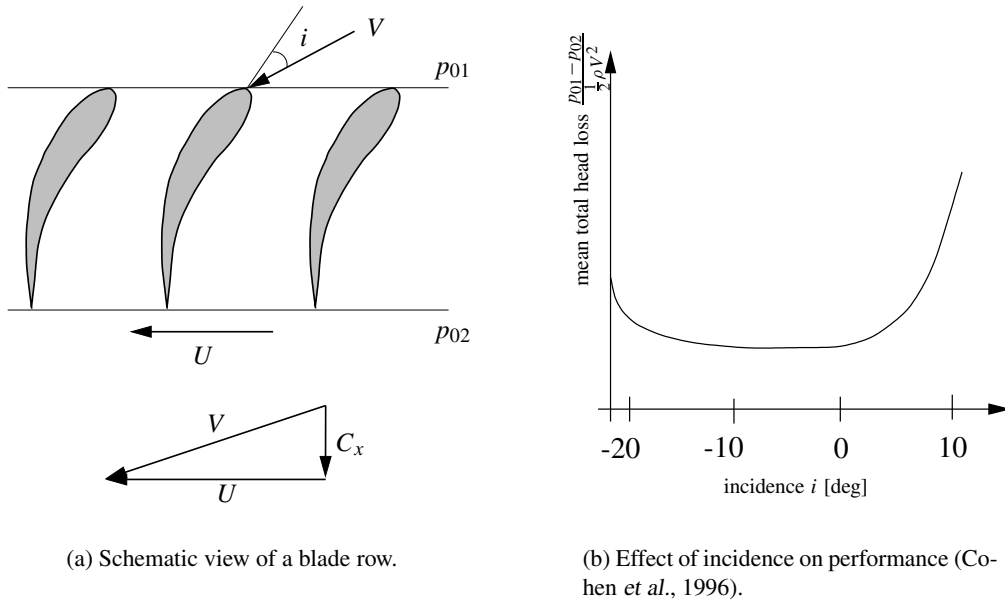


Figure 1.3: Incidence on a blade row.

line or *stall line*. As a rule, these aerodynamic flow instabilities occur at the top of the compressor characteristic or near the top in a point with a specific positive slope of the speed line (Greitzer, 1976a).

1.2 Rotating stall and surge

Various types of instabilities are encountered in compression systems, *e.g.*, combustion induced instabilities or aero-elastic instabilities such as flutter. This study is restricted to aerodynamic flow instabilities in axial and centrifugal compressors: *rotating stall* and *surge*. A review of several types of instabilities that are found in turbomachines can be found in Greitzer (1981).

Rotating stall

Rotating stall is a two-dimensional, local instability phenomenon in which one or more local regions of stagnant flow, so-called *stall cells*, rotate around the circumference of the compressor (see Fig. 1.4).

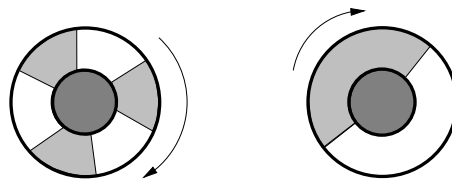


Figure 1.4: Rotating stall cells.

Depending on their size, these cells usually have a constant rotational speed between 20 and 80% of the rotor speed: larger cells rotate at a lower rotational speed than small cells (Greitzer, 1981). In

this flow regime, the annulus-averaged compressor mass flow is steady, but circumferentially non-uniform. In a compressor map, the occurrence of rotating stall is seen as a rapid movement from the unstalled characteristic (1) to a point on the stalled characteristic (2), as shown in Fig. 1.5. Rotating stall induces large vibratory stresses in the blading and can result in a large drop in performance and efficiency (De Jager, 1995; Greitzer, 1998). Moreover, in a gas turbine engine the reduced flow rates during rotating stall can lead to undesirable thermal loads in the turbine and to a reduction of the output power (Gu *et al.*, 1996; Hendricks and Gysling, 1994). More details about rotating stall are given in Appendix A.

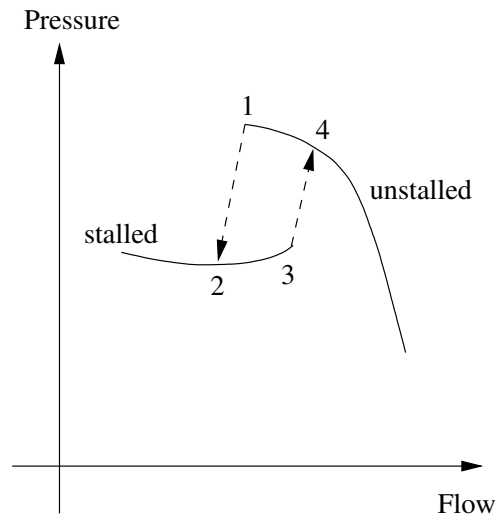


Figure 1.5: Rotating stall in compressor map.

Surge

Surge is characterized by large amplitude fluctuations of the pressure and by unsteady, but circumferentially uniform, annulus-averaged mass flow. This essentially one-dimensional instability affects the compression system as a whole and results in a limit cycle oscillation in the compressor map. Figure 1.6 shows a pressure trace for a compressor system, which was initially operated in a steady operating point. By throttling the compressor mass flow, the machine is run into surge. This figure illustrates the difference between pressure variations before and after surge initiation. Note that the surge frequency is around 20 [Hz]. Operation during surge often results in a considerable loss of performance and efficiency, and can lead to high blade and casing stress levels. In jet engines, surge can even lead to combustor flame-out (Dadd and Porter, 1993; Day and Freeman, 1994).

Based on the amplitude of mass flow and pressure fluctuations, four categories of surge can be distinguished (De Jager, 1995): mild surge, classic surge, modified surge, and deep surge. During mild surge, the frequency of oscillations is around the Helmholtz frequency (for details see Appendix C.1), *i.e.*, the resonance frequency of the compressor duct and the volume connected to the compressor (often called *plenum*) (Cumpsty, 1989). This frequency may be over an order of magnitude smaller than the maximal rotating stall frequency; for rotating stall, the frequencies are of the same order as the rotor frequency (see Fig. 1.7). Classic surge is a nonlinear phenomenon with larger oscillations and at a lower frequency than mild surge, but the mass flow fluctuations remain positive. A mix of

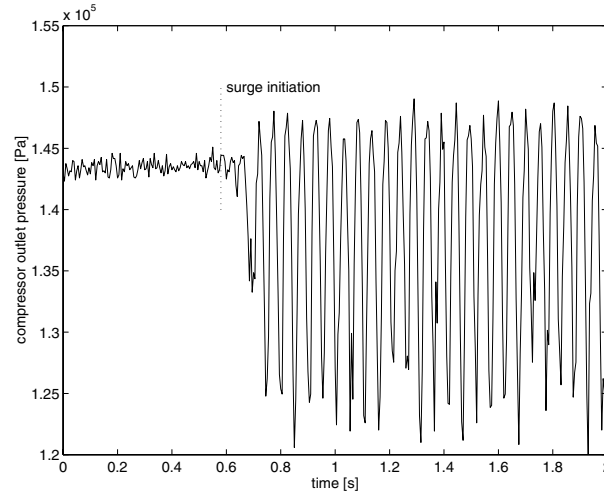


Figure 1.6: Surge initiation measured at the compressor outlet (Meuleman *et al.*, 1998).

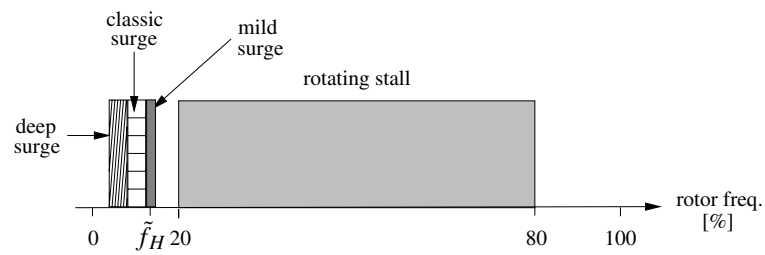


Figure 1.7: Frequencies of several types of aerodynamic flow instabilities (with scaled Helmholtz frequency $\tilde{f}_H = \frac{f_H}{f_{rotor}}$).

classic surge and rotating stall is called modified surge. Figure 1.8 shows a typical example of a deep surge cycle, which is associated with reverse flow over part of the cycle. The frequency of oscillations during deep surge is normally well below the Helmholtz frequency as it is set by the filling ($4 \rightarrow 1$) and emptying period ($2 \rightarrow 3$) of the plenum (Fink *et al.*, 1992). It is noted that Pinsley *et al.* (1991) have shown that mild surge transforms into other types of surge by throttling the compressor to lower mass flows.

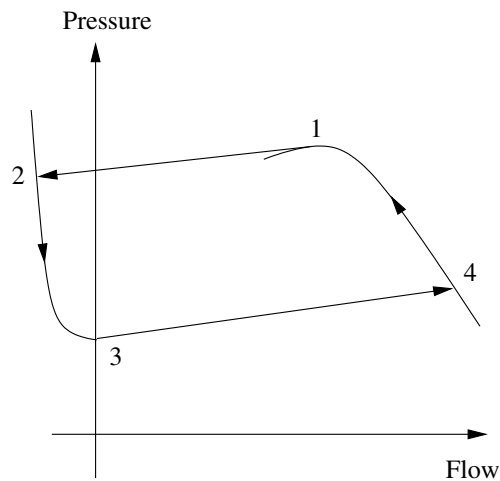


Figure 1.8: Compressor map with deep surge cycle (Willems and De Jager, 1998b).

As seen from Stenning (1980), surge only occurs in systems with compressible flow whereas rotating stall occurs in compressible as well as incompressible flows. Both flow phenomena are assumed to be related, since rotating stall can trigger surge (Epstein *et al.*, 1989; Greitzer, 1981); rotating stall and surge are seen as eigen modes of the system, with surge constituting the zeroth order (axisymmetric) mode and rotating stall representing higher order spatial modes.

Dynamic behavior of compressors

Regions of maximal efficiency and pressure rise are often located near the stall line (Gysling *et al.*, 1991; Pinsley *et al.*, 1991). In compressor designs, first the design operating point is specified based on the desired delivery pressure or mass flow. As the compressor will also be operated outside this point, a safety margin indicated by the *surge avoidance line* (also called *control line*) is accommodated to prevent the system from crossing the stall line (Badmus *et al.*, 1993a; Lawless and Fleeter, 1995). Then, the compressor is designed to maximize the efficiency in the design operating point under the constraint of the safety margin (Badmus *et al.*, 1993a; Cohen *et al.*, 1996). However, because of this margin the maximally achievable pressure is smaller than the peak pressure.

If a compressor is well designed, the machine is operated at a safe distance from the stall line during normal operation. Consequently, off-design conditions may lead to flow instabilities. Load variations, *e.g.*, by shutting off downstream processes or by temporal changes in the rate of production, can make the compressor's operating point move towards the stall line, as shown in Fig. 1.9. Stall could be avoided by decreasing the pressure rise Ψ , *e.g.*, by reducing the rotational speed or throttling the compressor mass flow, but this may conflict with the conceivable control objective of constant delivery pressure. This problem can be circumvented by using a compressor with a smaller capacity,

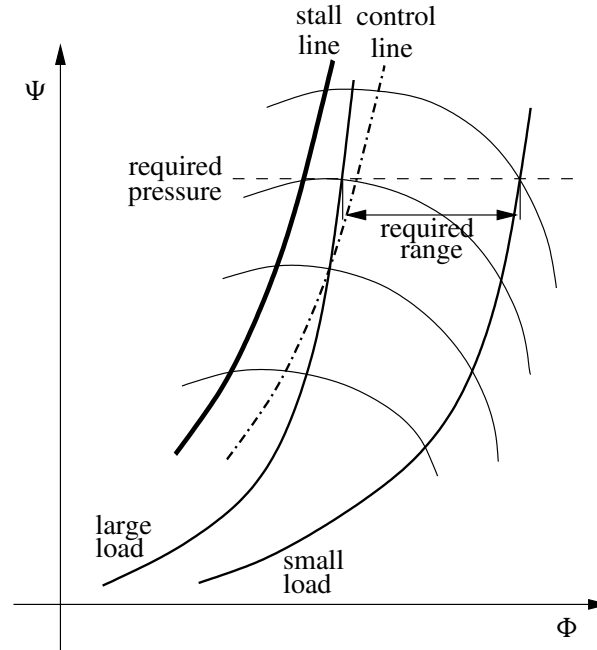


Figure 1.9: Effect of load variations.

which prevents the system from crossing the control line. However, for substantial load changes, a larger number of compressors may be required.

Set-point changes with fixed load may also cause the operating point to cross the stall line. For instance, in a compression system with a large volume, changes in mass flow ϕ will be faster than pressure rise changes and the operating point may cross the stall line during deceleration, as shown in Fig. 1.10. However, in case the compressor is accelerated, the operating point will initially move away from the stall line. In gas turbines with tightly integrated compressor/combustor/turbine such as in jet engines (see Fig. 1.11b), the compressor's operating point may cross the stall line during acceleration transients (Cohen *et al.*, 1996; De Jager, 1995), as shown in Fig. 1.11a. During an acceleration that follows upon an increase in fuel flow, first the turbine inlet temperature will rise significantly. As a result, the compressor outlet pressure may rise because of the increased back pressure of the turbine. Then, the operating point may initially move towards the stall line because of the slow response time of compressor speed and, thus, air mass flow. In aeroengines, stall is also caused by circumferential distortions, planar turbulence, and pressure pulsations due to a combustion chamber (Gu *et al.*, 1996).

For the cases shown in Figs. 1.10 and 1.11, the system's response time to changing operation requirements is constrained by the permissible pressure rise and mass flow variations. The operation of gas turbines is also constrained by the allowable inlet temperature of the turbine.

1.3 Suppression of rotating stall and surge

From the previous section, it is seen that rotating stall and surge can lead to failure of the system due to large mechanical loads in the blading. Furthermore, these instabilities restrict the machine's performance and efficiency. As these phenomena are unacceptable, they have to be avoided. Therefore, this thesis focuses on suppressing these aerodynamic flow instabilities, since this improves the life

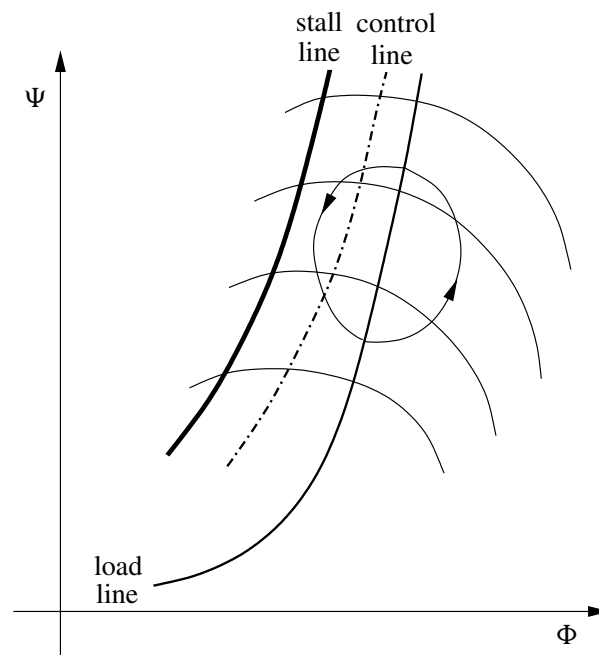


Figure 1.10: Transients in compression systems with a large volume.

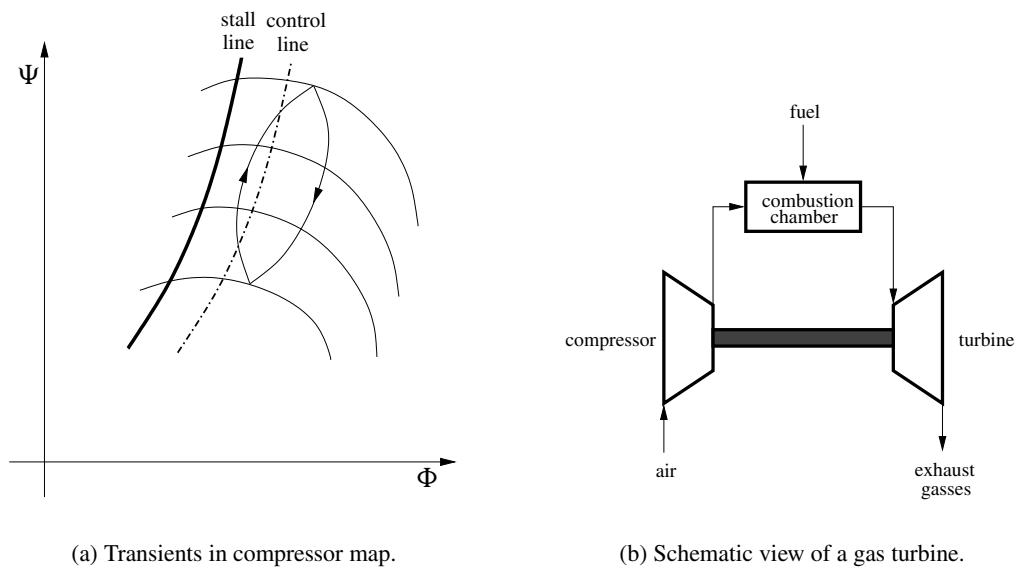


Figure 1.11: Transients in jet engines.

span and the performance of the compressor (Epstein *et al.*, 1989). In addition, enlarging the feasible operating region may reduce the operating costs and the required number of blade rows, and increases the effectiveness of compressor systems (De Jager, 1995; Epstein *et al.*, 1989). Note that in some cases the required number of compressors may even be reduced.

Several measures are known to increase the stable operating range of the compressor system (see, *e.g.*, Botros and Henderson (1994) or Greitzer (1981)). These measures can be grouped in three categories:

- Techniques that are focussed on **better compressor interior design**. Buse *et al.* (1996) showed that rotating stall can be suppressed by using a so-called low-solidity vaned diffuser. According to Greitzer (1981), the stable operating region can also be enhanced by casing treatment, and the use of backward leaning rotor blades, thickened rotor blades, or a vaneless diffuser. Other possibilities are increasing blade numbers (Freeman *et al.*, 1998), whereas Day (1993b) and McDougall *et al.* (1990) suggest to decrease the tip clearance. Elder and Gill (1985) present a comprehensive overview of factors involved in compressor design that influence surge in centrifugal compressors.
- Techniques that use **variable geometry**. Camp and Day (1998) and Rodgers (1991), for example, apply movable inlet guide vanes to increase the surge margin. These vanes change the shape of the compressor characteristic. Also, movable diffuser vanes can be used (Hunziker and Gyarmathy, 1994; Lawless and Fleeter, 1995).
- Techniques that attempt to **suppress these instabilities by control**. Main advantage of this approach is that this technique can be used for a wide range of machines and it can result in a considerable performance improvement compared to the other mentioned techniques. Moreover, it can easily be added to existing machines and designs.

The techniques based on redesign or variable geometry introduce relatively large efficiency penalties (Freeman *et al.*, 1998; Goto, 1994). According to De Jager (1995), the operating region can also be enhanced by better matching of compressor and discharge system specifications and by changes in the equipment in which the system discharges, *e.g.*, the volume (Fink *et al.*, 1992). In this thesis, the focus is on control.

Surge avoidance and detection

Stable operation can be guaranteed by operating the compressor at a safe distance from the unstable region (*surge avoidance* or *anti-surge control*). Control systems currently used in industry are based on this control strategy (Botros and Henderson, 1994; CCC, 1997; Gravdahl and Egeland, 1998). In this strategy, a control line is defined at some distance from the stall line, as shown in Fig. 1.12. This safety margin is set by (i) sensor and actuator limitations, (ii) uncertainty in the location of the stall line, and (iii) disturbances including load variations, inlet distortions, and combustion noise. If the compressor's operating point tends to cross the control line, it is stuck to the control line by, for example, opening a recycle or bleed valve (see, *e.g.*, Botros *et al.* (1991) or Staroselsky and Nadin (1979)). Another approach is to *fully* open the bleed valve.

Surge avoidance limits the performance of the compressor, since the maximal pressure is obtained close to the stall line (Gu *et al.*, 1996). Clearly, the bleed or recycle of the compressed fluid is not useful and reduces the overall efficiency. Furthermore, a narrow, feasible operating region can increase the required number of blade rows and decreases the effectiveness of compressor systems (De Jager, 1995; Epstein *et al.*, 1989). To decrease the wasteful safety margin, the controller can be activated if

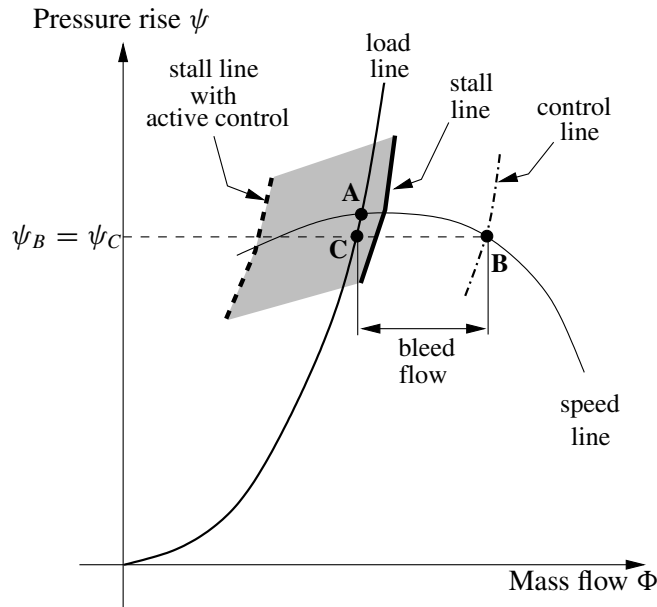


Figure 1.12: Scheme emphasizing the difference between surge avoidance and active control.

the onset of instabilities is detected (*surge detection and avoidance*). However, the main disadvantages of this strategy are problems associated with the detection of the instability onset and the necessity of large control actions and fast-acting control systems.

Active control

Epstein *et al.* (1989) proposed a fundamentally different strategy: *active control*. In this approach, controllers are used which stabilize unstable operating points by feeding back perturbations into the flow field. Based on information from sensors, which detect fluid fluctuations, the controller computes the desired perturbations to stabilize the system. These perturbations can be introduced, for instance, by a control valve or a loudspeaker. By feedback control, the compression system dynamics are modified such that the stable operating region is enlarged beyond the “natural” stall line, as illustrated in Fig. 1.12. Note that if small fluid fluctuations are fed back, small control actions with fluctuations at the surge frequency are required.

The difference between surge avoidance and active control is illustrated in Fig. 1.12. The desired operating point of the compression system is indicated as point A. In case of surge avoidance, a bleed or recycle valve is opened such that the actual operating point of the compressor is point B. For downstream processes, the compression system appears to operate in point C with a smaller pressure and mass flow than the desired values. Active control, on the other hand, enhances the stability of the compression system such that it can be operated in point A with the highest achievable performance: a high pressure rise in combination with the required low mass flow (Paduano *et al.*, 1994).

In the literature, up to 20% reduction in surge point mass flow is reported by applying active control to experimental set-ups (see, *e.g.*, Ffowcs Williams and Huang (1989) and Pinsley *et al.* (1991) for surge control and Paduano *et al.* (1994) for rotating stall control). For the gas turbine installation examined in this project, possible savings are studied using active control. This compression system is supposed to have a sinusoidal mass flow requirement (see Fig. 1.13) due to nocturnal load variations.

This can be the result, for instance, of nocturnal fluctuations in the demand of natural gas or electricity. The original system has to blow off compressed air if the required mass flow is smaller than the *control line mass flow*: 0.2 [kg/s]. Assuming a 20% reduction in surge point mass flow due to active control, the system can be operated without blow off. For a nominal delivery pressure of $1.36 \cdot 10^5$ [Pa], this results in a 3.4 [kW] reduction of the mean required power to drive the compressor. On a yearly basis, this means that the savings in energy costs are approximately EUR 3400 if the compressor is driven by an electro motor (calculated with electricity costs of 1000 [EUR/kWyear]). It is noted that the implemented active surge control system discussed in Chapter 5 is realized at a cost of approximately EUR 11,000.

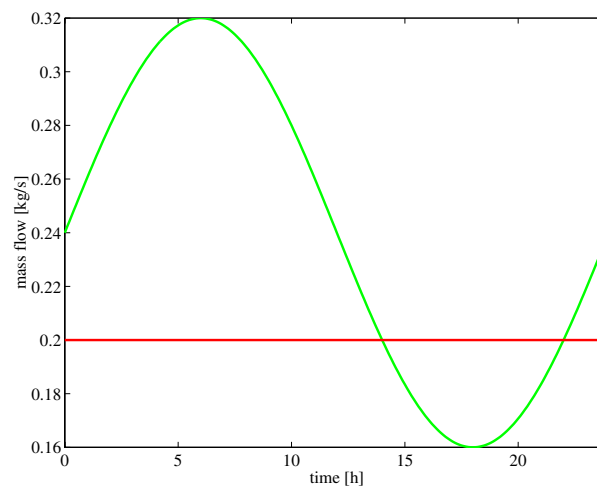


Figure 1.13: Required mass flow and constant control line mass flow (Willems and De Jager, 1999).

1.4 Research objectives

As seen from the vast amount of published literature, there has been considerable activity in the field of modeling and control of rotating stall and surge over the last 20 years. Currently, the behavior of the compressor subsequent to instability onset is understood reasonably well. Various models are capable of describing the time development of rotating stall or surge out of small perturbations (for a detailed overview of models, see, *e.g.*, Gravdahl and Egeland (1998), Gu *et al.* (1996), or Longley (1994)). However, a thorough understanding of the mechanisms that lead to the considered instabilities is lacking, especially in centrifugal compressors. According to Gravdahl and Egeland (1998), this difference between axial and centrifugal compressors might be explained from the fact that in this field a large amount of research is focused on the development of active stall controllers for jet engines. In these so-called *smart jet engines*, axial compressors are mainly applied. Therefore, less research is done into aerodynamic flow instabilities in centrifugal compressors. Furthermore, although there are examples of rotating stall in centrifugal compressors, see, *e.g.*, Buse *et al.* (1996) or Kämmer and Rautenberg (1986), rotating stall is believed to have little effect on compressor performance in centrifugal machines. Another reason might be that the situation in centrifugal machines is more complicated than in axial compressors because of the very wide range of speeds and compressor geometries, and the effect of matching between components (Elder and Gill, 1985; Fink *et al.*, 1992; Greitzer, 1981).

Recently, promising developments have been achieved in the field of rotating stall control (see, *e.g.*, Badmus *et al.* (1993b), Paduano *et al.* (1994), or Yeung and Murray (1997)), but there are still many problems to be solved (Gu *et al.*, 1996; De Jager, 1995): (i) reduction of the complexity of the control system, (ii) reduction of the required bandwidth of the actuator(s), and (iii) rotating stall control in high-speed machines is claimed to be a difficult problem due to compressibility effects. Active surge control, on the other hand, has evolved the last decade. In laboratory test rigs, up to 20% reduction in surge point mass flow is realized using active surge control. Nevertheless, actual implementation in industrial practice still has not taken place. The main problems seem the reliability penalties due to additional sensors, actuators, and controllers, the technological limitations, *e.g.*, limited bandwidth of actuators and difficulties to accurately measure mass flows, and the high costs to realize an active surge control system (Botros, 1994; Gravidahl and Egeland, 1998). In most cases, only simple proportional feedback controllers are applied to stabilize surge in experimental set-ups. More advanced controllers are expected to increase the achievable extension of the stable operating region; according to theoretical studies, for example, Van de Wal *et al.* (1997), stabilization of surge is possible in the *entire* unstable operating region. This thesis will concentrate on the practical limitations of active surge control in centrifugal compressors. More precisely, the objectives of this research are the following.

1. Investigation of the influence of actuators and sensors on controller performance.
2. Development of advanced controllers for surge stabilization in centrifugal compressors.
3. Validation of these controllers on an experimental set-up.

However, this research will also concentrate on the modeling of the examined compression system, since a model will be used to select appropriate actuators and sensors for surge control and to develop active surge controllers.

A better knowledge of the physical background of surge initiation may result in refinements to existing models, and may provide new insights into methods to suppress this instability. Therefore, the development of surge in centrifugal compressors as well as the initiation of surge are investigated in a companion research project: *Flow models for compressor surge*. Similar to the research project into compressor surge control, the companion project is part of the multi-disciplinary *Compressor Surge Project* at the Faculty of Mechanical Engineering, Eindhoven University of Technology.

1.5 What is new?

The main contributions of this research are the following:

- **Greitzer compression system model is applied to describe the behavior of the examined centrifugal compressor during fully-developed surge** (Chapter 2). Originally, the Greitzer model (Greitzer, 1976a) is developed for low pressure-ratio axial compressors. In this study, this model is applied to a centrifugal compressor which is part of a laboratory-scale gas turbine installation. The Greitzer model is identified and experimentally validated; the frequency and amplitude of the plenum pressure oscillations are predicted for a broad range of operating conditions. The results of this study can be found in Meuleman *et al.* (1998).
- **Systematic selection of actuators and sensors for active surge control** (Chapter 3). Based on the method presented in Van de Wal (1998), the influence of the number, type, and location of actuators and sensors on controller performance is studied (Van de Wal and Willems, 1996;

Van de Wal *et al.*, 1997). The results of this study guide the selection of an appropriate actuator and sensor for surge control. For the chosen control valve, the influence of the bandwidth and capacity on system behavior is examined (Willems, 1998; Willems and De Jager, 1998a).

- **Development of a novel, efficient surge control strategy** (Chapter 4). To avoid wasteful stationary bleed or recycle of compressed air, a one-sided controlled bleed valve is proposed for active surge control (Willems and De Jager, 1998a). This control valve is closed in the desired operating point and only opens to stabilize the system around this point. Surge is stabilized using static output feedback based on plenum pressure measurements. For the linearized system, a proof of the stability of this bounded output feedback controller is provided (see also Willems *et al.* (1999)).
- **Realization of an active surge control system** (Chapter 5). The proposed control system is implemented on the gas turbine installation (Willems, 1999; Willems and De Jager, 2000). Stabilization of surge is seen to be hampered by practical limitations. Application of a band-pass filter in combination with the novel surge control strategy overcomes these problems and results in a decreased surge point mass flow of 7%. Furthermore, experimental results are used to validate the applied model.

1.6 Scope of the thesis

This thesis is organized as follows. First, the studied compression system and the applied Greitzer compression system model are discussed in more detail in Chapter 2. In Chapter 3, the selection of sensors and actuators is motivated for active surge control in the studied compression system. Chapter 4 deals with the proposed control strategies for active surge control and the experimental results are presented in Chapter 5. Finally, conclusions are drawn and directions for future research are given.

Chapter 2

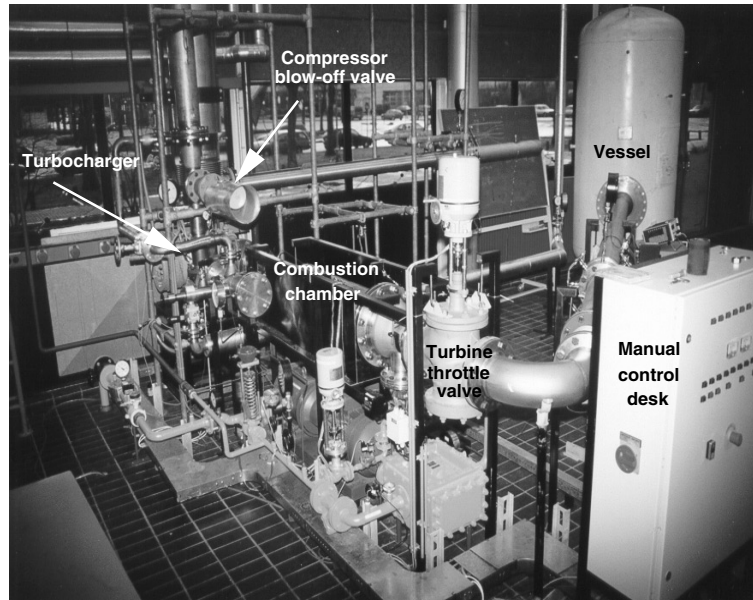
Compression System Modeling

An essential step in model-based controller design is to understand the physical phenomena in the system and to develop a mathematical model that describes the dynamics of the relevant phenomena. In this chapter, the examined compression system is presented in Section 2.1. The Greitzer lumped parameter model is applied to describe the dynamic behavior of the compression system during surge transients. This model with possible extensions and modifications is introduced in Section 2.2, whereas the identification of the model is dealt with in Section 2.3. Finally, simulation results are discussed in Section 2.4.

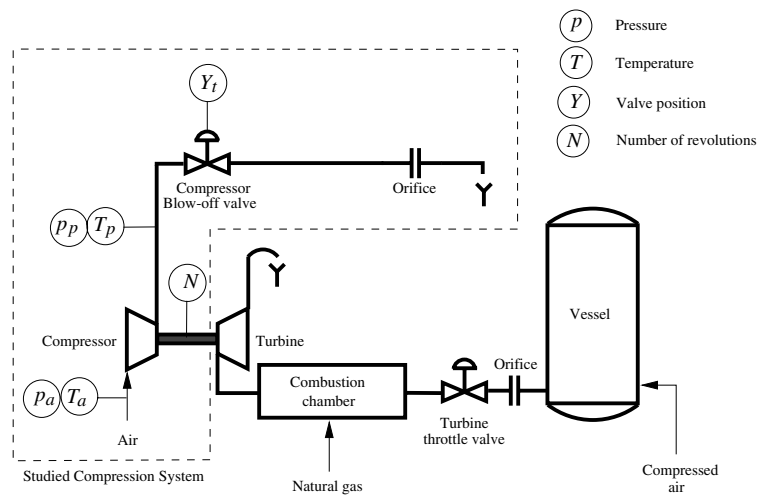
2.1 Experimental set-up

To study the dynamic behavior of turbomachinery, a laboratory-scale gas turbine installation was built in the Energy Technology Laboratory of the Eindhoven University of Technology, see Fig. 2.1a. This installation, designed by Van Essen (1995), consists of a single-stage, centrifugal compressor with a vaned diffuser, which is mounted on the same rotational axis as the axial turbine. In a standard gas turbine, as shown in Fig. 1.11b, mechanical power is produced at the shaft by expansion of a gas across a turbine. This expansion requires a pressure ratio across the turbine, so first the gas has to be compressed. By mounting the turbine on the same axis as the compressor, it can deliver the required compressor power to pressurize the incoming gas. To increase the net mechanical power provided at the shaft, the temperature of the working gas is raised by burning fuel in the combustion chamber. Details about gas turbines can be found in, *e.g.*, Cohen *et al.* (1996).

For surge studies, the gas turbine installation is used in the configuration shown in Fig. 2.1b. Similar to Fink *et al.* (1992), the mass flows through the compressor and turbine are decoupled; the compressor pressurizes the incoming air which is discharged via the compressor blow-off valve into the atmosphere. This modified configuration offers the following benefits. First, the occurring surge oscillations are assumed to be less harmful for the equipment, since the compressor discharges in a relatively small *plenum volume* compared to the large vessel of the standard gas turbine installation. Second, Fink *et al.* (1992) showed that in this small volume case the steady-state compressor characteristics can be determined up to smaller mass flows. Third, if the compressor and turbine mass flows are coupled, the number of steady operating points reduces significantly because a power and mass balance holds between both components. In the studied system, externally supplied compressed air flows via the turbine throttle valve into the combustion chamber where natural gas is added and burned. As the compressor and turbine mass flows can be varied independently, the modified system can in principle be operated in any desired operating point. However, in this configuration the



(a) Photograph of the installation.



(b) Scheme of the installation.

Figure 2.1: Experimental set-up.

rotational speed can be varied up to 25,000 [rpm] due to the limited mass flow rate of the externally supplied compressed air.

Measurement system

To determine the steady-state performance of the compressor, the compression system is equipped with temperature probes and pressure transducers, as shown in Fig. 2.1b. Moreover, steady turbine and compressor blow-off mass flows can be determined from two instrumented orifices whereas the rotational speed of the impeller is measured with a semi-conductor pulse tachometer. The angular displacement of the stem of the turbine throttle and compressor blow-off valve is also registered. This signal is a measure for the opening area of the valves. As these valves have a linear flow characteristic, the mass flow through the valve is proportional to the valve position (Van Essen, 1995). For data-acquisition, a NATIONAL INSTRUMENTS board is installed in a measurement PC. LABVIEW software controls the data storage on hard disk and real-time process monitoring on the computer screen. This system is run at 200 [Hz] sampling frequency. A second PC equipped with a dSPACE DS1103 controller board is used to run (surge) controllers and to gather a subset of the available data at high speeds (1 [kHz] sampling frequency).

Surge transients are observed using measurements of the high-frequency response pressure probe at the compressor outlet, of the compressor blow-off valve's rotation angle sensor, and of the rotational speed transducer. Reliable, transient mass flow measurements are not available. Further details about the installation and the measurement system can be found in Appendix B.

Compressor characteristics

Figure 2.2 shows the measured steady-state compressor map. The performance of the compressor is

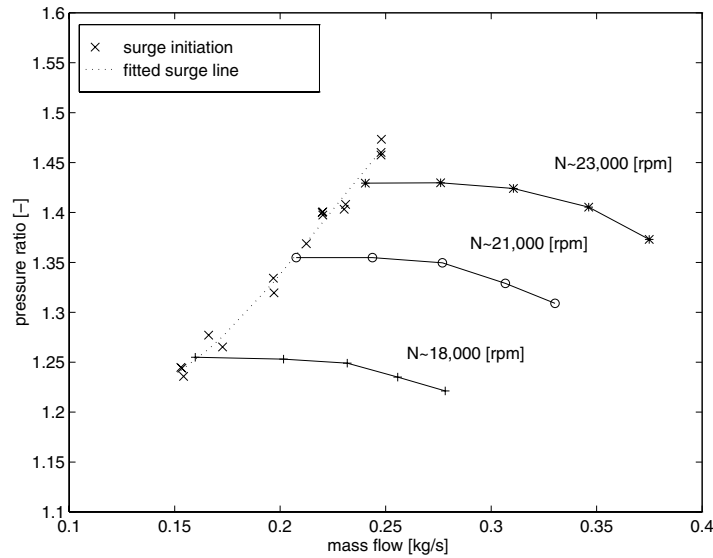


Figure 2.2: Measured compressor map (Meuleman *et al.*, 1998).

specified using the pressure ratio $\frac{p_p}{p_a}$, the compressor mass flow \dot{m} , and the rotational speed N . A compressor characteristic is determined by initially operating the system at a safe distance from the

surge line. The compressor mass flow is throttled by closing the compressor blow-off valve, so the system's operating point moves towards the surge line. As the rotational speed slightly increases for constant turbine power, it is kept constant by changing the externally supplied air or natural gas mass flow. Accordingly, various steady-state operating points can be measured at a speed line. The surge line is determined experimentally by detecting the surge initiation. During these experiments, first the compressor is operated in the stable operating region close to the surge line. Then, the compressor blow-off valve is slowly closed until the system exhibits surge. The surge initiation point corresponds to the point where the amplitude of the pressure oscillations starts to grow (as illustrated in Fig. 1.6).

2.2 Greitzer lumped parameter model

In the literature, various models can be found that describe rotating stall or surge. A comprehensive overview can be found in, *e.g.*, Gravdahl and Egeland (1998) or Longley (1994). In this study, we focus on the modeling of surge. Depending on the application, two important types of models can be distinguished: a **control model**, which predicts the time development of surge and directs the development of the controller. As the surge frequency is on the order of 10-20 [Hz], stabilization is supposed to require relatively fast control actions (50-200 [Hz]). Therefore, relatively low order models are required for real-time implementation of model-based controllers. On the other hand, more complex **simulation models** can be used for more detailed system dynamic analysis. This section deals with a compression system model that is suitable for surge control purposes. Furthermore, other models and possible extensions and modifications of the applied model are discussed.

To describe the dynamic behavior of the examined compression system, the Greitzer lumped parameter model (Greitzer, 1976a) is used, which is shown in Fig. 2.3. Ffowcs Williams and Huang (1989) and Pinsley *et al.* (1991), for example, showed that application of this model to experimental

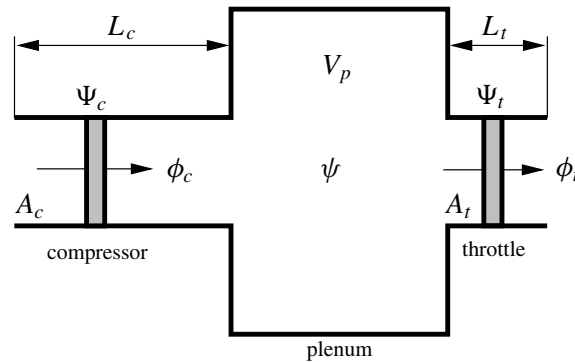


Figure 2.3: Greitzer lumped parameter model.

surge control studies in centrifugal compressors gives promising results. The lumped parameter model is originally developed for compression systems with low pressure-ratio axial compressors, and can describe surge transients initiated by disturbances from steady-state conditions. This model is based on a Helmholtz resonator type of model, as proposed by Emmons *et al.* (1955). The compression system is represented by a duct, in which the compressor works, that discharges in a large volume (often called *plenum*). The compressed gas flows via the plenum and the compressor blow-off valve (or throttle) into the atmosphere. In this model, compressibility effects are associated with isentropic compression of the gas in the plenum. Inertia effects, on the other hand, are lumped on momentum

changes of the gas in the compressor and throttle duct.

To come to the lumped parameter model, Greitzer (1976a) made the following assumptions. First, he assumed that the flow in the ducts is one-dimensional and incompressible. Second, in the plenum, the pressure is supposed to be uniformly distributed and the gas velocity is neglected. Third, the overall temperature ratio $\frac{T_p}{T_a}$ of the system is assumed to be near unity, so an energy balance is not required. Fourth, the influence of rotor speed variations on system behavior is neglected. An actuator disc placed in a straight duct is used to model the compressor and its ducting. This actuator disc represents a blade row as a plane across which the mass flow is continuous, but pressure changes can be discontinuous. The geometry of the *equivalent compressor duct* is chosen such that mass flow rate changes generate pressure differences which are equal to the pressure differences across the actual duct. A similar approach is followed to model the throttle.

For the description of the dynamic behavior of the compression system, the one-dimensional momentum equation is applied to the compressor and throttle ducts and the principle of mass conservation is used in the plenum. Dynamic compression behavior is described by a first order model with time constant $\tilde{\tau}$. Greitzer (1976a) incorporated this model to capture transients observed during the development of a stall cell. Introducing the dimensionless mass flow ϕ and the dimensionless pressure difference Ψ :

$$\phi = \frac{\dot{m}}{\rho_a A_c U_t} \quad \text{and} \quad \Psi = \frac{\Delta P}{\frac{1}{2} \rho_a U_t^2},$$

and scaling time t , as $\tilde{t} = t \omega_H$ using the Helmholtz frequency $\omega_H = a \sqrt{\frac{A_c}{V_p L_c}}$, leads to the following set of dimensionless equations:

$$\frac{d\phi_c}{d\tilde{t}} = B[\Psi_c - \psi] \quad (2.1)$$

$$\frac{d\phi_t}{d\tilde{t}} = \frac{B}{G}[\psi - \Psi_t] \quad (2.2)$$

$$\frac{d\psi}{d\tilde{t}} = \frac{1}{B}[\phi_c - \phi_t] \quad (2.3)$$

$$\frac{d\Psi_c}{d\tilde{t}} = \frac{1}{\tilde{\tau}}[\Psi_{c,ss} - \Psi_c] \quad (2.4)$$

where ϕ_c is the dimensionless compressor mass flow and ψ is the dimensionless plenum pressure rise. Furthermore, $\Psi_{c,ss}$ is the dimensionless steady-state compressor pressure rise given in the compressor map, whereas Ψ_c is the dimensionless dynamic compressor pressure rise. The throttle is assumed to behave quasi-stationary. For subsonic flow conditions, its behavior is described by (Meuleman *et al.*, 1998; Van de Wal and Willems, 1996):

$$\phi_t = c_t u_t \sqrt{\Psi_t} \quad \text{if} \quad \Psi_t > 0 \quad (2.5)$$

with dimensionless throttle mass flow ϕ_t , dimensionless throttle position u_t , and dimensionless pressure drop Ψ_t across the throttle. The dimensionless throttle parameter c_t is a measure for the capacity of the fully opened throttle (for details, see Appendix B.2.2). The meaning of other variables and parameters used in the Greitzer model is listed in Table 2.1. Details about the derivation of the Greitzer

Table 2.1: Parameters and variables used in the Greitzer model.

<i>Symbol</i>	<i>Meaning</i>
a	Speed of sound [m/s]
\dot{m}	Mass flow [kg/s]
P_a	Ambient pressure [Pa]
ΔP	Pressure difference $P - P_a$ [Pa]
ρ_a	Air density [kg/m ³] at ambient conditions
A_c	Compressor duct area [m ²]
A_t	Throttle duct area [m ²]
L_c	Equivalent compressor duct length [m]
L_t	Equivalent throttle duct length [m]
R_t	Rotor tip radius [m]
U_t	Rotor tip speed [m/s]
V_p	Plenum volume [m ³]
ω_H	Helmholtz frequency [rad/s]
c_t	Dimensionless throttle parameter
u_t	Dimensionless throttle position
\tilde{t}	Dimensionless time
$\tilde{\tau}$	Dimensionless time constant associated with development of stall cells
B	Greitzer stability parameter
G	Dimensionless parameter
ψ	Dimensionless plenum pressure rise
Ψ_c	Dimensionless compressor pressure rise
$\Psi_{c,ss}$	Dimensionless steady-state compressor pressure rise
Ψ_t	Dimensionless pressure drop across throttle
ϕ_c	Dimensionless compressor mass flow
ϕ_t	Dimensionless throttle mass flow

model are given in Appendix C.2.

Note that (2.1) and (2.2) are the dimensionless 1-D momentum equations for the compressor and throttle duct, respectively, whereas (2.3) is the dimensionless mass balance of the plenum. The dynamic compressor behavior is described by (2.4). This model is also capable of describing transitions from steady flow conditions to rotating stall if the stalled characteristic is included in $\Psi_{c,ss}$ (see Greitzer (1976b)). Recall that the flow description in the Greitzer model is one-dimensional, so only changes in the dimensionless annulus-averaged compressor mass flow ϕ_c and the dimensionless plenum pressure rise ψ can be described; information about circumferential variations is not available.

Scaling of the equations results in the introduction of three dimensionless system parameters:

$$B = \frac{U_t}{2\omega_H L_c}, \quad G = \frac{L_t A_c}{L_c A_t}, \quad \text{and} \quad \tilde{\tau} = \frac{2\pi R_t N_\tau}{U_t} \omega_H,$$

where N_τ is the lag associated with the formation of stall cells, which is expressed in number of rotor revolutions. The Greitzer stability parameter B appeared to be a quantitative measure to predict the behavior of the compression system subsequent to instability onset; systems with B -values above a critical value B_{crit} exhibit surge, while small B systems will tend to rotating stall. This critical

parameter B_{crit} is seen to vary between 0.25 and 2.7 for different compression systems (Willems, 1997). Further increase of the B -parameter beyond B_{crit} results in a change of classic surge into deep surge (Greitzer, 1976b). Linear analyses of the Greitzer model demonstrate that the system stability is locally set by the relation between the slope of the compressor characteristic, the slope of the throttle characteristic, and the Greitzer stability parameter (Greitzer, 1981; Simon *et al.*, 1993). More precisely, from an analysis of a nonlinear compression system, Simon and Valavani (1991) showed that the stability strongly depends on the *shape* of the compressor and throttle characteristics.

The dimensionless parameter G , on the other hand, can be interpreted as a measure for the importance of the inertia effects in the throttle duct compared to those in the compressor duct. Recall that the dimensionless time constant $\tilde{\tau}$ accounts for the time needed for the full development of rotating stall after initiation. This time constant is a different dimensionless parameter as B and G , since it depends on the system response and can not be set before the experiments.

Compressibility effects In the Greitzer model, the flow in the ducts is assumed to be incompressible and pressure rise characteristics are concentrated in a blade row. However, according to Ishii and Kashiwabara (1996) this approach is not valid for systems with a large number of stages. It is also noted that compressibility effects are important in high-speed machines (Day and Freeman, 1994; Gu *et al.*, 1996). For high-speed, multi-stage compressors, Feulner *et al.* (1996) present a linear compressible flow model that distributes compressibility through the compressor. This model consists of one-dimensional models for the flow in the blade passages and two-dimensional models of the flow in the interblade row gaps and in the inlet and outlet ducts. Ishii and Kashiwabara (1996), on the other hand, developed a complete two-dimensional, compressible flow model for the description of rotating stall and surge in high-speed, multi-stage axial compressors. Similar to Moore and Greitzer (1986), this nonlinear model can describe the development of both rotating stall and surge, and the coupling between these instabilities.

Additionally, compressibility effects may be important in centrifugal compressors, since they normally achieve larger pressure ratios (Gu *et al.*, 1996). Recall that the Greitzer model is originally developed for low pressure-ratio axial compressors. Application of the Greitzer model to centrifugal compressors shows conflicting results. Hansen *et al.* (1981) and Fink *et al.* (1992) modeled deep surge in a small single-stage centrifugal compressor. For a suitable choice of the dimensionless time constant $\tilde{\tau}$ associated with dynamic compressor response, the Greitzer model shows qualitatively good agreement with experiments in Hansen *et al.* (1981). Fink *et al.* (1992), on the contrary, found poor agreement between simulations and measurements due to rotor speed variations. For a multi-stage centrifugal compressor, Arnulfi *et al.* (1999b) reasonably predict deep surge transients using a third order Greitzer model which neglects the dynamics in the throttle duct. Macdougall and Elder (1983) derived a model much similar to Greitzer (1976a) for a centrifugal compressor. This model can describe mild surge transients and can deal with non-ideal gases and changes in gas composition. A different approach is followed by Botros (1994) and Badmus *et al.* (1995a). They developed models that start from a general description by applying principles of conservation of mass, energy, and momentum for a calorically perfect gas. Both one-dimensional models can be applied to generic compression systems and describe the dynamic behavior of axial as well as centrifugal compressors during surge. However, these models are relatively complex. Nonetheless, the control-oriented high-frequency model has been reported to be successfully applied for controller design in Badmus *et al.* (1995b).

Influence of rotor speed variations According to Botros (1994), rotor shaft inertia has to be included in cases where fast transients are expected. Note that rotor speed variations are considerably smaller in low-speed compressors with large shaft inertia. From the results of Hansen *et al.* (1981), it is seen that these variations can be negligible in small high-speed machines during deep surge. Fink *et al.* (1992), on the other hand, found poor results for deep surge in a centrifugal compressor within a small turbocharger. Inclusion of rotor speed variations in the Greitzer model significantly improved the qualitative and quantitative agreement with experiments. Gravdahl and Egeland (1997b,c), included rotor shaft dynamics in the Moore-Greitzer and Greitzer model, respectively, to study the simultaneous control of stall and the rotational speed. Rotor speed variations are also incorporated in the model proposed by Botros (1994).

Compressor characteristics To specify the behavior of the compressor, Greitzer (1976a) used a steady-state compressor characteristic. This characteristic is generally not known for mass flows smaller than the surge point mass flow. Often, a third or higher-order polynomial is used to approximate the steady compressor characteristic (see, *e.g.*, Badmus *et al.* (1996), Hansen *et al.* (1981), and Pinsley *et al.* (1991)). However, Gravdahl and Egeland (1997c) determine a second-order approximation of the characteristic from compressor geometry and energy considerations for a centrifugal compressor; a characteristic based on ideal energy transfer is modified by including incidence and frictional losses. Analogously, Ishii and Kashiwabara (1996) developed an approach which deals with the influence of blade geometry on compressor performance. In this approach, the characteristic of a blade row is described in terms of the total pressure loss and deviation angle δ (*i.e.*, the difference between the air outlet angle α_2 and blade outlet angle α'_2 , see Fig. 2.4) as a function of the incidence angle i . Botros (1994) and Macdougall and Elder (1983), on the other hand, use relations for a

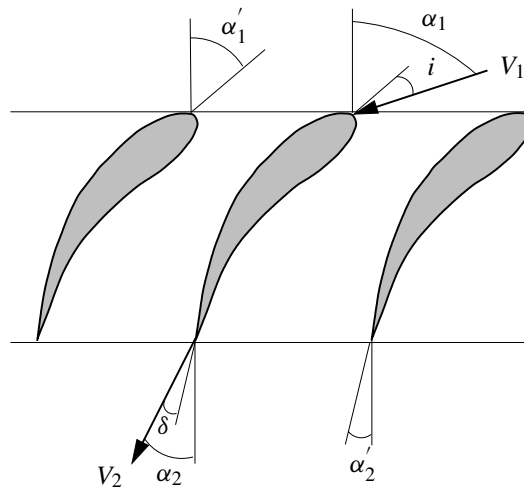


Figure 2.4: Scheme of a blade row with important angles.

polytropic compression process in combination with an approximation of the steady compressor characteristic to describe the behavior of a centrifugal compressor. For a detailed stability analysis, Elder and Gill (1985) modeled various components of a centrifugal compressor (*i.e.*, inducer, impeller tip, semi-vaneless space and diffuser channel). The dynamic behavior of each component is described by conservation laws in combination with its measured, steady characteristic. Lastly, in Moore and Greitzer (1986), a description of the *stalled* characteristic is suggested that follows from the application

of a Galerkin procedure. This procedure assumes that the general solution of the model can be represented by a sequence of basic functions; a single term harmonic wave approximation is used to describe the circumferential mass flow perturbation associated with rotating stall, whereas, *e.g.*, Haynes *et al.* (1994) and Paduano *et al.* (1994) apply higher order harmonics.

In summary, the models discussed in this section and their main properties are listed in Table 2.2.

Table 2.2: Overview of the properties of the examined models. Legend: *Rotor speed variations* ΔN – +: included, –: not included; *Type of machine described by the model* – A: axial compressor, C: centrifugal compressor; *Instability described by the model* – S: surge, R: rotating stall.

<i>Model</i>	<i>Flow description</i>	ΔN	<i>Mach.</i>	<i>Instab.</i>
Greitzer (1976a)	1D Incompressible	–	A	S
Hansen <i>et al.</i> (1981)	1D Incompressible	–	C	S
Fink <i>et al.</i> (1992)	1D Incompressible	+	C	S
Gravdahl and Egeland (1997c)	1D Incompressible	+	C	S
Macdougall and Elder (1983)	1D Compressible	–	AC	S
Elder and Gill (1985)	1D Compressible	–	C	S
Botros (1994)	1D Compressible	+	AC	S
Badmus <i>et al.</i> (1995a)	Quasi-1D Compressible	–	AC	S
Moore and Greitzer (1986)	2D Incompressible	–	A	SR
Gravdahl and Egeland (1997b)	2D Incompressible	+	A	SR
Feulner <i>et al.</i> (1996)	1D/2D Compressible	–	A	SR
Ishii and Kashiwabara (1996)	2D Compressible	–	A	SR

Applied compression system model

To describe the behavior of the examined compression system during surge, the two state Greitzer lumped parameter model is applied:

$$\begin{aligned}\frac{d\phi_c}{d\tilde{t}} &= B[\Psi_{c,ss} - \psi] \\ \frac{d\psi}{d\tilde{t}} &= \frac{1}{B}[\phi_c - \phi_t]\end{aligned}\tag{2.6}$$

with:

$$\Psi_c = \Psi_{c,ss} \quad \text{and} \quad \Psi_t = \psi$$

Application of this model is based on the following assumptions:

- ***G* parameter in (2.2) is small.** As $A_t \approx A_c$ in the studied system, this means that the equivalent throttle duct length L_t is significantly smaller than L_c . This seems reasonable since L_t is on the order of the length of the flow path in the throttle: $L_t \approx 0.1$ [m].
- **Compressor behaves quasi-stationary.** Greitzer (1976b) investigated an axial compressor, in which both rotating stall and surge were present. To account for the development of rotating stall, (2.4) was incorporated. However, in the studied centrifugal compressor, rotating stall is not assumed to be important, so this equation is omitted.

- **Rotational speed variations are negligible.** This is verified from experiments; during surge the rotational speed is seen to be approximately constant for constant throttle position. However, surge initiation transients are associated with considerable rotational speed variations. The rotational speed can be kept constant by implementing a speed controller on the gas turbine. Then, the natural gas mass flow and the externally supplied air mass flow can be used as control inputs. This will result in a relatively slow response due to the slow turbine throttle valve, the constraint on the turbine inlet temperature, and the time constant associated with the combustion chamber response (see Van Essen (1998)). These problems can be circumvented if an electro motor is applied to drive the compressor.
- **Overall temperature ratio $\frac{T_p}{T_a}$ is near unity.** In the studied speed range, the plenum temperature is around $T_p = 340$ [K], so $\frac{T_p}{T_a} \approx 1.1$. From (C.26), it is seen that if T_p differs from T_a this can be interpreted as a change of B (and thus of V_p). An appropriate choice of V_p will compensate for this effect, so T_p can be replaced by the ambient temperature. Then, an extra equation of state is not needed.

It is noted that this second order Greitzer model is a special case of the two-dimensional Moore-Greitzer model (Moore and Greitzer, 1986): the *pure surge case*. Besides the pure surge mode, the Moore-Greitzer model is capable to predict a mix of rotating stall and surge, and to describe the coupling between rotating stall and surge.

2.3 Identification of the Greitzer model

For the examined compression system, the compressor characteristic $\Psi_{c,ss}$, the throttle characteristic ϕ_t , and the Greitzer parameter B in (2.6) have to be determined. This identification problem is split up in two parts. First, the steady compressor and throttle characteristics are approximated using stationary measurements. Second, applying these approximated characteristics, measured surge transients are used to identify the Greitzer stability parameter B .

2.3.1 Compressor and throttle characteristics

For the approximation of the steady-state compressor characteristic, the cubic polynomial proposed by Moore and Greitzer (1986) is used:

$$\Psi_c(\phi_c) = \Psi_c(0) + H \left[1 + \frac{3}{2} \left(\frac{\phi_c}{F} - 1 \right) - \frac{1}{2} \left(\frac{\phi_c}{F} - 1 \right)^3 \right].$$

The parameters $\Psi_c(0)$, H , and F are determined from steady-state measurements of the compressor characteristics shown in Fig. 2.5; $\Psi_c(0)$ is the valley point of the characteristic located at the compressor pressure rise axis, whereas $\phi_c = 2F$ corresponds to the dimensionless compressor mass flow at the top of the characteristic (see also Fig. 2.10). Using the data of the three parameters obtained for different speeds, they are interpolated by polynomials in N . Details can be found in Appendix B.2.1. Note that steady-state measurements cannot be performed for mass flows lower than the surge point mass flow. For the region in which stationary measurements are available, the approximated characteristics $\Psi_c(\phi_c)$ are shown in Fig. 2.5.

For the estimation of the dimensionless throttle parameter c_t in (2.5), the same steady-state measurements are used as for the compressor characteristics. This estimation is straightforward, since stationary measurements of ϕ_t , ψ , and u_t are available (see Appendix B.2.2).

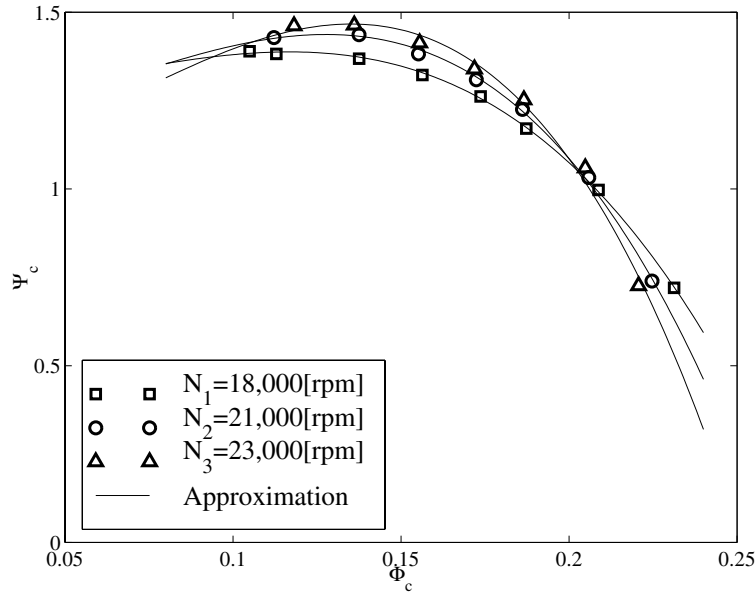


Figure 2.5: Dimensionless compressor map.

2.3.2 Greitzer stability parameter

To specify the B -parameter, the compressor duct area A_c , the equivalent duct length L_c , and the plenum volume V_p have to be determined. Similar to Greitzer (1976a), A_c is chosen to be equal to the compressor exit area. Recall that reliable, transient mass flow measurements are not available, so the equivalent compressor duct length L_c cannot be obtained from experiments using (C.13). Furthermore, the plenum volume V_p is not exactly known. It is chosen to be equal to the approximated volume of the volute of the centrifugal compressor and of the duct between the compressor outlet and the compressor blow-off valve. The length of the volute and the duct is small compared to the wavelength of the pressure oscillations of the surge oscillations. Therefore, the measured pressure oscillations in the compressor outlet duct are not associated with a standing pressure wave pattern (Ribi and Gyarmathy, 1995).

The B -parameter can be estimated from measurements; combining the equations of (2.6) yields:

$$B = \frac{-\frac{d\phi_c}{dt}}{\frac{d^2\psi}{dt^2} - \Psi_c(\phi_c) + \psi}.$$

This estimation is expected to be inaccurate since the measured plenum pressure rise ψ has to be differentiated twice and $\frac{d\phi_c}{dt}$ has to be approximated using (2.5). Therefore, measurements of plenum pressure variations during fully-developed surge are used to determine the B -parameter in the Greitzer model. Contrary to other types of transients, *e.g.*, set-point changes in the stable operating region or surge initiation, in the studied case the rotational speed is nearly constant. Moreover, we are especially interested in the prediction capability of the model in case of surge. During experiments, surge is triggered by first operating the compressor in the stable operating region close to the surge line. Then, the compression system is throttled by closing the compressor blow-off valve until surge occurs. For a constant throttle position, the system is operated in surge for 15 [s]. This is done for varying throttle positions and rotational speeds. The throttle position and rotational speed during fully-developed

surge are the inputs of the two state Greitzer model.

In the simulations, the compression system is perturbed from its equilibrium point (ϕ_{c0}, ψ_0) associated with the given throttle position and rotational speed. If ϕ_{c0} is smaller than the surge point mass flow, this leads to a limit cycle oscillation in the compressor map. The measured and predicted dimensionless plenum pressure oscillations are compared with each other. More precisely, the dominant frequency of the dimensionless plenum pressure oscillations is obtained from a spectral analysis of the pressure oscillations during fully-developed surge. This way the *surge frequency* is determined with an accuracy of 0.4 [Hz]. Moreover, the agreement between the measured and predicted amplitude of the dimensionless plenum pressure oscillations is studied from time traces.

Assuming that A_c and V_p are chosen correctly, the identification of B boils down to the determination of L_c ; this length has to be specified such that the frequency and amplitude of the measured and predicted plenum pressure oscillations agree.

Sensitivity analysis

To make an appropriate choice for L_c , simulations are performed for various values of the Helmholtz frequency and the Greitzer stability parameter. For the four cases listed in Table 2.3, the predicted

Table 2.3: Parameters used in sensitivity analysis.

<i>Parameter</i>	<i>Case I</i>	<i>Case II</i>	<i>Case III</i>	<i>Case IV</i>
L_c [m]	0.66	1.53	1.8	1.8
f_H [Hz]	41.6	27.3	25.2	25.2
B	0.51-0.65	0.34-0.42	0.31-0.39	0.31-0.39
Δ	0	0	0	0.3

surge frequency is shown in Figs. 2.6 and 2.7 for various dimensionless throttle positions u_{t0} and B parameters, respectively. Other parameters used in the Greitzer model can be found in Table 2.4.

Initially, simulations are done with the approximation of the compressor characteristic ($\Delta = 0$; see Fig. 2.10), which is presented in Appendix B.2.1. For these cases, it is seen that L_c strongly influences the predicted surge frequency, as shown in Fig. 2.6. This is reasonable, since time is scaled with ω_H in the simulations. Therefore, L_c is chosen such that the Helmholtz frequency f_H is on the order of the observed surge frequency (Case III, lower left-hand figure). Note that the outliers are associated with the mild and classic surge cases. In this study, the classification of surge types is based on De Jager (1995). As seen from Fig. 2.7, mild surge occurs for small B -values. For increasing B , the surge type changes into classic surge and deep surge. These results are in accordance with the experimental results of Greitzer (1976b).

During mild surge, the frequency of oscillations is on the order of the Helmholtz frequency. Furthermore, this type of surge is associated with small amplitude oscillations, as shown in Fig. 2.8. The upper left-hand figure shows the limit cycle oscillation in the compressor map. This result can only be shown for the simulation, because transient mass flow measurements are not available. The compressor and throttle characteristics are shown for reference. In the upper right-hand figure, the time traces of the measured and predicted dimensionless plenum pressure oscillations during fully-developed surge are shown in detail. The lower figure shows the power spectral density estimates of the predicted and measured ψ .

Classic surge, on the other hand, is a nonlinear phenomenon with larger oscillations and at a lower

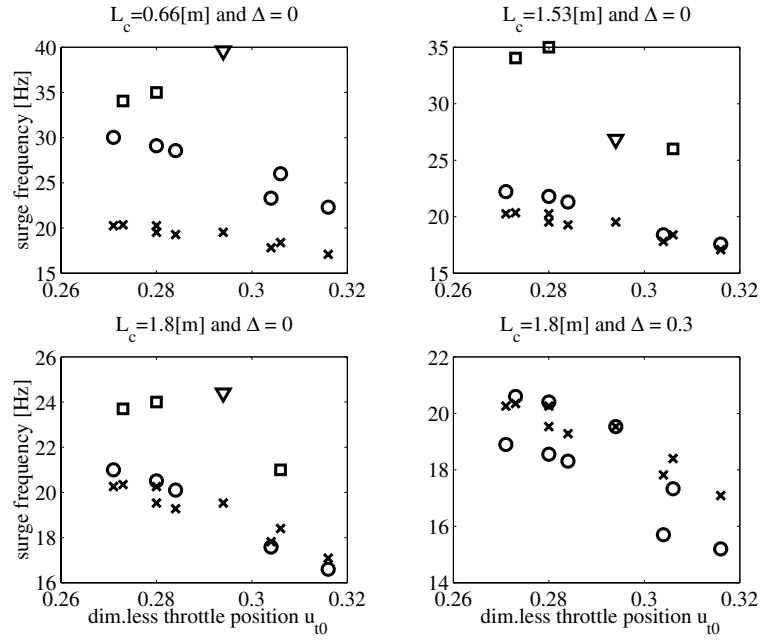


Figure 2.6: Effect of nominal throttle position u_{t0} on measured and predicted surge frequency (Measurements (x), Simulations: deep surge (O), classic surge (\square), and mild surge (∇)).

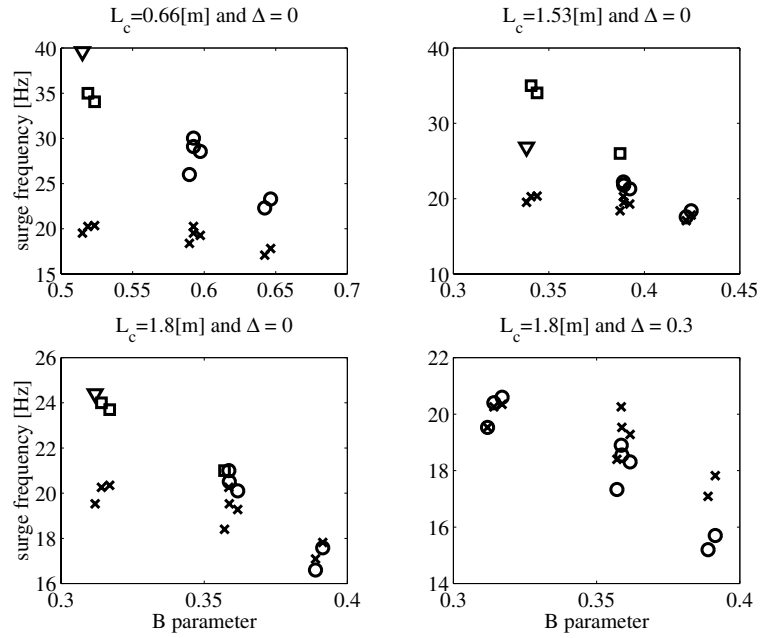


Figure 2.7: Effect of B -parameter on measured and predicted surge frequency (Measurements (x), Simulations: deep surge (O), classic surge (\square), and mild surge (∇)).

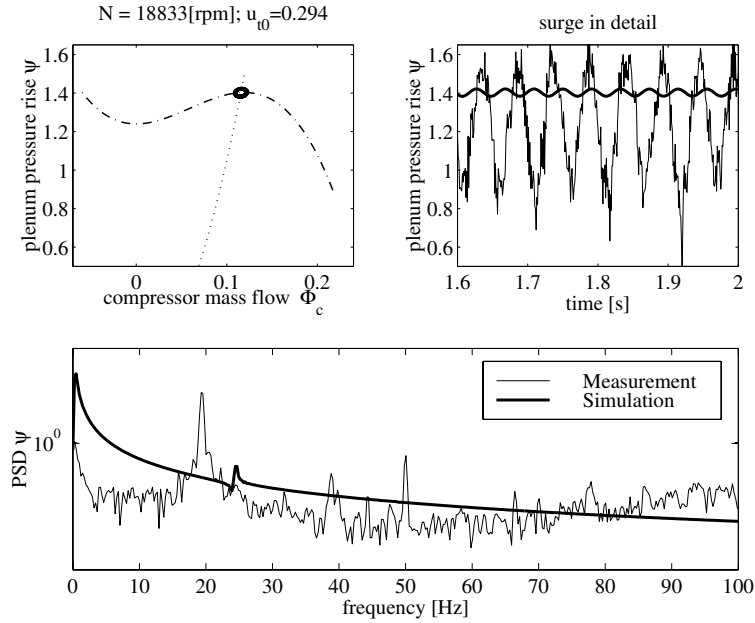


Figure 2.8: Results for mild surge case ($B = 0.312$, $L_c = 1.8$ [m] and $\Delta = 0$).

frequency than mild surge. This is illustrated in Fig. 2.9; for the simulation, the first higher order harmonic can clearly be observed in the lower figure. From the upper left-hand figure, it is concluded that ψ differs significantly from the steady compressor characteristic $\Psi_c(\phi_c)$ during surge. This is due to the relatively large inertia of the gas in the compressor duct.

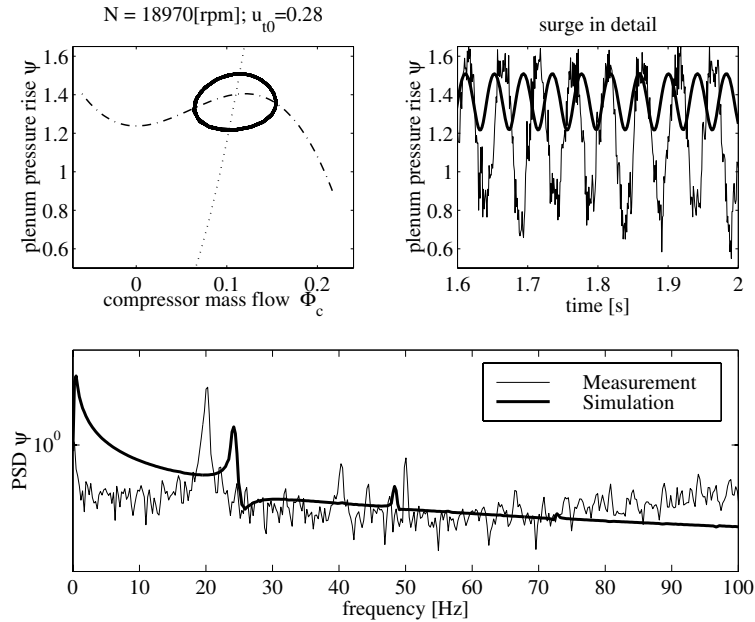


Figure 2.9: Results for classic surge case ($B = 0.314$, $L_c = 1.8$ [m] and $\Delta = 0$).

In Case III, the surge frequency is reasonably predicted, but the amplitude of the plenum pressure oscillations is underestimated (see Fig. 2.9). Remarkably, the maximal plenum pressure during a surge cycle is approximated well. Similar results are found for the deep surge cases. Consequently,

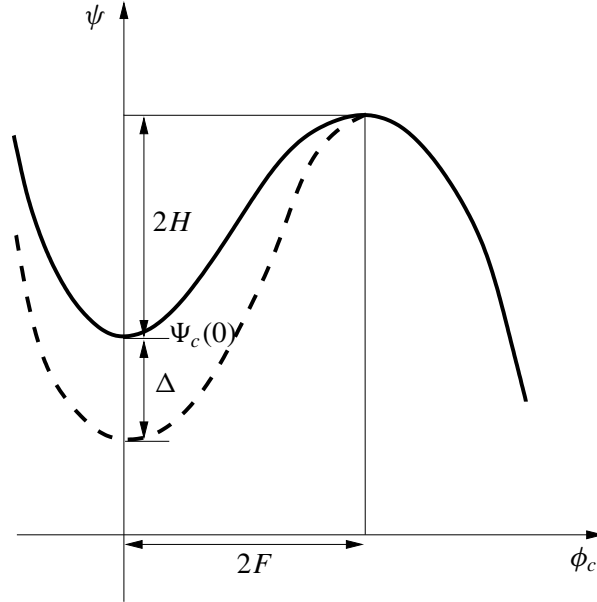


Figure 2.10: Scheme illustrating the effect of Δ on $\Psi_c(\phi_c)$.

to improve the agreement between the estimated and measured amplitude of the plenum pressure rise oscillations, the valley point $\Psi_c(0)$ is moved without changing the measured part of the compressor characteristics $\Psi_c(\phi_c)$ (see Fig. 2.10):

$$\begin{aligned} H' &= H & \text{and } \Psi'_c(0) &= \Psi_c(0) & \phi_c &\geq 2F \\ & & & & \text{if} \\ H' &= H + \frac{1}{2}\Delta & \text{and } \Psi'_c(0) &= \Psi_c(0) - \Delta & \phi_c &< 2F \end{aligned}$$

Doing so, comparison of the lower plots in Fig. 2.6, learns that the prediction of the surge frequency is improved and *only* deep surge occurs for $\Delta = 0.3$. This surge type is associated with reverse flow over part of the cycle. The trend observed in the measurements is reasonably described by the Greitzer model for a wide range of rotational speeds and nominal throttle positions. Moreover, the prediction of the amplitude of ψ is significantly improved; for the case examined in Fig. 2.9, the results are shown in Fig. 2.11 using the modified compressor characteristic. The measured surge frequency and first higher order harmonic are perfectly matched. During deep surge, the frequency of the plenum pressure oscillations is normally well below the Helmholtz frequency, since it is set by the filling and emptying periods of the plenum (Fink *et al.*, 1992; Hansen *et al.*, 1981). Nonetheless, the difference between the frequency during classic and deep surge is small in the studied cases. This is expected because of the relatively small plenum volume. As seen from the lower plots of Figs. 2.6 and 2.7, the occurring surge type is also affected by the shape of the compressor characteristic. Unless otherwise specified, in the sequel simulations are performed with the parameters listed in Table 2.4.

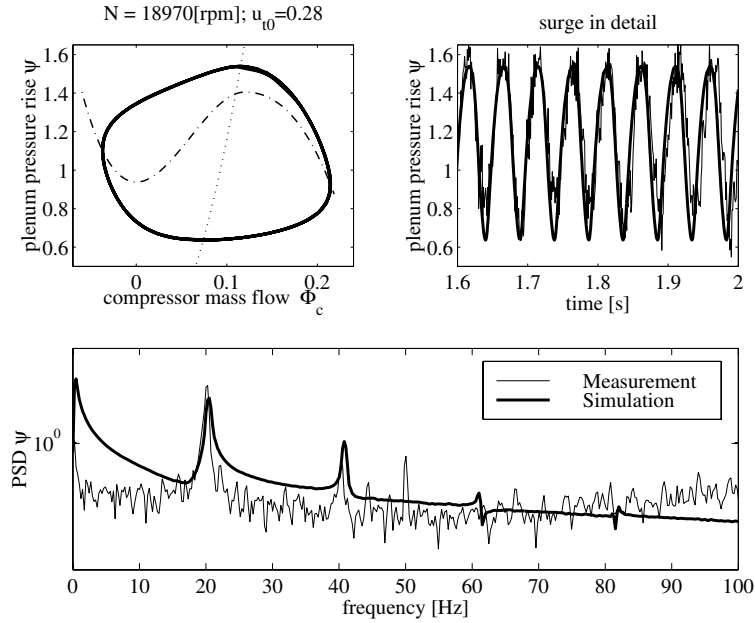


Figure 2.11: Results for deep surge case ($B = 0.314$, $L_c = 1.8$ [m] and $\Delta = 0.3$).

2.4 Discussion

From the sensitivity analysis, it is concluded that the surge frequency is influenced by the Helmholtz frequency f_H and the shape of the compressor characteristic Ψ_c . The amplitude of the plenum pressure oscillations, on the other hand, is seen to strongly depend on the shape of the compressor characteristic and the occurring surge type (thus, the B -parameter); plenum pressure oscillations during classic surge are seen to be smaller than for deep surge. Good results are obtained if L_c is chosen such that f_H is

Table 2.4: Parameters used in Greitzer model.

Parameter	Value
Compressor duct area A_c [m ²]	$7.9 \cdot 10^{-3}$
Plenum volume V_p [m ³]	$2.03 \cdot 10^{-2}$
Compressor duct length L_c [m]	1.8
Speed of sound a [m/s]	340
Helmholtz frequency f_H [Hz]	25.2
Impeller tip radius r [m]	0.09
Density ρ_a [kg/m ³]	1.20
Throttle parameter c_t	0.3320
Compressor characteristic shift Δ	0.3

on the order of the surge frequency and the valley point $\Psi_c(0)$ of the original cubic polynomial is lowered by $\Delta = 0.3$. Recall that Ψ_c is unknown for mass flows ϕ_c smaller than the surge point mass flow. Fink *et al.* (1992) showed that compressor characteristics can be determined down to smaller

mass flows by decreasing the plenum volume (and, thus, the B parameter). Locally the stability is set by the slopes of the compressor and throttle characteristics. Arnulfi *et al.* (1999a) mounted a throttle directly on their compressor to determine the compressor characteristics down to very small positive mass flows. In Hansen *et al.* (1981), the negative flow branch of the compressor characteristic is measured by forced air flow. This part was fitted by a parabola whereas the stable part for positive mass flows was described by a cubic approximation. Both parts were smoothly connected by another cubic polynomial. Greitzer (1976b) and Arnulfi *et al.* (1999b), on the other hand, used deep surge measurements to determine the negative flow branch of the compressor characteristic; their systems behave quasi-stationary during the emptying period of the plenum.

From experiments, it is seen that the surge frequency increases for decreasing throttle position u_{t0} . A similar trend is observed by Pinsley *et al.* (1991) in a single-stage centrifugal compressor. For a multi-stage centrifugal compressor, Arnulfi *et al.* (1999a) found that further throttling the compressor will finally result in a decrease of the observed surge frequency. The relation between the surge frequency and the throttle position u_t and the B -parameter is predicted reasonably well by the applied Greitzer model for $L_c = 1.8$ [m] and $\Delta = 0.3$. In this case, only deep surge is found in the simulations. It cannot be verified if deep surge occurs in the experimental set-up, because mass flow transients cannot be measured accurately. As an alternative in the future, similar to Greitzer (1976b), the compressor mass flow can probably be calculated from the continuity equation for the plenum using plenum pressure measurements, the approximated throttle behavior, and an isentropic relation for the compression process in the plenum.

For the examined compression system, Meuleman *et al.* (1998) found reasonable agreement between measurements and simulation results for different values of A_c , V_p , and L_c . The applied parameter values are listed in Table 2.5. Compared to this study, the experiments in Meuleman *et al.* (1998)

Table 2.5: Model parameters used in simulations.

Parameter	Value	Meuleman <i>et al.</i> (1998)
Compressor duct area A_c [m ²]	$7.9 \cdot 10^{-3}$	$9.56 \cdot 10^{-3}$
Plenum volume V_p [m ³]	$2.03 \cdot 10^{-2}$	$3.75 \cdot 10^{-2}$
Equivalent compressor duct length L_c [m]	1.8	1.0
Speed of sound a [m/s]	340	340
Helmholtz frequency f_H [Hz]	25.3	27.3
Rotational speed N [10 ³ · rpm]	18 - 25	18 - 25
Greitzer stability parameter B	0.31 - 0.49	0.49 - 0.69
Throttle parameter c_t	0.3320	0.2994
Compressor characteristic shift Δ	0.3	0

are done without the flange ($V = 2.0 \cdot 10^{-3}$ [m³]) that is placed between the compressor outlet and the blow-off valve to install the actuators. This extra volume results in a reduction of the surge frequency of approximately 2 [Hz]. In Meuleman *et al.* (1998), the area A_c is equal to the compressor outlet duct area, and for $L_c = 1.0$ [m] the plenum volume is tuned such that the Helmholtz frequency is of the order of the measured surge frequency. This results in a plenum volume equal to the volume of the compressor discharge system (*i.e.*, the duct between the compressor and the compressor blow-off valve and the blow-off duct). However, additional experiments *without* the blow-off duct show that this duct does not influence the compression system behavior during surge transients, as illustrated in Fig. 2.12. For $N = 21, 100$ [rpm] and $u_{t0} = 0.284$, the plenum pressure oscillations measured

in the system with blow-off duct have a dominant frequency of 21.1 [Hz]. Removing the blow-off

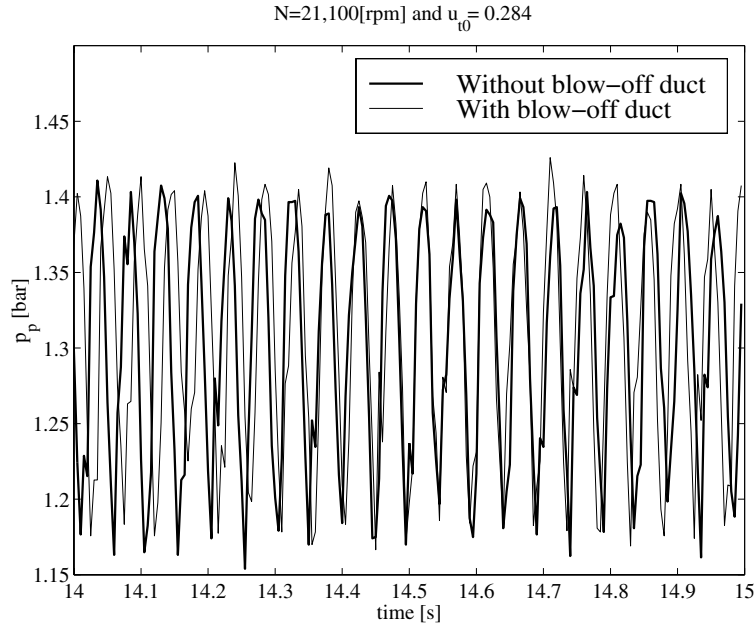


Figure 2.12: Influence of blow-off duct on compression system behavior during surge.

duct ($V = 2.94 \cdot 10^{-2}[\text{m}^3]$) leads to a 0.5 [Hz] reduction of the surge frequency. Similar results are obtained for $N = 22,600$ [rpm] and $u_{t0} = 0.295$. From these results, it is also concluded that the Helmholtz frequency is an important parameter to predict the frequency of the measured plenum pressure oscillation; as long as the product $V_p L_c$ in:

$$\omega_H = a \sqrt{\frac{A_c}{V_p L_c}}$$

is chosen appropriately, reasonable results are obtained. This is supported by the results of Case I and II in Table 2.3, which correspond to the same B and f_H values, respectively, as in Meuleman *et al.* (1998).

Chapter 3

Design of the Surge Control System

Active surge control systems consist of sensors for the detection of fluid perturbations, actuators to introduce the desired perturbations, and a controller that determines appropriate control actions from sensor information. This chapter mainly deals with the design of a control system, especially the selection of sensors and actuators, for active surge control in the compression system presented in Chapter 2. Section 3.1 discusses the active control concept. In Section 3.2, we present an overview of sensors, actuators, and controllers applied in experimental surge control studies. Section 3.3 motivates the selection of a plenum pressure sensor and a bleed valve. Specifications for this valve are derived in Section 3.4 and the valve selection is discussed in Section 3.5.

3.1 Active control of aerodynamic compressor flow instabilities

Roughly a decade ago, Epstein *et al.* (1989) posed the basic ideas for active control of aerodynamic flow instabilities, as illustrated in Fig. 3.1. They assumed that rotating stall and surge are initiated

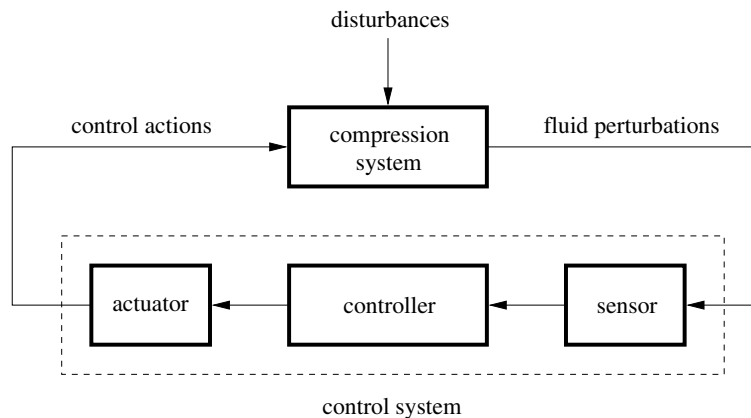


Figure 3.1: Block scheme of compression system with active control system.

by small amplitude perturbations or disturbances which move the system, being essentially unstable, from its equilibrium point. Feedback can stabilize the system, and so prevent these perturbations from initiating large perturbations or a limit cycle. If active control is based on small flow variations, low-power, small amplitude control actions are required (Epstein *et al.*, 1989; Pinsley *et al.*, 1991).

By feedback of fluid perturbations into the flow field, the compression system dynamics are modified such that the region of feasible operating points is enlarged.

3.2 Experimental active surge control systems

Applicability of active control to experimental set-ups is first demonstrated by Ffowcs Williams and Huang (1989). During the 1990s, active control evolved to a mature research field. Currently, active stall control is studied in high-speed aeroengines (Eveker *et al.*, 1998); in these transonic machines, the situation is extremely complicated due to the compressible flow in the machine and high bandwidth requirements for actuators. Table 3.1 gives an overview of the developments of active surge control in experimental set-ups. From this table, it is seen that early experimental surge control studies are done

Table 3.1: Overview of active surge control systems applied in experiments. Legend: *Type of machine* - A: axial, C: centrifugal, l: low speed, h: high speed, s: single-stage, m: multi-stage. *Control of type of instability* - S: surge, R: rotating stall.

<i>Ref.</i>	<i>Mach.</i>	<i>Inst.</i>	<i>Sensor</i>	<i>Actuator</i>	<i>Control</i>
Ff. Williams and Huang (1989)	C	S	diffuser pressure	loudspeaker	proportional feedback
Gysling <i>et al.</i> (1991)	C	S	plenum pressure	movable wall	structural feedback
Pinsley <i>et al.</i> (1991)	C	S	plenum pressure	throttle	proportional feedback
Nakagawa <i>et al.</i> (1994)	C	S	plenum pressure	suction-side valve	proportional feedback
Jungowski <i>et al.</i> (1996)	C	S	duct pressure	valve/loudspeaker	proportional feedback
DiLiberti <i>et al.</i> (1996)	C	S	plenum pressure	plenum bleed valve	proportional feedback
Billoud <i>et al.</i> (1991)	A	S	plenum pressure	loudspeaker	adaptive control
Badmus <i>et al.</i> (1995b)	As	S	plenum pressure	throttle	\mathcal{H}_∞ loop shaping
Badmus <i>et al.</i> (1996)	Al	S	inlet pressure	throttle	I/O feedb. linearization
Ffowcs Williams <i>et al.</i> (1993)	C	SR	diffuser pressure	air injector	proportional feedback
Day (1993a)	Alm	SR	hot wires	air injectors	proportional feedback
Eveker <i>et al.</i> (1998)	Ahm	SR	compr. pressure	compr. bleed valve	nonlinear control

in centrifugal compressor systems. This is reasonable since rotating stall is expected to play no role in many centrifugal machines. As a result, surge control is sufficient to significantly increase the stable operating region (Greitzer, 1998).

A review of sensors, actuators, and controllers employed in experimental surge control systems will now be presented. A scheme of a compression system with sensors and actuators proposed in the literature (also in numerical studies) is shown in Fig. 3.2.

Sensors and actuators

From Table 3.1, it is concluded that surge can be stabilized using a single actuator (often called a 1-D or axisymmetric actuator). Furthermore, a single sensor provides sufficient information to the controller. Van de Wal and Willems (1996) showed from an analysis of the linearized Greitzer model that the compression system is controllable and observable if a single actuator and sensor are used from those mentioned in Simon *et al.* (1993). Experimental results demonstrate that significant shifts can be achieved in surge point mass flow, as predicted by Epstein *et al.* (1989). For example, in Gysling *et al.* (1991), a decrease of 25% in surge point mass flow is reported, whereas Ffowcs Williams and Huang (1989) achieved approximately 20% reduction using a loudspeaker. The movable wall in Gysling

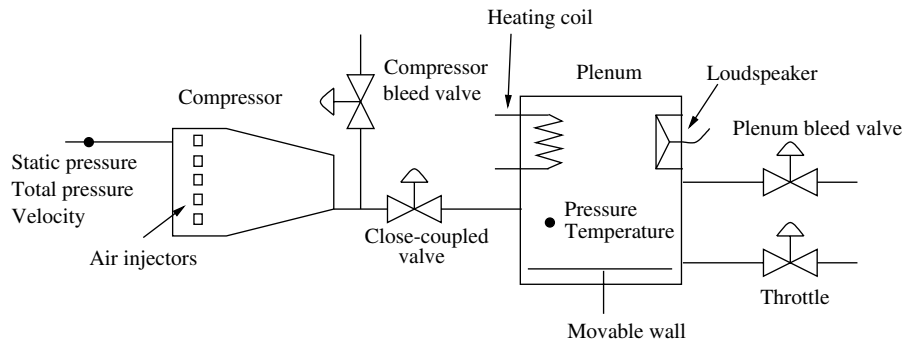


Figure 3.2: Compression system with candidate sensors and actuators.

et al. (1991) is a *passive* element; the plenum pressure oscillations are damped by dissipation of the energy in the damper attached to the movable wall. All other actuators are active (*i.e.*, these elements can absorb and supply energy).

Day (1993a) examined active control in a four-stage axial compressor using hot wires and air injectors, which are placed around the circumference at the compressor inlet (2-D sensing and actuation). In this machine, deep surge is triggered by rotating stall. By stabilizing rotating stall, surge is also suppressed and a 5% reduction in stall point mass flow is realized. A similar approach is applied in Ffowcs Williams *et al.* (1993) for a single-stage centrifugal compressor. However, the controller obtains information from pressure sensors positioned in several diffuser channels and a single air injector is used for actuation. In the examined engine, the surge point mass flow is reduced by 2.6%. Eveker *et al.* (1998) demonstrated *integrated* rotating stall and surge control on a high-speed, three-stage axial compressor. This machine exhibits rotating stall at part-speed operations and surge for high speeds. Because of the strong interaction between the two aerodynamic compressor flow instabilities, these instabilities are addressed simultaneously to increase the feasible operating region. For actuation, control valves are placed around the circumference at the compressor discharge. These valves are operated simultaneously, so this can be seen as 1-D actuation. Information about stall is determined from circumferentially distributed pressure sensors (2-D sensor) located in the compressor.

Controllers

The “first generation” of active surge controllers was based on stabilization by proportional feedback. The objectives of these controllers are to stabilize unstable operating points and to obtain a large stable operating region. The motivation for this approach is that stable compressor operation can be guaranteed as long as the perturbed system stays in the domain (region) of attraction¹ of the stabilized equilibrium point. To stabilize surge, Epstein *et al.* (1989) proposed a *complex-valued proportional feedback controller*. This controller describes the gain and phase relation between the sensed signal and control signal. The idea of complex-valued controllers originates from active rotating stall control (see Epstein *et al.* (1989)); measurements obtained from 2-D sensors are *spatially* Fourier transformed. These measurements are processed in an amplifier and phase shifter before they are applied to a 2-D actuator. Details about this approach can be found in Haynes *et al.* (1994) or Paduano *et al.* (1994). For surge control, suitable values for the gain and phase shift are determined from an analysis of the

¹Let $x = 0$ be an asymptotically stable equilibrium point. If any trajectory starting from a neighborhood Ω of the origin converges to $x = 0$, Ω is called the domain of attraction of the origin. Details can be found in, *e.g.*, Khalil (1996).

linearized Greitzer model. Application of this control scheme to experimental setups shows promising results for surge control (Ffowcs Williams and Huang, 1989; Pinsley *et al.*, 1991; Jungowski *et al.*, 1996).

The main drawback of proportional feedback is the limited operating region in which the linear controller is valid. However, Ffowcs Williams and Huang (1989) and Pinsley *et al.* (1991) have shown that stabilization is possible using proportional feedback if the surge limit cycle is contained in the domain of attraction of a nominal operating point. If the domain of attraction is too small, gain scheduling or LPV based controllers may circumvent this. Furthermore, nonlinear controllers deal with the nonlinearities directly, and they are expected to enlarge the domain of attraction of an equilibrium point. An important assumption in all studies is that both the compressor characteristic in the “surge” region and the load or throttle line are known *a priori*, so the desired operating point can be determined. For instance, in Badmus *et al.* (1995a), the control-oriented high-frequency modeling approach is used to model a generic turbojet engine and a generic compression system. But, the pressure requirements in, for example, jet engines or a natural gas compressor station generally are not known. Consequently, to stabilize these systems in a nominal operating point, (1) techniques have to be applied that do not require an equilibrium point (*e.g.*, D-action only for systems with slowly varying equilibrium points), or (2) techniques have to be developed that determine a nominal operating point *without* requiring a description of the entire system.

Limited experimental results are known of studies addressing disturbance rejection and robustness of the controlled system. Recently, a \mathcal{H}_∞ surge controller was implemented (Badmus *et al.*, 1995b) whereas Eveker *et al.* (1998) examined the robustness of their nonlinear control strategy for disturbances and variations in compressor designs.

3.3 Selection of sensors and actuators

An important issue in the process of control system design is the selection of an appropriate number, place, and type of sensors and actuators. Besides aspects like hardware expenses and system complexity, the employed set of actuators and sensors (IO-set) also affects the achievable performance of the control system. Furthermore, in aeroengines the implementation of extra sensors and actuators introduce weight penalties. Therefore, it is worthwhile to investigate which type of sensor and actuator is most suitable for surge control.

3.3.1 Results of selection methods

Simon *et al.* (1993) studied the effect of five actuators (closed-coupled valve (CCV), plenum bleed valve, air injector at compressor inlet, plenum heat addition and movable wall) and four sensors (plenum pressure, compressor mass flow, and static and total compressor inlet pressure) on system behavior. Based on an analysis of the linearized Greitzer model, the maximal stabilizable compressor slope is determined for the mentioned sensor-actuator pairs using static output feedback. A CCV or an injector as actuator, in combination with a mass flow sensor appears to be most promising. In Van de Wal *et al.* (1997, 1999), the selection method developed by Van de Wal (1998) is applied for an IO-set without air injection and heat addition. In this quantitative analysis, the performance of the closed-loop linearized system under exogenous disturbances and actuator limitations is specified using the \mathcal{H}_∞ norm of the closed-loop. This analysis indicates a mass flow sensor in combination with a CCV and movable wall as the best IO-set.

The influence of the valve position on compressor performance has been studied in Jungowski

et al. (1996) using proportional feedback. In this study, it was concluded that a CCV and a bleed valve positioned close to the compressor are effective. Both Jungowski *et al.* (1996) and Nakagawa *et al.* (1994) have shown that a valve placed on the suction side of the compressor also gives promising results. Montazeri-Gh *et al.* (1996) examined the effect of the location of compressor bleed valves in a multi-stage axial compressor on system behavior. Using full-state feedback, the performance for each actuator location is specified in terms of an energy cost criterion (LQR control). From this study, it is seen that the performance increases if the actuator is placed further downstream.

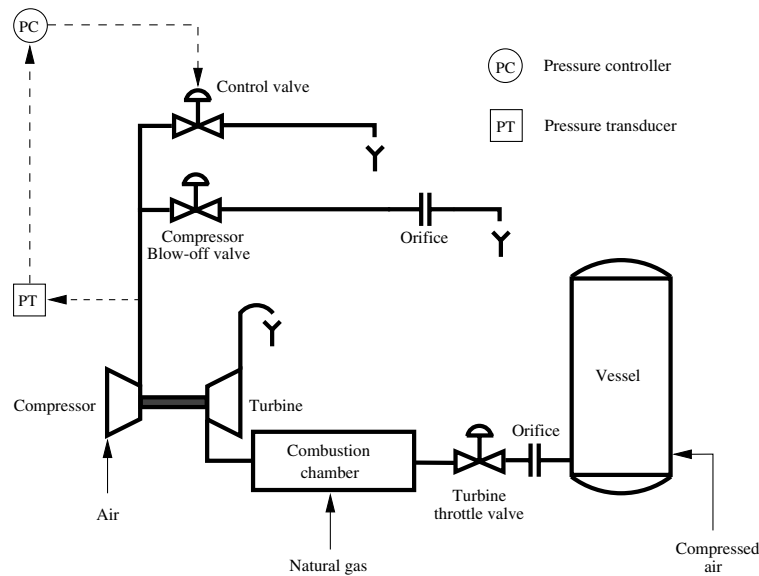


Figure 3.3: Scheme of the modified gas turbine installation.

3.3.2 Motivation of the selected sensor and actuator

In the gas turbine installation which is introduced in Chapter 2, reliable, unsteady mass flow measurements are not available. As a result, the easily measurable plenum pressure is used for surge control, so expensive mass flow sensors are not required. From the results in Simon *et al.* (1993), it is concluded that the plenum pressure sensor in combination with a plenum bleed valve is expected to give the best performance. If the bleed valve is closed in the desired equilibrium point, the overall efficiency of the compression system is expected to improve compared to studies which accept a nonzero stationary recycle flow (Botros *et al.*, 1991) or a pressure drop across a CCV (Simon and Valavani, 1991; Gravdahl and Egeland, 1997a). Simon *et al.* (1993) show that for the bleed valve and for small B values steeper compressor characteristics can be stabilized if a static or total pressure sensor is placed at the compressor inlet.

Simulations show that the compressor blow-off valve is too slow for surge control in the studied compression system. Therefore, analogous to DiLiberti *et al.* (1996), a *fast response bleed valve* is placed in parallel with the compressor blow-off valve, as shown in Fig. 3.3; the large blow-off valve represents the system's pressure requirements, *e.g.* downstream processes or losses due to resistance in the piping, whereas the control valve has to stabilize the compression system around its nominal operating point. This system is supposed to be a better representation of a real process, since in many cases the system's load is difficult to control. Nonetheless, the throttle in Pinsley *et al.* (1991) or

in Badmus *et al.* (1995b, 1996) can be interpreted as a throttle in parallel with a plenum bleed valve.

For the large plenum system ($V_p = 2.66 \text{ [m}^3\text{]}$) studied in Van de Wal *et al.* (1997), the results are poor for a plenum bleed valve. However, the compression system examined in this study has a relatively small plenum volume: $V_p = 2.03 \cdot 10^{-2} \text{ [m}^3\text{]}$. Promising results are reported for similar systems using plenum pressure measurements in combination with a fast response *throttle* for surge control (Badmus *et al.*, 1995b; Eveker *et al.*, 1998; Pinsley *et al.*, 1991).

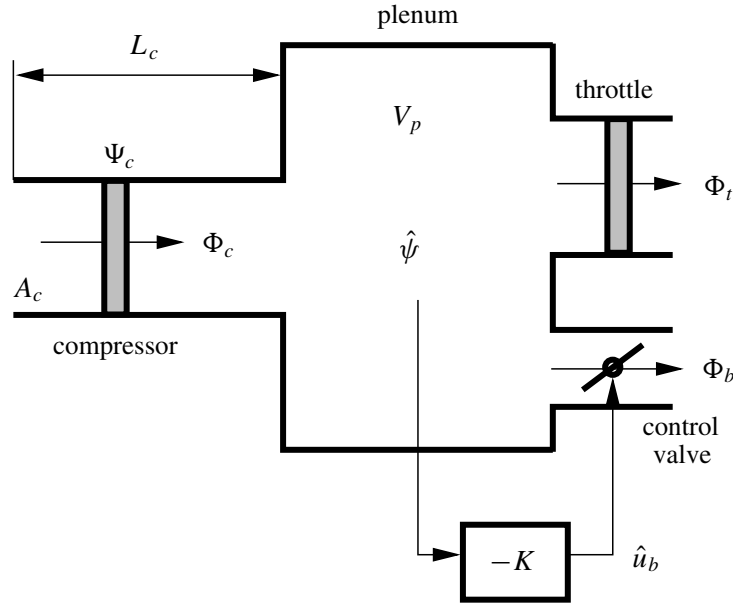


Figure 3.4: Compression system model with the proposed surge control system.

3.3.3 Compression system with surge control system

The compression system with the selected surge control system can be modeled, as shown in Fig. 3.4. For this case, the set of dimensionless equations (2.1)-(2.2) has to be modified in the following way:

$$\begin{aligned} \frac{d\phi_c}{d\tilde{t}} &= B[\Psi_c(\phi_c) - \psi] \\ \frac{d\psi}{d\tilde{t}} &= \frac{1}{B}[\phi_c - \phi_t(u_t, \psi) - \phi_b(u_b, \psi)] \end{aligned} \quad (3.1)$$

where the control valve behavior is described in a similar way as the throttle behavior:

$$\phi_b(u_b, \psi) = c_b u_b \sqrt{\psi}.$$

Linearization of (3.1) around $(\phi_{c0}, \psi_0, u_{t0}, u_{b0})$ gives:

$$\dot{\mathbf{x}} = \begin{bmatrix} \dot{\hat{\phi}}_c \\ \dot{\hat{\psi}} \end{bmatrix} = \begin{bmatrix} Bm_c & -B \\ \frac{1}{B} & -\frac{1}{Bm_{te}} \end{bmatrix} \begin{bmatrix} \hat{\phi}_c \\ \hat{\psi} \end{bmatrix} + \begin{bmatrix} 0 \\ -\frac{v}{B} \end{bmatrix} \hat{u}_b \quad (3.2)$$

The subscript 0 indicates quantities corresponding to the nominal operating point and $\hat{\cdot}$ expresses deviations from the nominal operating point. The meaning of the new variables introduced in (3.2) can be found in Table 3.2. Applying the static output feedback controller:

$$\hat{u}_b = -K\hat{\psi} \quad (3.3)$$

with $\hat{\psi} = \psi - \psi_0$, leads to the following closed-loop transfer function:

$$H_{cl}(j\tilde{\omega}) = \frac{\frac{-VK}{B}(s - Bm_c)}{s^2 + \left(\frac{1}{Bm_{te}} - Bm_c - \frac{VK}{B}\right)s + \left(1 - \frac{m_c}{m_{te}} + VKm_c\right)} \quad (3.4)$$

where $\tilde{\omega} = \frac{\omega}{\omega_H}$ is the normalized angular frequency.

For the region of interest, *i.e.* $0 \leq \phi_{c0} \leq 2F$, m_c is positive and (3.4) has a right-half plane zero, which impose fundamental limitations to the control of this *non-minimum phase* system; the bandwidth of the closed-loop system can only be increased up to frequencies equal to the magnitude of the smallest right-half plane zero. Moreover, disturbance attenuation is possible in a limited frequency range. These limitations do not occur if static pressure is measured at the compressor inlet (Simon *et al.*, 1993).

Table 3.2: Meaning of variables.

Variable	Meaning
Dimensionless slope of compressor characteristic m_c	$\left. \frac{\partial \Psi_c}{\partial \phi_c} \right _{\phi_{c0}}$
Dimensionless slope of equivalent throttle parameter m_{te}	$\left[\left. \frac{\partial(\phi_t + \phi_b)}{\partial \psi} \right _{(\psi_0, u_{t0}, u_{b0})} \right]^{-1}$
Dimensionless slope of bleed valve characteristic V	$\left. \frac{\partial \phi_b}{\partial u_b} \right _{(\psi_0, u_{b0})}$

From the Routh-Hurwitz stability criterion (for details, see, *e.g.*, Bosgra and Kwakernaak (1995)), it is seen that (3.3) can stabilize the linearized system around an equilibrium point if and only if the following condition holds:

$$m_c < \frac{1}{B} \quad (3.5)$$

The Greitzer parameter B is proportional to the rotational speed N . As a result, stabilization is more difficult for increasing N , because smaller slopes of the compressor characteristic (thus, higher mass flows ϕ_{c0}) are allowed. In the examined compression system, for $N = 18,000$ [rpm] this boils down to $\phi_{c0} > 1.65F$. Roughly speaking, the *uncontrolled* compression system is stable if $\phi_{c0} \geq 2F$. As a result, a 17.5% increase of the stable operating region is expected using static output feedback based on plenum pressure measurements and bleed valve actuation. In case of $N = 25,000$ [rpm], the linearized system can be stabilized by (3.3) for $\phi_{c0} \geq 1.87F$, which corresponds with a 6.5% increase.

The applied output feedback controller is supposed to be most limiting; other controllers are assumed to (i) stabilize the compression system in the entire unstable operating region (*e.g.*, full state feedback (Willems *et al.*, 1999) or \mathcal{H}_∞ control (Van de Wal *et al.*, 1997)), (ii) realize a larger domain of attraction, or (iii) require smaller control actions.

3.4 Control valve specification

Final step in the design of the surge control system is the specification of the required control valve *bandwidth* and *capacity* for surge stabilization in the examined compression system. This section discusses the effect of these parameters on closed-loop stability.

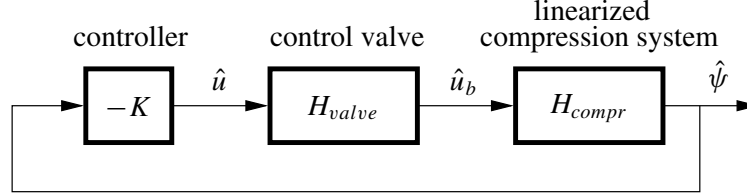


Figure 3.5: Block scheme of the linearized closed-loop system.

To study the influence of the valve dynamics on system behavior, analogous to Botros *et al.* (1991) the control valve is modeled as a second order linear system:

$$H_{valve}(j\tilde{\omega}) = \frac{\tilde{\omega}_{co}^2}{s^2 + 2\zeta\tilde{\omega}_{co}s + \tilde{\omega}_{co}^2} \quad (3.6)$$

where:

$$\tilde{\omega}_{co} = \frac{2\pi f_{co}}{\omega_H}$$

This results in the linearized closed-loop system shown in Fig. 3.5. In this system, the transfer function H_{compr} is given by:

$$H_{compr}(j\tilde{\omega}) = \frac{\frac{-V}{B}(s - Bm_c)}{s^2 + \left(\frac{1}{Bm_{te}} - Bm_c\right)s + \left(1 - \frac{m_c}{m_{te}}\right)} \quad (3.7)$$

Control valve bandwidth

To examine the influence of f_{co} on closed-loop stability, the root-locus technique is applied. In this method, the closed-loop poles λ are plotted in the complex plane for varying control gains K (*root-locus*). If all closed-loop poles are in the open complex left-half plane (LHP), *i.e.*, $\text{Real}(\lambda) < 0$, the closed-loop system is stable. More information about this technique is given, *e.g.*, in Bosgra and Kwakernaak (1995).

For varying natural valve frequencies f_{co} , closed-loop stability is studied. This is done for the maximal realizable rotational speed $N = 25,000$ [rpm] and for $\phi_{c0} = 1.9F$; according to (3.5) this case is most difficult. Moreover, for the considered speed line we are interested in the stabilizable equilibrium point with the smallest compressor mass flow. In that case, maximal extension of the stable region is realized. The results of the stability analysis are shown in Fig. 3.6. The upper figures show the root-loci for three f_{co} values and K varying between -20 and 0 . Furthermore, the open-loop poles and open-loop zero are plotted for reference. The arrows indicate the direction in which $|K|$ increases. From these figures, it can be verified that for $f_{co} = 30$ [Hz] and 40 [Hz], the closed-loop system cannot be stabilized with (3.3); for each K , the closed-loop system has poles in the

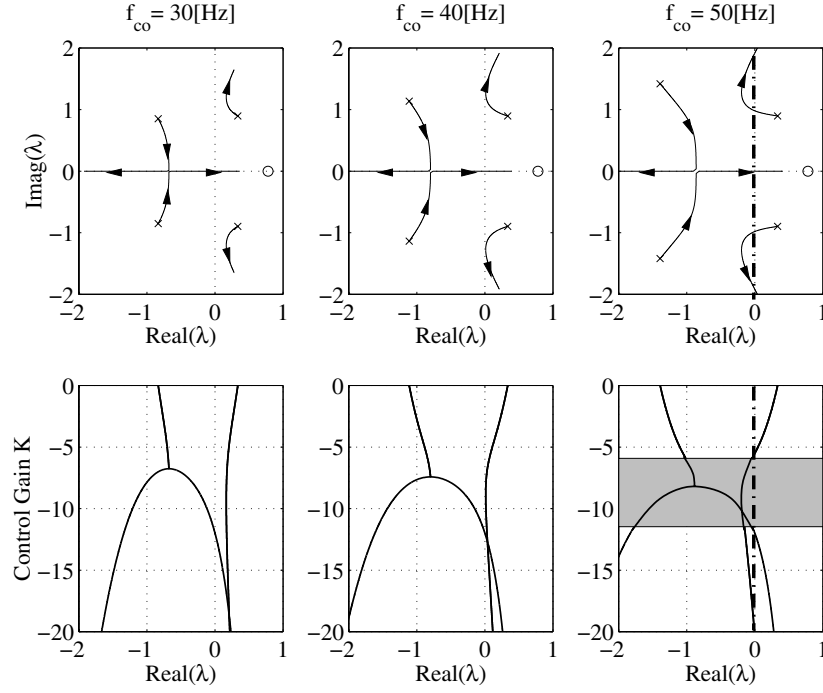


Figure 3.6: Effect of f_{co} on system stability (open-loop poles (x), open-loop zero (o), stability boundary (— ·); $N = 25,000$ [rpm], $\phi_{c0} = 1.9F$, $c_b = 0.1c_t$, $u_{b0} = 0$, and $\zeta = 0.7$).

open complex right-half plane. For $f_{co} = 50$ [Hz] the situation is more complicated. To determine the control gains K , for which all closed-loop poles are located in the LHP ($\text{Real}(\lambda) < 0$), in the lower figures the control gain K is plotted, which corresponds to the real parts of the close-loop poles shown in the upper figures. It is seen that there is a small range of K , indicated by the grey region, for which all closed-loop poles are in the LHP. For these control gains, the examined equilibrium point is stable. This case is most limiting; for larger ϕ_{c0} values, the compression system can be stabilized, e.g., for $f_{co} = 40$ [Hz]. Similar results are found for $N = 18,000$ [rpm] and $\phi_{c0} = 1.7F$. Therefore, we concluded that in the examined compression system surge stabilization requires a control valve bandwidth of $f_{co} = 50$ [Hz] if static output feedback based on plenum pressure measurements is applied.

Control valve capacity c_b

The results in Fig. 3.6 are obtained for a nominally closed control valve ($u_{b0} = 0$) and valve capacity $c_b = 0.1c_t$. For given values of ϕ_{c0} , c_b , c_t , and u_{b0} , the nominal throttle position is determined from:

$$u_{t0} = \frac{1}{c_t} \left[\frac{\phi_{c0}}{\sqrt{\psi_0}} - c_b u_{b0} \right] \quad \text{with} \quad \psi_0 = \Psi_c(\phi_{c0})$$

In that case, the root-locus does **not** depend on the chosen nominal control valve position u_{b0} since the variables m_{te} and V only depend on the nominal compressor mass flow ϕ_{c0} , nominal plenum pressure rise ψ_0 , and the control valve capacity c_b :

$$m_{te} = \frac{2\psi_0}{\phi_{c0}} \quad \text{and} \quad V = c_b \sqrt{\psi_0}$$

Furthermore, it can easily be verified that V is multiplied by K in the closed-loop transfer function (see, *e.g.*, (3.4) for the case without valve dynamics). This means that if VK is kept constant the same root-locus will be found. More precisely, for every control valve capacity c_b the linearization can be stabilized if K is chosen appropriately. However, the presented stability analysis does not deal with the constrained input $u_b \in [0, 1]$. For small c_b values, stabilization requires large control gains K , so the valve will saturate and stability can no longer be guaranteed. Hence, the required control valve capacity for surge stabilization will be determined from simulations with the nonlinear compression system model. These results are presented in Chapter 4.

3.5 Discussion

This chapter discusses the design of an active surge control system for the examined compression system. The results in Simon *et al.* (1993) and Van de Wal (1998) are used to select an appropriate sensor and actuator for surge control. Given the available equipment, a *plenum pressure sensor* in combination with a *bleed valve*, which is placed closely to the compressor, is used. The control valve bandwidth is specified using a stability analysis of the linearized compression system. From this analysis, it is seen that in the examined compression system surge stabilization requires a minimal valve bandwidth of 50 [Hz]. The required control valve capacity c_b has to be determined from simulations with the nonlinear compression system model (see Chapter 4). As the desired capacity can be realized by placing valves in parallel, an appropriate valve can already be selected, as follows.

Table 3.3: Control valve specifications.

<i>Criteria</i>	<i>Spec</i>
Valve actuator	electric
Valve bandwidth	≥ 50 [Hz]
Process medium	air
Maximal process temperature	420 [K]
Maximal pressure difference	1.5 [bar]

Smith and Vivian (1995) and Whitehouse (1993) discussed several criteria for valve selection: *e.g.*, valve actuation, process medium, and process conditions. For the studied application, the main specifications are listed in Table 3.3. Valves can be operated by hydraulic, pneumatic, and electric actuators. Hydraulic actuators can realize very high operating forces, but require an expensive hydraulic power supply system. Most important drawback of pneumatic actuation is the compressibility of air, which limits the ability to hold a specific valve position and to realize fast displacements. Consequently, valves with electric actuation will be applied. Contacted valve manufacturers did not provide any information about the bandwidth of their valves. Because of its relatively fast response time (*i.e.*, time needed to fully open a closed valve), a small proportional solenoid valve is selected. For this valve, the natural frequency of the valve mechanics based on the determined core mass m and spring stiffness k is approximately 50 [Hz]. Consequently, it meets the bandwidth specification if the control valve electronics are fast. Details about the selected valve are given in Appendix B.4.

Chapter 4

Active Surge Control

This chapter presents simulation results of the nonlinear compression system model including a detailed valve model. From these simulations, we studied the effect of the nominal control valve position on control system performance (Section 4.1). This results in a new efficient surge control strategy: *one-sided surge control*. In this strategy, the control valve is nominally closed and only opens to stabilize the system around its equilibrium point. In Section 4.2, clear design parameters are presented for the proposed bounded output feedback controller. Simulation results for this controller are discussed in Section 4.3. Furthermore, the required control valve capacity for surge stabilization is determined and stability robustness of the proposed controller is examined for uncertainties in the compressor characteristic and in the B parameter. Finally, we discuss the results in Section 4.4.

4.1 Effect of nominal control valve position

The linear stability analysis presented in Section 3.4 provides no information about the effect of the nominal control valve position u_{b0} and of the control valve capacity c_b on closed-loop stability. Here, both effects are examined from simulations with a nonlinear model. This model consists of the Greitzer compression system model and a control valve model, which accounts for the effects of the valve dynamics and valve saturation. Details about this simulation model can be found in Willems (1998).

For the specification of the control valve, stabilization of fully-developed surge is most limiting; smaller disturbances from equilibrium conditions will require smaller control actions. If $\phi_{c0} < 2F$, these disturbances ultimately result in a surge limit cycle. As a result, this case requires the *maximal* control valve capacity for surge stabilization. In practice the controller will be activated before surge is fully-developed. Only *non-persistent* disturbances (*i.e.*, disturbances with bounded energy) are considered, though persistent disturbances such as steps may also occur. The latter could be due to load changes, which are manifested as stepwise changes in the throttle characteristic ϕ_t . This results in a different equilibrium point, which can only be reached with non-zero stationary control action. But, this is inefficient and undesired. In that case, manipulation of the rotational speed seems a better solution than continuous bleed, although this may conflict with the control goal, *e.g.*, constant delivery pressure (see De Jager (1995)).

In the simulations, the *uncontrolled* system is initially disturbed from its equilibrium point (ϕ_{c0}, ψ_0) . This results in a limit cycle oscillation for $\phi_{c0} < 2F$. Then, the controller is switched on and the controlled system behavior is observed. A similar approach can be found in Pinsley *et al.* (1991) and Badmus *et al.* (1996). We consider the case associated with $\phi_{c0} = 1.9F$ and with the maximal realizable speed $N = 25,000$ [rpm]. As seen from (3.5), stabilization in this operating point is relatively

difficult to accomplish using static output feedback based on plenum pressure measurements. The compressor characteristic is obtained from extrapolation of the approximation $\Psi_c(\phi_c, N)$ presented in Appendix B.2.1. Unless stated otherwise, the modified compressor characteristic ($\Delta = 0.3$) is applied. Furthermore, the natural frequency of the selected valve is seen to be approximately $f_{co} = 50$ [Hz] and, based on information from MOOG (1999), $\zeta = 0.7$ seems a suitable value.

First, the effect of u_{b0} is investigated. For two cases, $u_{b0} = 0$ and 0.5 , the results are shown in Fig. 4.1. These simulations are performed using a control valve with a capacity of 10% of the throttle:

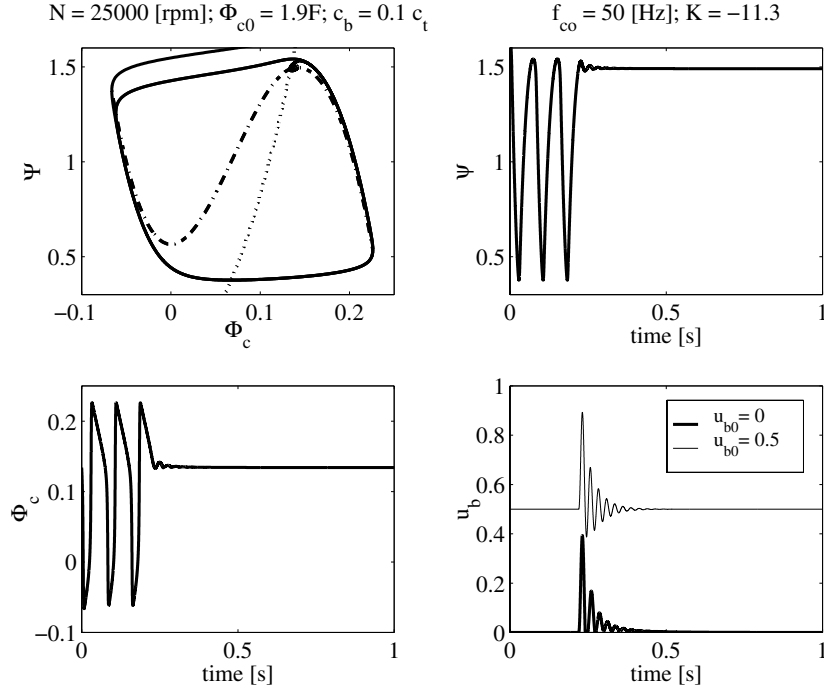
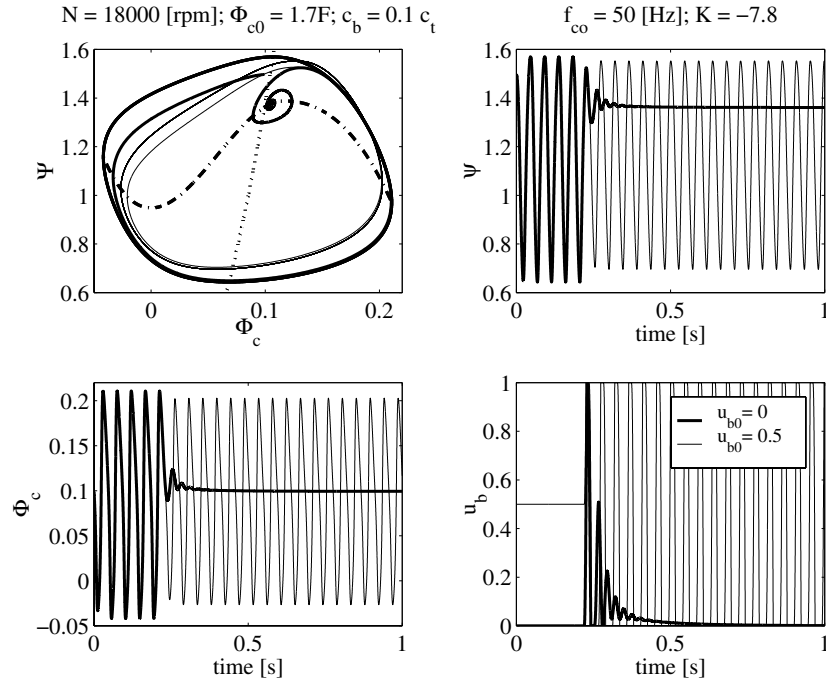


Figure 4.1: Effect of u_{b0} on system behavior ($t_s = 0.22$ [s])

$c_b = 0.1c_t$. To stabilize surge, the static output feedback (3.3) is used. The controller is activated at $t_s = 0.22$ [s]. For $u_{b0} = 0.5$, the switch on time t_s can not be chosen arbitrarily; if the controller is activated when $\hat{\psi} < 0$, the system is not stabilized. Willems (1998) showed that t_s does not affect the qualitative behavior of the controlled system for $u_{b0} = 0$. The upper left-hand plot shows the system's response in the compressor map. In this map, the dash-dotted and dotted lines are the compressor and throttle characteristic respectively, which are shown for reference. The other plots show the plenum pressure rise ψ , compressor mass flow ϕ_c , and control valve position u_b as a function of time. The latter illustrates that the desired operating point, which corresponds to u_{b0} , is finally reached. This is realized without violating the upper constraint $u_b = 1$. The effect of the control system can clearly be observed; if the controller is activated, in both cases the system exhibits a (damped) oscillation with a frequency around 40 [Hz].

In addition, the case is examined with the lowest rotational speed, for which compressor data is available. For $N = 18,000$ [rpm] and $\phi_{c0} = 1.7F$, the plenum pressure deviations $\hat{\psi}$ are relatively large (see Fig. 4.2). If $u_{b0} = 0$, the domain of attraction contains the limit cycle, so the equilibrium point is reached with zero stationary bleed valve mass flow. In case the bleed valve is opened initially ($u_{b0} = 0.5$), the amplitude of the oscillations can only be slightly decreased. From these cases, it

Figure 4.2: Effect of u_{b0} on system behavior ($t_s = 0.22$ [s]).

is concluded that opening the valve ($u_b > u_{b0}$) is effective to stabilize surge in particular; closing the valve ($u_b < u_{b0}$) has hardly any effect because the plenum pressure rise becomes significantly smaller than ψ_0 and the valve saturates immediately. The domain of attraction can be enlarged by increasing c_b . However, we aim to determine the *minimal* required control valve capacity for surge stabilization. Furthermore, for $u_{b0} = 0.5$ the stabilized equilibrium point is reached with *non-zero* stationary bleed valve mass flow. Therefore, the $u_{b0} = 0$ case will be examined in more detail. This is termed *one-sided control*, since \hat{u}_b can only become positive.

4.2 One-sided surge control

As the actual control input is bounded between 0 (closed) and 1 (fully opened), we also want to deal with input constraints in our stability analysis. So far, only results are known in case \hat{u}_b is constrained between $-a$ and b ($a, b > 0$). However, no solutions are found in the literature for $\hat{u}_b \in [0; 1]$. Chen and Kuo (1997) studied the practical stability (a definition can be found in Chen and Leitmann (1987)) of a one-sided controlled nonlinear system using a Lyapunov-based technique. For the compression system, the *sufficient* conditions for practical stability are not met (Willems, 1999). Instead, the theory, developed by Heemels and Stoorvogel (1998), of positive feedback stabilization is used. This theory is restricted to linear systems and it does not deal with the upper constraint on \hat{u}_b .

Consider a linear system:

$$\dot{x}(t) = \mathbf{A}x(t) + \mathbf{B}u(t)$$

with the *non-negative* state feedback:

$$u(t) = \max(0, \mathbf{K}x(t)) = \begin{cases} 0 & \text{if } \mathbf{K}x(t) \leq 0 \\ \mathbf{K}x(t) & \text{if } \mathbf{K}x(t) \geq 0 \end{cases} \quad (4.1)$$

The control input $u(t) \in \mathbb{R}_+^m$ is assumed to belong to the Lebesgue space of measurable, square integrable (i.e., $\int_0^\infty |u(t)|^2 dt$ is finite) functions denoted by L_2^m . Switching occurs between the *controlled mode* (linear state feedback active) and the *uncontrolled mode*. The system is said to be **positive feedback stabilizable**, if there exists a \mathbf{K} such that all solutions $x(t) \in \mathbb{R}^n$ are contained in L_2^n . Heemels and Stoorvogel (1998) state the following theorem that gives a solution to this problem if the system matrix \mathbf{A} has only one unstable complex conjugated pole pair.

Theorem *Suppose that the linear system (\mathbf{A}, \mathbf{B}) has a scalar input ($m = 1$) and \mathbf{A} has at most one pair of unstable, complex conjugated eigenvalues. The problem of positive feedback stabilization is solvable if and only if (\mathbf{A}, \mathbf{B}) is stabilizable and $\sigma(\mathbf{A}) \cap \mathbb{R}_+ = \emptyset$.*

In this formulation, $\sigma(\mathbf{A})$ denotes the set of eigenvalues of \mathbf{A} . The linear system (\mathbf{A}, \mathbf{B}) is stabilizable if and only if:

$$\text{rank}(\mathbf{A} - \lambda I, \mathbf{B}) = n \quad \text{for all } \lambda \in \mathbb{C}_+.$$

Consider the case where \mathbf{A} has one pair of complex conjugated eigenvalues with non-zero imaginary parts. There exists a nonsingular transformation \mathbf{S} and a decomposition of the new state variable $\bar{x} = \mathbf{S}x$ in $(x_1^T, x_2^T)^T$ such that the system description becomes:

$$\dot{x}_1(t) = \mathbf{A}_{11}x_1(t) + \mathbf{B}_1u(t) \quad (4.2)$$

$$\dot{x}_2(t) = \mathbf{A}_{22}x_2(t) + \mathbf{B}_2u(t) \quad (4.3)$$

with \mathbf{A}_{11} anti-stable (i.e., $-\mathbf{A}_{11}$ stable), \mathbf{A}_{22} stable, and $(\mathbf{A}_{11}, \mathbf{B}_1)$ controllable. The eigenvalues of \mathbf{A}_{11} are denoted by $\sigma_0 \pm j\omega_0$. Heemels and Stoorvogel (1998) formulate the following easily verifiable, sufficient condition:

If we can construct a feedback $u(t) = \max(0, \mathbf{K}_1x_1(t))$ (depends only on x_1) and \mathbf{K}_1 is designed such that the eigenvalues of $\mathbf{A}_{11} + \mathbf{B}_1\mathbf{K}_1$ are contained in:

$$\left\{ \lambda = \sigma + j\omega \in \mathbb{C} \mid \sigma < 0 \quad \text{and} \quad \left| \frac{\omega}{\sigma} \right| < \left| \frac{\omega_0}{\sigma_0} \right| \right\} \quad (4.4)$$

then, the resulting closed-loop system (4.2) is stable.

The relation (4.4) can be interpreted as a cone in the open complex left-half plane, as illustrated in Fig. 4.3. If the closed-loop poles are placed inside this cone, the feedback $u(t) = \max(0, \mathbf{K}_1x_1(t))$ stabilizes the system (4.2)-(4.3).

For details about the proof, the interested reader is referred to Heemels and Stoorvogel (1998) or Willems *et al.* (1999).

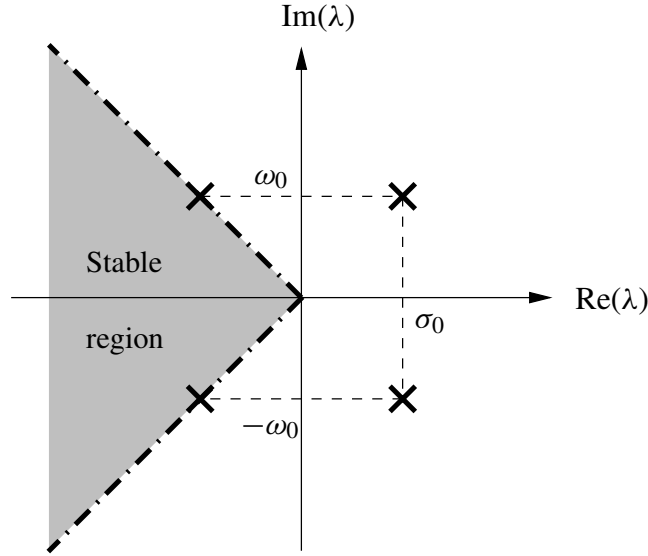


Figure 4.3: Stabilizing closed-loop poles according to (4.4).

4.2.1 Compression system without valve dynamics

Positive feedback stabilization is first examined for the constrained linearized system *without* valve dynamics:

$$\begin{bmatrix} \dot{\hat{\phi}}_c \\ \dot{\hat{\psi}} \end{bmatrix} = \begin{bmatrix} Bm_c & -B \\ \frac{1}{B} & -\frac{1}{Bm_{te}} \end{bmatrix} \begin{bmatrix} \hat{\phi}_c \\ \hat{\psi} \end{bmatrix} + \begin{bmatrix} 0 \\ -\frac{V}{B} \end{bmatrix} \hat{u}_b \quad (4.5)$$

Then, (4.3) can be ignored. It can easily be verified that the linearizations of the compression system are stabilizable in the complete unstable working range: $0 \leq \phi_{c0} < 2F$. Furthermore, the system matrix \mathbf{A} has no positive real eigenvalues for $N = 18,000$ [rpm], so the linearizations are positive feedback stabilizable in this operating region. For rotational speeds larger than $N = 19,000$ [rpm], this region decreases due to open-loop poles on the positive real axis: for instance, the linearizations for $N = 25,000$ [rpm] are positive feedback stabilizable if $1.73F < \phi_{c0} < 2.0F$.

State feedback

The poles of the resulting closed-loop system (4.2) can be arbitrarily placed within the cone (4.4) using the state feedback:

$$\hat{u}_b = \max(0, \mathbf{K}[\hat{\phi}_c, \hat{\psi}]^T). \quad (4.6)$$

Recall that the actual constraint on \hat{u}_b is more restrictive than only being positive. For sufficiently small values of $x = [\hat{\phi}_c, \hat{\psi}]^T$ the feedback satisfies the upper bound on \hat{u}_b . Hence, local stability is always guaranteed. To obtain a large domain of attraction, the amplitude of the control input has to be made as small as possible. Application of the *Kalman-Jakubovič-Popov* equality (see, *e.g.*, Bosgra and Kwakernaak (1995)) learns that for LQ-control the least control energy (L_2 -norm) is needed to stabilize the system if the closed-loop poles approach the mirror images of the “unstable” open-loop poles. Nevertheless, in that case the upper constraint on the control input may still be violated.

Another solution to overcome problems caused by the upper constraint is to increase the control valve capacity c_b .

Static output feedback

A drawback of (4.6) is that accurate measurements of $[\hat{\phi}_c, \hat{\psi}]^T$ are required. In the installation, only reliable measurements of the plenum pressure are available. One possibility is to apply an observer, as in Badmus *et al.* (1996), but this complicates the implementation. We study what can be achieved with static output feedback based on plenum pressure measurements:

$$\hat{u}_b = \max(0, \mathbf{K}\hat{\psi}). \quad (4.7)$$

Using the output equation $y(t) = \mathbf{C}x(t)$, it can easily be seen that (4.7) is a special case of (4.6):

$$\hat{u}_b = \max(0, \mathbf{K}\mathbf{C}[\hat{\phi}_c, \hat{\psi}]^T).$$

As \mathbf{K} is simply a scalar (*i.e.*, $-K$), the root-locus technique can be applied to decide if there exists control gains \mathbf{K} that places the eigenvalues of $\mathbf{A} + \mathbf{B}\mathbf{K}\mathbf{C}$ (with $\mathbf{C} = [0 \ 1]$ and \mathbf{A} , \mathbf{B} as in (4.5)) in the cone (4.4). Details about this technique can be found, *e.g.*, in Bosgra and Kwakernaak (1995). For $N = 25,000$ [rpm], the results are shown in Fig. 4.4 for three equilibrium points. In the upper plots,

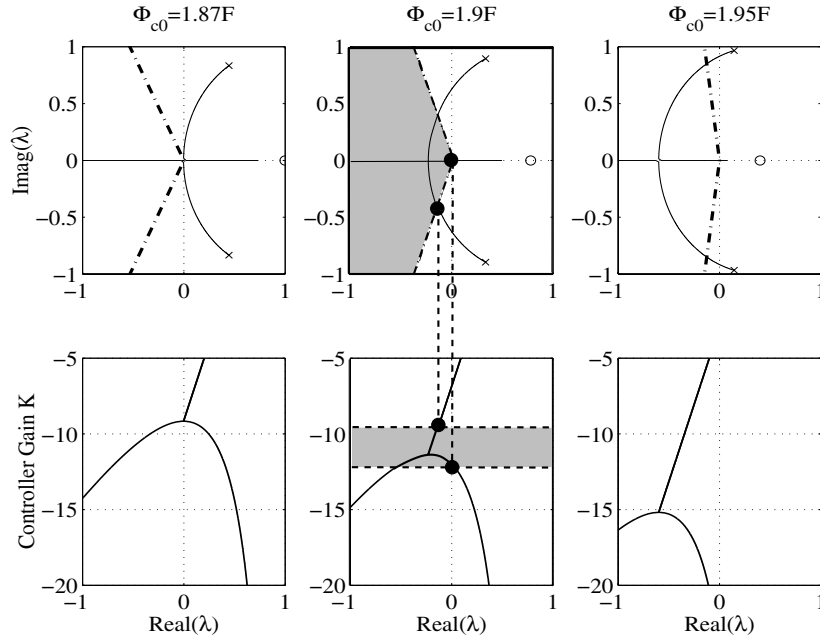


Figure 4.4: Root-loci for the static output feedback $\hat{u}_b = -K\hat{\psi}$ (cone $(-\cdot)$, open-loop poles (x), open-loop zero (o); $N = 25,000$ [rpm], $c_b = 0.1c_t$, and $u_{b0} = 0$)

the location of the closed-loop poles in the complex plane is shown for a range of control gains K . The dash-dotted lines represent the bounds of the cone (4.4). In the lower figures, control gains are shown as a function of the real parts of the closed-loop poles. Note that for small $|K|$ there is only one branch, since the system has complex conjugated eigenvalues. The upper plots illustrate that the closed-loop poles can not be placed arbitrarily using the applied output feedback; for a specific range

of control gains K , which is indicated by the grey area for $\phi_{c0} = 1.9F$, the closed-loop poles are placed inside the cone (4.4). By decreasing ϕ_{c0} , the range of stabilizing control gains K_{stab} reduces significantly and finally no K_{stab} exists. For $N = 25,000$ [rpm], the linearizations corresponding to $1.87F \leq \phi_{c0} < 2F$ can be stabilized by (4.7). Consequently, using static output feedback the operating region in which the system is positive feedback stabilizable is reduced compared to state feedback. However, compared to the unconstrained linearized compression system the positive input does not affect the stability of the controlled system, but only the range of stabilizing control gains.

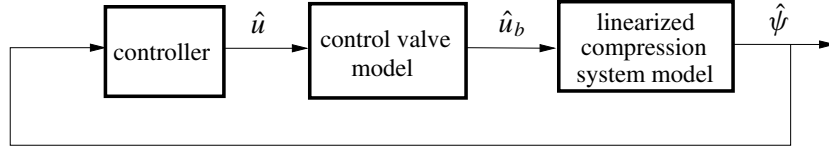


Figure 4.5: Block scheme of linearized compression system with valve dynamics.

4.2.2 Compression system with valve dynamics

To study the effect of the control valve dynamics on stability, the compression system model is extended with a second order linear valve model (see Fig. 4.5). Linearization of (3.1) and (3.6) around $(\phi_{c0}, \psi_0, \dot{u}_{b0}, u_{b0})$ results in the following state equations ($\dot{u}_{b0} = u_{b0} = 0$):

$$\begin{bmatrix} \dot{\hat{\phi}}_c \\ \dot{\hat{\psi}} \\ \dot{\hat{u}}_b \\ \dot{\hat{u}}_b \end{bmatrix} = \begin{bmatrix} Bm_c & -B & 0 & 0 \\ \frac{1}{B} & -\frac{1}{Bm_{te}} & 0 & -\frac{V}{B} \\ 0 & 0 & -2\zeta\tilde{\omega}_{co} & -\tilde{\omega}_{co}^2 \\ 0 & 0 & 1 & 0 \end{bmatrix} \begin{bmatrix} \hat{\phi}_c \\ \hat{\psi} \\ \hat{u}_b \\ \hat{u}_b \end{bmatrix} + \begin{bmatrix} 0 \\ 0 \\ \tilde{\omega}_{co}^2 \\ 0 \end{bmatrix} \hat{u} \quad (4.8)$$

Then, we can only manipulate \hat{u} instead of controlling \hat{u}_b directly. This means that we do not have a control constraint, but a *state* constraint. One possibility to tackle this more difficult problem is to implement an inverse model of the control valve dynamics. In case of exact cancellation, the system (4.8) reduces to the second order system (4.5), so the controllers discussed in Section 4.2.1 can be applied. However, two problems obstruct the real implementation of this method: (i) the cancellation is never exact and (ii) implementation of the exact inverse valve dynamics requires differentiation of measured signals, which is not reliable due to non-smoothness and noise. Therefore, the following realization is suggested:

$$\hat{u} = \frac{\tilde{\omega}_1^2}{\tilde{\omega}_{co}^2} \left(\frac{s^2 + 2\zeta'\tilde{\omega}_{co}'s + \tilde{\omega}_{co}'^2}{s^2 + 2\zeta_1\tilde{\omega}_1s + \tilde{\omega}_1^2} \right) \hat{u}^* \quad (4.9)$$

where ζ' and $\tilde{\omega}_{co}'$ are approximations of ζ and $\tilde{\omega}_{co}$ and \hat{u}^* is one of the controllers (4.6) or (4.7). If the approximation of the inverse model is accurate enough for the relevant frequencies of the system, the closed-loop behavior is expected to remain stable. This will be verified from simulations.

Note that \hat{u}_b is not necessarily non-negative, although \hat{u}^* is. However, if the control valve dynamics (3.6) are overdamped ($\zeta > 1$), the non-negativity of \hat{u} implies that \hat{u}_b is non-negative for all t . This follows from the non-negativity of the impulse response corresponding to an overdamped second order linear system and of \hat{u} .

State feedback

For (4.8), it is possible to decompose the system and to construct a state feedback:

$$\hat{u} = \max(0, \mathbf{KS}^{-1}[x_1, x_2]^T) \quad (4.10)$$

which only depends on $x_1(t)$ and places the closed-loop poles of $\mathbf{A}_{11} + \mathbf{B}_1\mathbf{K}_1$ inside the cone (4.4). In case the control valve dynamics are overdamped ($\zeta > 1$), the state constraint is met. For $\zeta \leq 1$, a realization (4.9) can be implemented with $\zeta_1 > 1$ and \hat{u}^* equal to (4.10). If the control valve dynamics are exactly canceled, (3.6) can be replaced by:

$$H'_{valve}(j\tilde{\omega}) = \frac{\tilde{\omega}_1^2}{s^2 + 2\zeta_1\tilde{\omega}_1s + \tilde{\omega}_1^2}$$

Static output feedback

The main disadvantage of (4.10) is the need for measurements of the states of the compression system and the control valve:

$$[x_1, x_2]^T = \mathbf{S} [\hat{\phi}_c, \hat{\psi}, \hat{u}_b, \hat{u}_b]^T$$

For the static output feedback:

$$\hat{u} = \max(0, \mathbf{KCS}^{-1}[x_1, x_2]^T). \quad (4.11)$$

stabilization can not be guaranteed, because \hat{u} does not necessarily depend on $x_1(t)$. However, if a realization (4.9) is used such that the control valve dynamics can be neglected, this case boils down to the static output feedback case discussed in Section 4.2.1. Alternatively, as in Badmus *et al.* (1996), state observers can be applied to determine the full state $[\hat{\phi}_c, \hat{\psi}, \hat{u}_b, \hat{u}_b]^T$ from the measured output, and then we can use (4.10).

4.3 Simulation results

Static output feedback based on the easily measurable plenum pressure measurements is interesting for practical implementation. However, stability can not be guaranteed for the constrained compression system with valve dynamics. Simulations are run with the nonlinear model discussed in Section 4.1 to investigate the possibilities of static output feedback. Furthermore, the required control valve capacity for surge stabilization is determined and stability robustness is studied. Finally, state feedback is examined, because this stabilizes the compression system down to smaller mass flows compared to static output feedback.

4.3.1 Static output feedback

By analyzing linearizations, the local behavior of the nonlinear system can be predicted. However, essentially nonlinear phenomena like, for instance, multiple isolated equilibria or limit cycles, can not be described by linear systems (Khalil, 1996; Slotine and Li, 1991). In the literature, a bifurcation analysis is frequently applied to study the stability of the nonlinear compression system, see, *e.g.*, Gu *et al.* (1999), Liaw and Abed (1992), or McCaughan (1989). Here, the results of a simulation study are presented for $N = 25,000$ [rpm] and $\phi_{c0} = 1.9F$.

Effect of control gain K

In this study, controller gains are chosen based on a stability analysis of the linearized compression system *without* valve dynamics. This seems reasonable if the valve dynamics are relatively fast. In that case, their effect on closed-loop system behavior can be neglected. This simplifies the implementation of the controller, since (4.9) is not needed. It is verified whether this approach is suitable for $f_{co} = 50$ [Hz]. For the applied static output feedback controller, three cases can be distinguished.

1. Stable equilibrium point Neglecting the control valve dynamics, the linearized compression system is seen to be positive feedback stabilizable in a limited range control gains using (4.7): $K_{stab} = [-12.0; -9.8]$. For two K -values, the system responses are shown in Fig. 4.6. In case of $K = -9.8$,

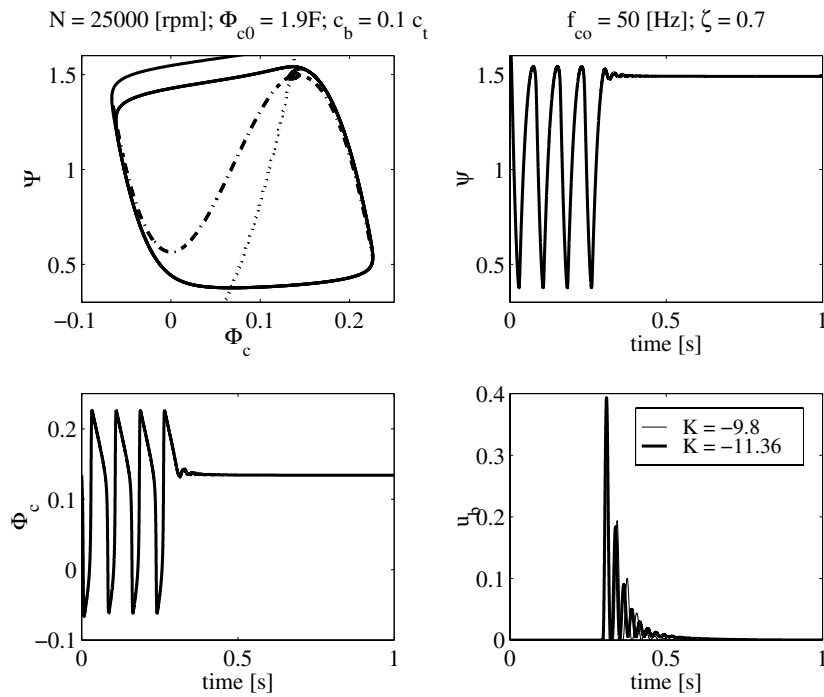


Figure 4.6: Simulation results for static output feedback.

the closed-loop poles lay just inside the cone (4.4). The control gain $K = -11.36$ is the smallest $|K|$ for which the closed-loop poles are real. The exact location of the closed-loop poles corresponding to the applied K values is given in Table 4.1. Although the valve dynamics are not dealt with in the stability analysis, the system is stabilized in the desired equilibrium point. If the closed-loop poles are complex ($K = -9.8$), the system frequently switches between the controlled and uncontrolled mode; during the uncontrolled mode the state has time to grow, so more time is needed to reach the equilibrium point. For the real closed-loop poles, we also find a damped oscillation. This can be explained from the location of the closed-loop poles of the unconstrained compression system with valve dynamics (see right column of Table 4.1); for $f_{co} = 50$ [Hz], the closed-loop poles associated with the compressor dynamics are complex.

For control gains associated with closed-loop poles outside the cone (4.4), the following cases occur.

Table 4.1: Location of the closed-loop poles of the linearized compression system.

K	<i>Closed-loop poles</i>	
	<i>without valve dynamics</i>	<i>with valve dynamics</i>
−9.8	$-0.1446 \pm j0.3832$	$-0.1811 \pm j1.4171$ $-0.2110; -1.5386$
−11.36	$-0.2139; -0.2280$	$-0.1534 \pm j1.5298$ $-0.0463; -1.7585$

2a. Limit cycle One possibility is that the closed-loop system exhibits a limit cycle oscillation, as shown in Fig. 4.7. The trajectory in the compressor map is slightly changed during the controlled

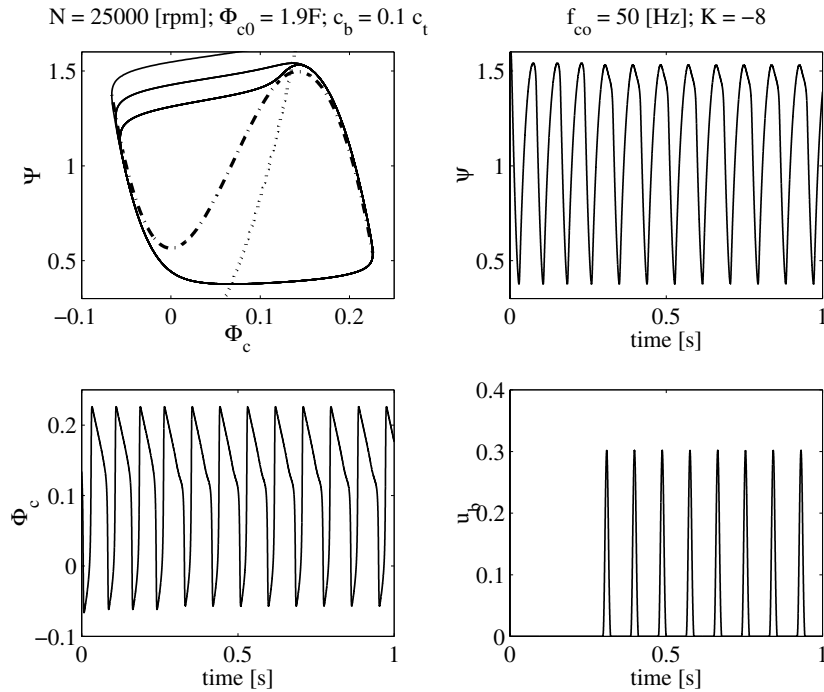


Figure 4.7: Limit cycle oscillation.

mode. However, the states grow during the uncontrolled mode such that the amplitude of the plenum pressure and compressor mass flow oscillations are hardly changed compared to the uncontrolled compression system. Note that the frequency of the oscillation is decreased when the controller is switched on. In this case, the closed-loop poles of the linearized system without valve dynamics are located outside the cone (4.4), but in the LHP.

2b. Distinct equilibrium point Alternatively, the compression system can be stabilized in an operating point with *non-zero* stationary control valve mass flow, as shown in Fig. 4.8. The upper left-hand figure shows the compressor map with the limit cycle in detail. The location of the new equilibrium point varies for different control gains; for $K = -13$ and -20 , the system is stabilized in a point

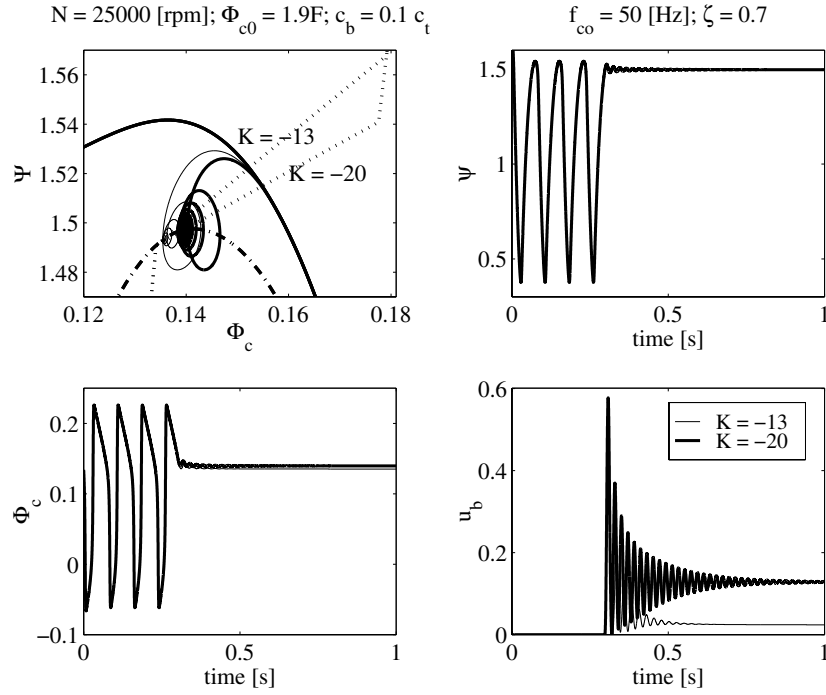


Figure 4.8: Distinct equilibrium point.

on the compressor characteristic corresponding to $\phi_c = 1.91F$ and $1.98F$, respectively. Applying these control gains, the desired equilibrium point (ϕ_{c0}, ψ_0) is unstable; in both cases, one pole of the linearized system is in the RHP.

The existence of a distinct equilibrium point can be explained from the shape of the *equivalent* throttle characteristic:

$$\phi_{te} = (c_t u_{t0} + c_b \hat{u}_b) \sqrt{\psi_0 + \hat{\psi}}$$

where \hat{u}_b is given by:

$$\begin{cases} \hat{u}_b = 0 & -K\hat{\psi} \leq 0 \\ \hat{u}_b = -K\hat{\psi} & \text{if } 0 < -K\hat{\psi} < 1 \\ \hat{u}_b = 1 & -K\hat{\psi} \geq 1 \end{cases}$$

Stationary operating points of ϕ_{te} are indicated by the dotted lines in the upper left-hand plot of Fig. 4.8. Increasing $|K|$ results in a decreased slope of ϕ_{te} for $\hat{u}_b \in [0; 1]$. Consequently, the new equilibrium point moves towards higher mass flows and can even be shifted to the right of the surge line ($\phi_c > 2F$). In that case, effectively we perform surge avoidance.

Effect of control valve capacity c_b

For fully-developed surge, the control valve capacity c_b is determined, which is required to stabilize the compression system using the proposed output feedback. Simulations for $N = 25,000 \text{ [rpm]}$ and $\phi_{c0} = 1.9F$ show that surge stabilization can be realized with a valve capacity of $c_b = 0.04c_t$ (see

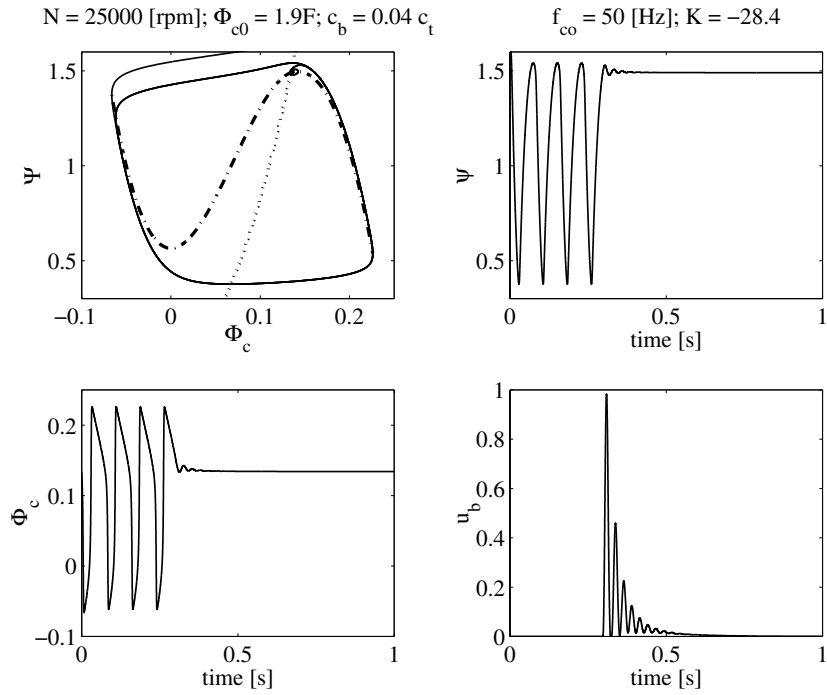
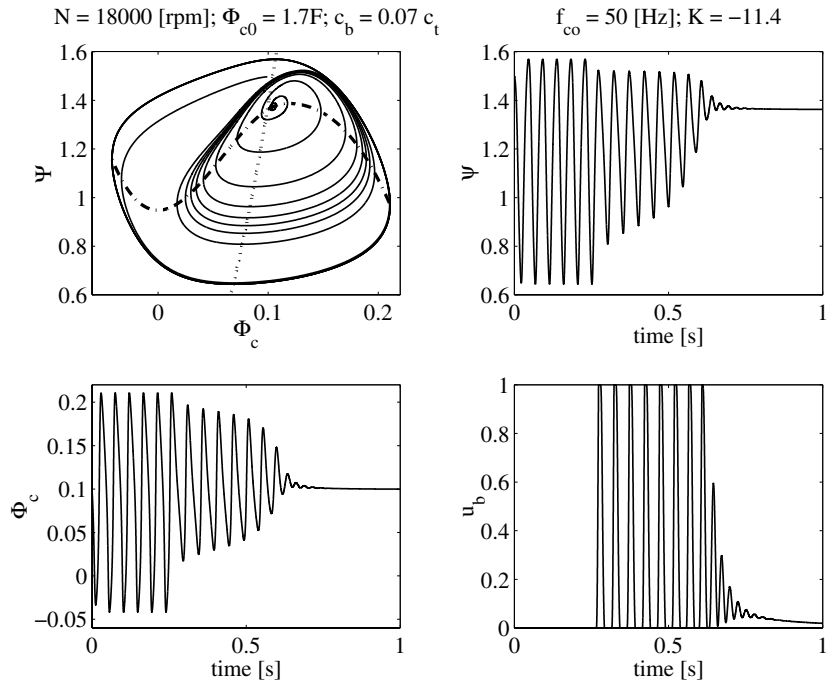
Figure 4.9: Simulation result for $c_b = 0.04c_t$.

Figure 4.10: Maximal extension of examined operating region.

Fig. 4.9). As the equilibrium point is close to the top of the compressor characteristic, a relatively small domain of attraction is needed. Therefore, stabilization is expected to be relatively simple.

We are also interested in the maximal reduction of the surge point mass flow in the examined operating region, 18,000-25,000 [rpm], using (4.7); for $N = 18,000$ [rpm], the system can be stabilized down to $\phi_{c0} = 1.7F$ (as shown in Fig. 4.10). This requires a capacity of $c_b = 0.07c_t$. For smaller capacities, the compression system can be stabilized in a smaller operating region; *e.g.*, for $N = 18,000$ [rpm] and $c_b = 0.06c_t$ stabilization from surge is possible down to $\phi_{c0} = 1.75F$.

In conclusion, a control valve with a capacity of $c_b = 0.07c_t$ will be used in the experiments. Recall from Section 3.3.3 that the uncontrolled compression system is stable if $\phi_{c0} \geq 2F$. As a result, for the bounded static output feedback controller the surge point mass flow is reduced by 15% for $N = 18,000$ [rpm] and by 5% for $N = 25,000$ [rpm].

Stability robustness

An important aspect of a controller is its robustness for uncertainties in the system. The applied controller is designed based on the Greitzer model. However, in this model the compressor characteristic $\Psi_c(\phi_c)$ is uncertain for $\phi_c < \phi_{surge}$ and the B parameter is identified using plenum pressure measurements. In this study, the effect of uncertainties in the compressor slope m_c and in B on the stability of the constrained system without valve dynamics is investigated. This is done by varying both parameters by 10%. For three m_c -values, the results are shown in Fig. 4.11. From these figures, it is

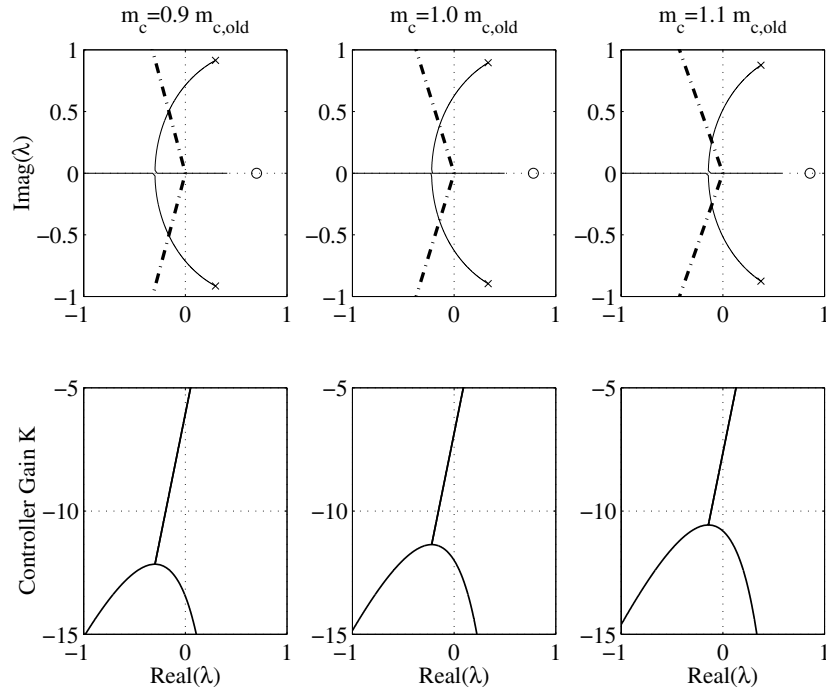


Figure 4.11: Effect of uncertainty in m_c on system stability (cone (---), open-loop poles (x), open-loop zeros (o); $N = 25,000$ [rpm], $\phi_{c0} = 1.9F$, and $u_{b0} = 0$).

concluded that it is better to overestimate m_c ; for $m_c = 1.1m_{c,old}$ each stabilizing control gain K_{stab} will also stabilize the compression system for smaller m_c values. In case of $m_c = 0.9m_{c,old}$, the region

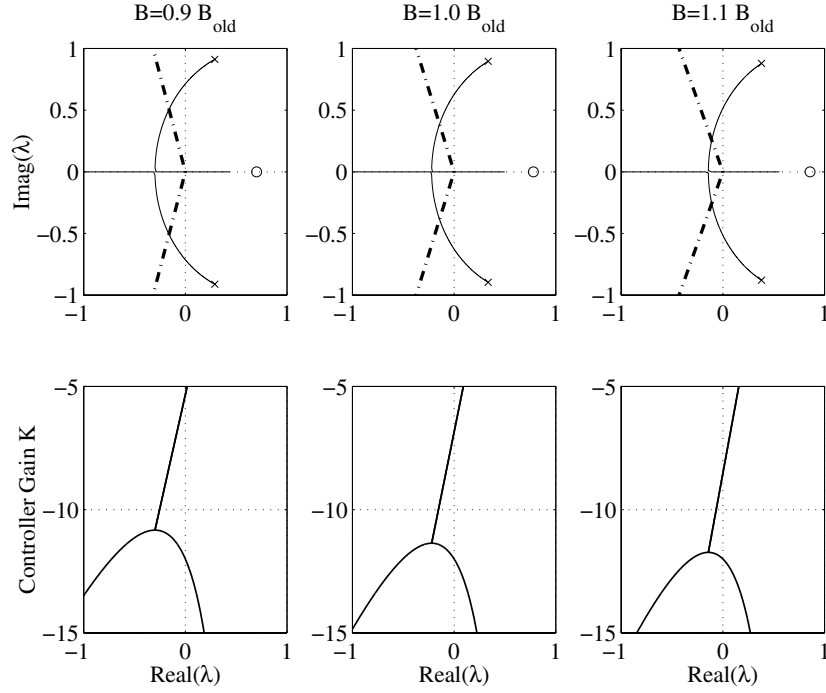


Figure 4.12: Effect of uncertainty in B on system stability (cone (---), open-loop poles (x), open-loop zeros (o); $N = 25,000$ [rpm], $\phi_{c0} = 1.9F$, and $u_{b0} = 0$).

of stabilizing control gains is largest, so the stabilized compression system can become unstable if m_c is increased. A similar trend is observed for uncertainties in B (see Fig. 4.12). For $m_c > 1.29m_{c,old}$ and $B > 1.29B_{old}$ the linearized system becomes unstable. Note that the range of acceptable parameter variations is identical for both B and m_c . This can be explained from the stability condition (3.5): $m_c < \frac{1}{B}$. The linearization corresponding to $N = 18,000$ [rpm] and $\phi_{c0} = 1.7F$ is stable for $m_c \leq 1.16m_{c,old}$ and $B \leq 1.16B_{old}$.

In conclusion, the robustness of the applied static output feedback controller for uncertainties in m_c and B is moderate; for $N = 18,000$ [rpm] and $\phi_{c0} = 1.7F$, variations larger than 16% destabilize the system. Therefore, it will not be easy to stabilize the compression system in practice.

4.3.2 State feedback

From Section 4.2, it is seen that static output feedback places fundamental constraints on the stabilizable operating region. These limits can be removed by applying state feedback. In that case, stability can be guaranteed for the compression system with valve dynamics if the resulting valve dynamics are overdamped: $\zeta_1 > 1.0$. In the studied case, $\zeta = 0.7$. Consequently, the valve dynamics are compensated using (4.9) with $\tilde{\omega}'_{co} = \tilde{\omega}_{co}$, $\zeta' = \zeta$, $\tilde{\omega}_1 = \frac{2\pi 10^3}{\omega_H}$, and $\zeta_1 = 1.1$. As shown in Fig. 4.13, for $N = 25,000$ [rpm] the system can be stabilized down to $\phi_{c0} = 1.78F$ (compared to $1.87F$ for static output feedback). It is noted that the surge line can even be shifted to smaller mass flows if c_b is increased. Furthermore, it is seen that the valve dynamics make the closed-loop system unstable; surge is experienced if we do not compensate for the valve dynamics. Additional simulations show that the nonlinear system is robust for non-exact cancellation: for $0.85\tilde{\omega}_{co} \leq \tilde{\omega}'_{co} \leq 1.2\tilde{\omega}_{co}$, surge is

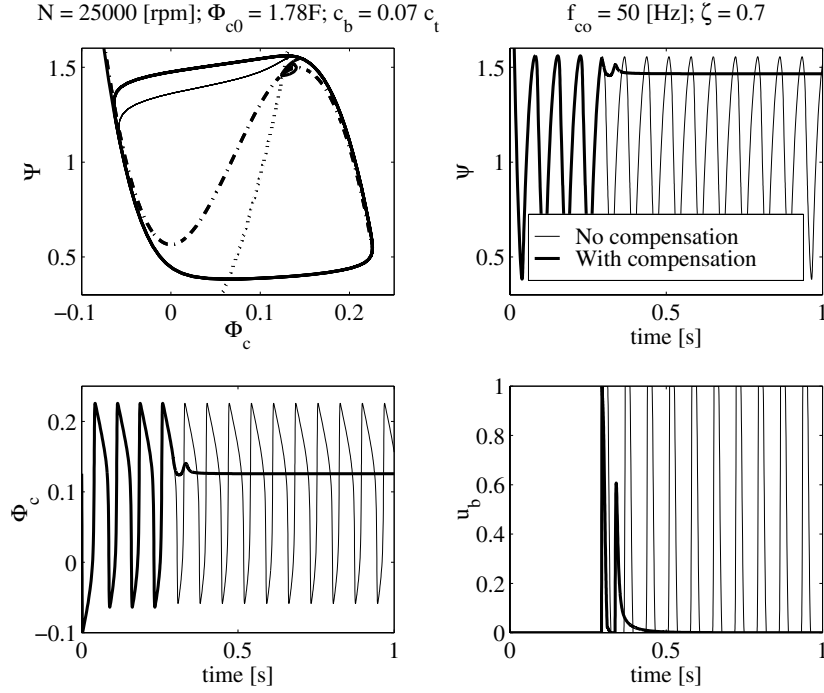


Figure 4.13: Simulation results for state feedback (Closed-loop poles: $\lambda_1 = -2.0$ and $\lambda_2 = -0.1$).

still stabilized.

Furthermore, the effect of the pole location on closed-loop system behavior is examined. For two cases, the results are shown in Fig. 4.14. For the real poles (Case I), the system stays in the controlled mode and reaches the desired equilibrium within one cycle. In Case II, the closed-loop poles are placed closely to the mirror images of the open-loop poles. From LQ-control, we know that in this case the energy of \hat{u}_b is minimized, so \hat{u}_b is kept as small as possible. Note that this can only be guaranteed for the controlled mode. The system frequently operates in the uncontrolled mode. During this period, the state has time to grow, so overall the energy is not minimized and the response is slower than in Case I. From these results, it is concluded that the fastest response will be obtained if the closed-loop poles are real. Additional simulations show that if the real closed-loop poles are shifted further to $-\infty$ the upper constraint is limiting and the system becomes unstable.

4.4 Discussion

Simulation results of a nonlinear model are presented. In this model, the effects of valve dynamics and valve saturation are included. To stabilize surge, we propose a bounded static output feedback controller based on plenum pressure measurements. Using this controller, the stabilized equilibrium point is reached with zero stationary control valve mass flow if disturbances are absent. This is beneficial for the overall efficiency of the compression system. From simulations, it is seen that for $N = 18,000$ [rpm] the surge point mass flow can be reduced by 15% in the examined operating region. This requires a control valve capacity of $c_b = 0.07c_t$, which can be realized by placing 15 selected control valves in parallel (see Appendix B.4).

The stability of the constrained compression system is examined using the theory of positive

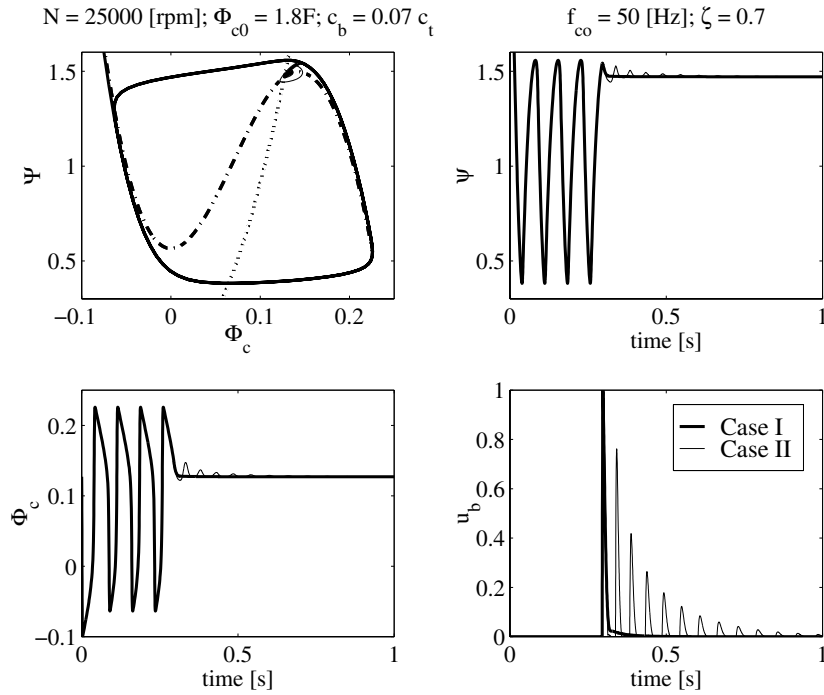


Figure 4.14: Effect of pole-placement for state feedback (Open-loop poles: $\lambda_{open-loop} = 0.6859 \pm j0.6128$; Case I: $\lambda_1 = -2.0$; $\lambda_2 = -0.1$; Case II: $\lambda_{KJP} = -0.6959 \pm j0.6128$).

feedback stabilization (Heemels and Stoorvogel, 1998). This linear theory can not deal with the upper constraint on the control input, so only *local* stability can be guaranteed. For the system *without* valve dynamics, stabilization is possible in a limited region using static output feedback based on plenum pressure measurements; *e.g.*, for $N = 25,000$ [rpm] the controlled system can be stabilized in the region $1.87F \leq \phi_{c0} \leq 2F$. The stable region can be further increased by applying full-state feedback. Then, information about the full state is required, but in practice these measurements are often not available. This problem can be overcome by applying an observer, as in Badmus *et al.* (1996). Control system performance can also be improved by using a dynamic output feedback controller.

The situation for the compression system *with* valve dynamics is more complicated, because we have a *state* constraint instead of a control constraint. In that case, stabilization of the constrained compression system can not be guaranteed for static output feedback. However, simulations with the nonlinear compression system show that surge stabilization is possible in case the controller design is based on a stability analysis of the compression system without valve dynamics.

Main drawback of the proposed nonlinear controller is that it is applicable in a limited operating region of the nonlinear compression system; the linearization varies for different nominal operating points. Gain scheduling can circumvent this design problem. Alternatively, the use of LPV based controllers can be investigated. It would also be useful to estimate the domain of attraction of the examined equilibrium. Then, it can be verified if the domain of attraction contains the limit cycle. In this case, the theory developed by Smirnov (1996) seems a useful starting point. Furthermore, a bifurcation type of analysis, just like in Eveker *et al.* (1998), can be performed.

Chapter 5

Experimental Results

Surge stabilization using the proposed static output feedback is experimentally investigated in the examined compression system. In Section 5.1 the valve model is validated for the selected control valve and the open-loop behavior of the compression system with control valves is examined. The stabilization of fully-developed surge and the possible extension of the stable operating region is studied in Section 5.2. These experimental results are compared with simulation results. Finally, the compression system model and the practical limitations of the applied control strategy are discussed (Section 5.3).

5.1 Open-loop behavior

5.1.1 Control valve model

Before presenting experimental results of the compression system with control valves, the dynamic behavior of the selected control valve is discussed. In Willems (1999), it is shown that the applied solenoid valves can be modeled as in Fig. 5.1. In this model, the control valve electronics convert the dimensionless control valve input

$$u = \frac{Y_b}{Y_{b,max}}$$

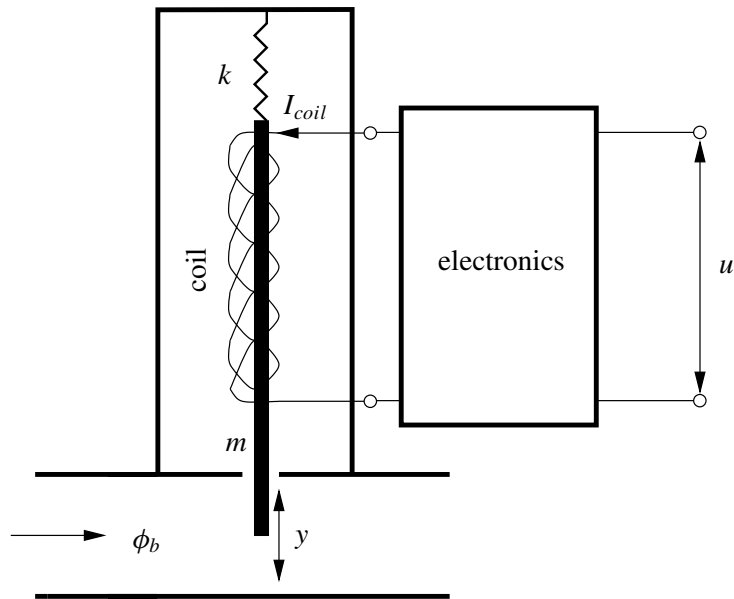
into a coil current I_{coil} . In this relation, Y_b is the actual control valve input (in [V]) and $Y_{b,max} = 10$ [V]. The coil generates a Lorentz force which excites the core mass m . This results in a dimensionless core displacement y . A nonlinear flow curve describes the relation between y and u_b , which is a measure for the opening area of the valve. The dimensionless control valve mass flow ϕ_b is given by the relation

$$\phi_b = c_b u_b \sqrt{\psi}$$

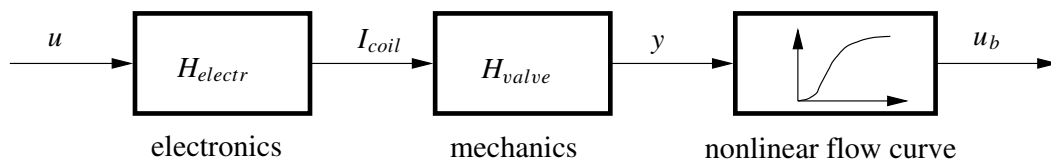
with control valve capacity c_b and dimensionless pressure difference ψ across the valve.

The nonlinear flow curve is determined from stationary measurements (see Section 5.1.3). In addition, *sine sweeps* are performed to estimate the transfer functions $H_{electr}(j\tilde{\omega})$ and $H_{valve}(j\tilde{\omega})$. Measurements of the control valve input u and the coil current I_{coil} show that the control valve electronics is relatively slow; the transfer function $H_{electr}(j\tilde{\omega})$ can be described by (Willems, 1999):

$$H_{electr}(j\tilde{\omega}) = \left(\frac{\tilde{\omega}_2^4}{\tilde{\omega}_1^2} \right) \cdot \frac{s^2 + 2\zeta_1\tilde{\omega}_1s + \tilde{\omega}_1^2}{(s^2 + 2\zeta_2\tilde{\omega}_2s + \tilde{\omega}_2^2)^2} \quad (5.1)$$



(a) Scheme of applied solenoid valve.



(b) Block scheme of dimensionless control valve model.

Figure 5.1: Dimensionless control valve model.

with $\tilde{\omega}_1 = \frac{2\pi 8}{\omega_H}$, $\tilde{\omega}_2 = \frac{2\pi 23}{\omega_H}$, $\zeta_1 = 0.7$, and $\zeta_2 = 0.6$. In other words, the control valve electronics has *break frequencies* $f_1 = 8$ [Hz] and $f_2 = 23$ [Hz]. To describe the valve mechanics, a second order model is used:

$$H_{valve}(j\tilde{\omega}) = \frac{\tilde{\omega}_{co}^2}{s^2 + 2\zeta\tilde{\omega}_{co}s + \tilde{\omega}_{co}^2} \quad (5.2)$$

with $\tilde{\omega}_{co} = \frac{2\pi 50}{\omega_H}$ and $\zeta = 0.6$. The undamped natural frequency $f_{co} = 50$ [Hz] is in agreement with the natural frequency based on the determined core mass m and spring stiffness k :

$$f_{co} = \frac{1}{2\pi} \sqrt{\frac{k}{m}} = 52.6 \text{ [Hz]}.$$

The dynamic behavior of the control valve is illustrated in Fig. 5.2. These results are obtained for a control valve mass flow of $3.4 \cdot 10^{-3}$ [kg/s]. This figure shows the transfer function between u and

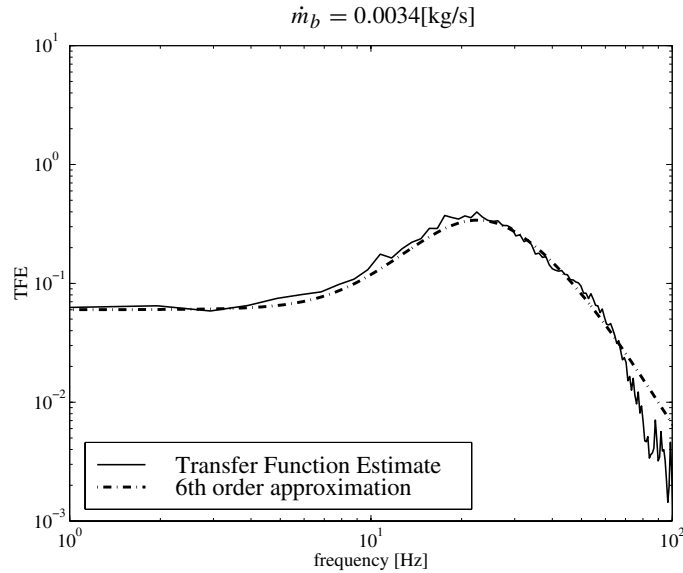


Figure 5.2: Measured and approximated valve dynamics ($u_0 = 0.5$).

$\sqrt{\frac{1}{\psi}}$. The valve dynamics is approximated by:

$$H_{dyn}(j\tilde{\omega}) = H_{electr}(j\tilde{\omega}) \cdot H_{valve}(j\tilde{\omega}).$$

It is concluded that the dynamic valve behavior is reasonably described up to 70 [Hz]. Further details can be found in Willems (1999). From a stability analysis of the unconstrained linearized compression system, it is seen that the valve electronics makes the closed-loop system unstable. This will be verified from experiments.

For active surge control, the integrated effect of all control valves on compression system behavior is of particular interest. The total capacity and the flow curve of the installed control valves are determined from stationary measurements. Furthermore, the dynamics of all control valves is studied from frequency response measurements.

5.1.2 Control valve capacity c_b

Recall from Section 4.3 that a control valve capacity of $c_b = 0.07c_t$ is required for surge stabilization in the examined equilibrium points. The following procedure is used to determine the total capacity of the 15 installed control valves. Initially, the compression system is operated in an operating point (ψ_1, N_1) far from the surge line with fully-opened control valves (Stage 1). The corresponding dimensionless compressor mass flow is supposed to be given by:

$$\phi_{c1} = [c_t u_{t1} + c_b u_{b1}] \sqrt{\psi_1} \quad (5.3)$$

Next, the fully-opened control valves are closed. This results in an increase of the plenum pressure rise ψ and the compressor will accelerate because the power delivered by the turbine is kept constant. By further opening the throttle valve, the operating point is moved until the initial stationary operating conditions are reached again (Stage 2). In that case, $\psi_2 = \psi_1$ and $\phi_{c2} = \phi_{c1}$, so the total control valve capacity can be determined from:

$$c_b = \frac{u_{t2} - u_{t1}}{u_{b1} - u_{b2}} c_t$$

with $u_{b1} - u_{b2} = 1$. Precise results are hampered by hysteresis in the throttle valve and inaccuracies associated with the exact realization of (ψ_1, N_1) in Stage 2. For these experiments, the determined control valve capacity c_b ranges from $c_b = 0.051c_t$ to $c_b = 0.066c_t$. In this chapter, $c_b = 0.06c_t$ will be used in simulations.

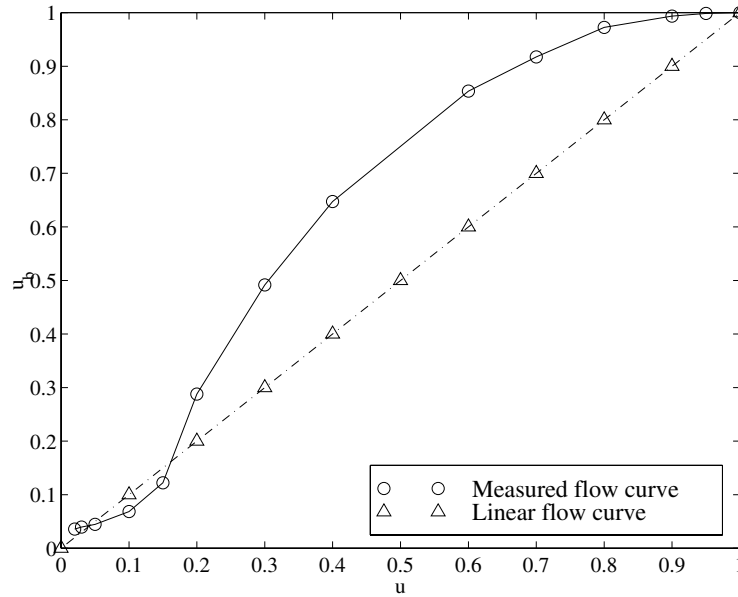


Figure 5.3: Measured nonlinear flow curve ($\psi = \text{constant}$).

5.1.3 Nonlinear flow curve

For each control valve, the dimensionless control valve input u and the control valve mass flow are varied for a constant pressure drop across the valve. These stationary measurements lead to a combined *flow curve* (see Fig. 5.3); for a specific u , the sum of the mass flows measured for the individual

control valves is determined. This flow curve shows

$$u_b = \frac{\phi_b}{\phi_{b,max}}$$

as a function of the dimensionless control valve input u . Willems (1998) demonstrated that a nonlinear flow curve can degrade the performance of the control system. Although each valve is equipped with a control unit to adjust the shape of the individual flow curve, we did not succeed in linearizing the combined flow curve.

By applying slowly varying control inputs u , the compression system is supposed to behave quasi-stationary, so the effect of the valve dynamics $H_{dyn}(j\tilde{\omega})$ can be ignored. Moreover, the effect of the nonlinear flow curve on compression system behavior will be most prone for large amplitude control valve inputs. Therefore, experiments are done for $u = 0.5 + 0.45 \sin(2\pi t)$. This results in a plenum pressure oscillation, which is shown in Fig. 5.4. The measurements are filtered with a low-

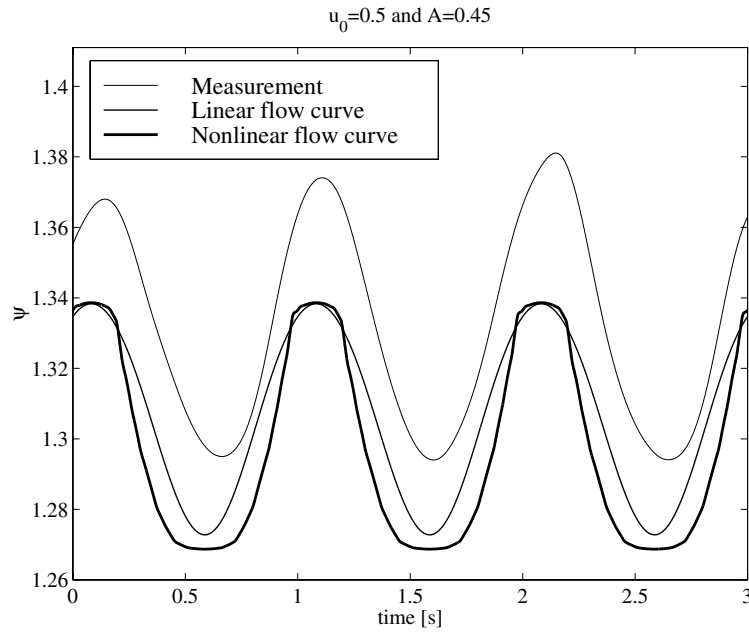


Figure 5.4: Effect of flow curve on frequency response (*Experiment*: $N = 18, 200$ [rpm], $u_{t0} = 0.399$; *Simulation*: $N = 18, 200$ [rpm], $\phi_{c0} = 2.62F$, $u_{t0} = 0.399$).

pass Butterworth filter. In the filtered plenum pressure signal, the excitation frequency, $f = 1$ [Hz], can clearly be observed. Experimental results are compared with the results of the Greitzer compression system model without valve dynamics. In this model, the effect of the flow curve is included. Comparison of the simulation results learns that the measured nonlinear flow curve modifies the shape of the plenum pressure oscillations; application of the linear flow curve leads to sinusoidal plenum pressure variations. For the nonlinear flow curve, on the other hand, the control valve is opened more than 80% if $u > 0.6$, so ψ is small over a relatively larger period of time. Furthermore, in this case ψ variations are faster, since the nonlinear flow curve is steeper between $u = 0.15$ and 0.6 than the linear flow curve. The response for the nonlinear flow curve is seen to show reasonable agreement with the measured plenum pressure oscillation. However, in both cases the nominal plenum pressure

rise is predicted too small. Additional simulations show that these differences can be explained from inaccuracies in the predicted nominal operating point (ϕ_{c0}, ψ_0) .

5.1.4 Frequency response measurements

To study the dynamic behavior of the installed control valves, frequency response measurements are performed on the gas turbine installation. More precisely, the compression system is excited with the input:

$$u(t) = A \sin(2\pi ft)$$

around a nominal operating point (N, u_{t0}, u_0) . Accordingly, the plenum pressure variations ψ are observed for different excitation frequencies f . Simulations are done with the Greitzer compression system model. Analogous to Chapter 4, the effect of the control valve dynamics and valve saturation is included in the nonlinear simulation model (see Fig. 5.5). Moreover, the measured nonlinear flow

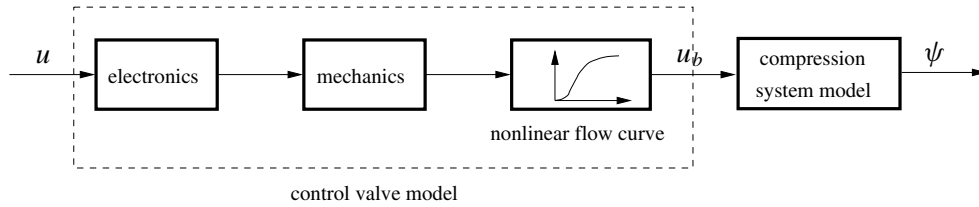


Figure 5.5: Simulation model for frequency responses.

curve is applied. The nominal throttle position u_{t0} , the rotational speed N , and the control valve input $u(t)$ from the experiments are the inputs for the simulation model.

For a nominal operating point corresponding to $N = 18,000$ [rpm], $u_{t0} = 0.506$, and $u_0 = 0.3$, experimental and simulation results are given in Fig. 5.6. This figure shows the frequency responses for four excitation frequencies. As the measured plenum pressure signal is noisy, these measurements are filtered with a low-pass Butterworth filter. In the simulations, first the control valve is supposed to have ideal electronics: $H_{electr} = 1$. For $f = 1$ [Hz], the simulation result is in reasonable agreement with the measurement. In the other cases, the amplitude of ψ is seen to be underestimated considerably. Furthermore, the nominal plenum pressure rise ψ_0 is predicted 0.04 too small in the examined cases. From additional simulations, it is seen that the predicted nominal plenum pressure rise ψ_0 is strongly influenced by the computed nominal operating point corresponding to the measured u_{t0} , u_0 and N . Due to inaccuracies in the approximated compressor, throttle, and control valve characteristics, the nominal operating point (ϕ_{c0}, ψ_0) of the compressor system is not exactly predicted. Inaccuracies are felt severely if the compressor slope is steep.

For $f = 10$ and 20 [Hz], the prediction capability of the applied model is studied from the power spectral density estimates of the measured and predicted plenum pressure oscillations ψ . As seen from Fig. 5.7, nonlinearities are not captured very well by the simulation model. For $f = 10$ [Hz], the excitation frequency is seen to be accurately approximated. But, the higher harmonics associated with 16.6 and 22.0 [Hz] also have an important contribution in the measured ψ . These phenomena can not be described by the applied compression system model. If the system is excited with $f = 20$ [Hz], the amplitude of the measured plenum pressure oscillations is slowly varying with a frequency of approximately 2 [Hz], as illustrated in the lower left-hand figure of Fig. 5.6. This *beating* appears for

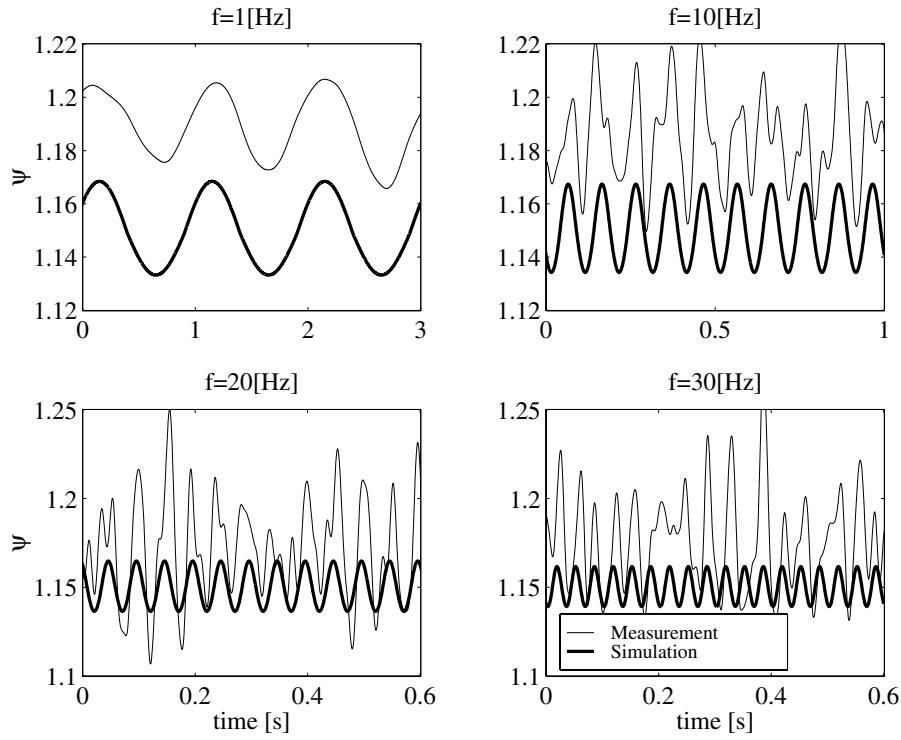


Figure 5.6: Frequency responses ($N = 18,000$ [rpm], $u_{t0} = 0.506$, $u_0 = 0.3$ and $A = 0.1$; *Simulation*: valve dynamics: $f_{co} = 50$ [Hz] and $\zeta = 0.6$).

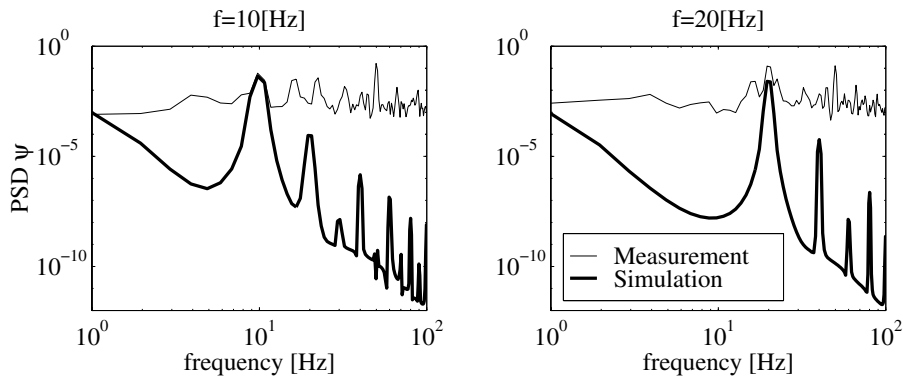


Figure 5.7: Power spectrum ($N = 18,000$ [rpm], $u_{t0} = 0.506$, $u_0 = 0.3$ and $A = 0.1$; *Simulation*: valve dynamics: $f_{co} = 50$ [Hz] and $\zeta = 0.6$).

a combination of two sinusoidal signals which have nearly the same frequency; in this case, $f = 16.1$ and 20.0 [Hz]. However, in the model only a peak at $f = 20.0$ [Hz] is found.

Extension of the simulation model with the valve electronics (5.1) significantly improves the prediction accuracy of the amplitude of ψ (see Fig. 5.8). The control valve electronics amplify

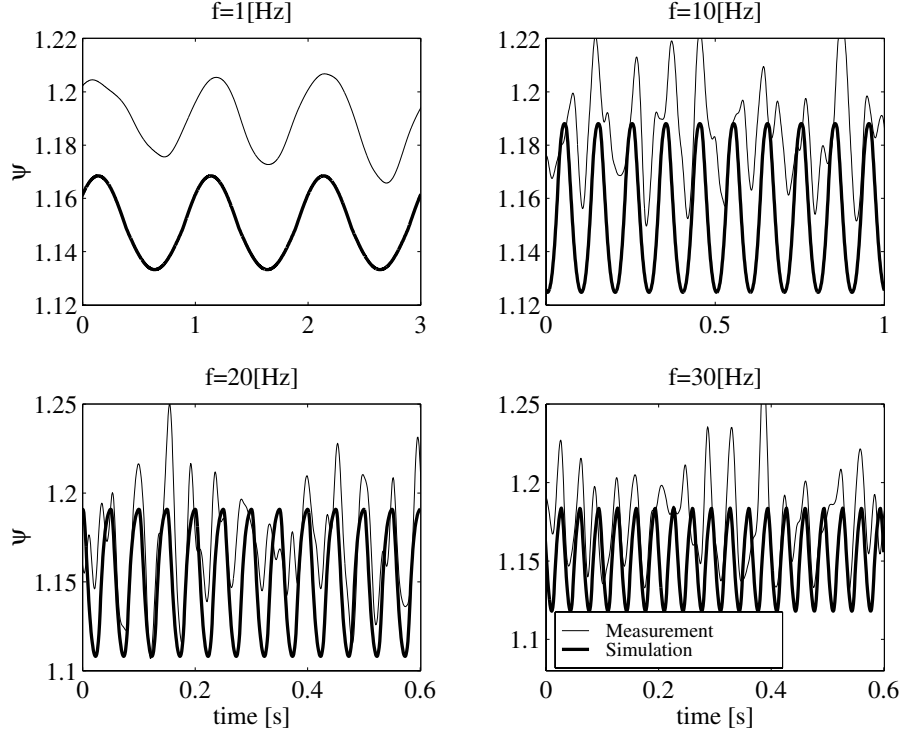


Figure 5.8: Effect of control valve electronics ($N = 18,000$ [rpm], $u_{t0} = 0.506$, $u_0 = 0.3$ and $A = 0.1$; *Simulation*: valve dynamics: $f_{co} = 50$ [Hz] and $\zeta = 0.6$).

($|H_{electr}| > 1$) the power of input signals with a frequency between 3 and 60 [Hz]. Then, the control valves are seen to saturate for 20 [Hz] in the simulation. As measurements of the core displacement are not available, this can not be verified from experiments. Compared to the case with ideal valve electronics, the effect of the valve electronics is manifest in the power spectrum by the increased power of higher harmonics up to 60 [Hz] (see Fig. 5.9). Consequently, if the system is excited with 20 [Hz], the estimate of the power spectral density around the excitation frequency is improved. For $f = 10$ [Hz], the amplitude is even slightly overestimated. Note that there are still unmodeled dynamics associated with 16.1 and 20 [Hz].

5.1.5 Surge avoidance

Open-loop experiments show that the control valves are effective. Before examining the closed-loop behavior of the compression system, surge avoidance is studied. This is done to demonstrate the conceptual difference between surge avoidance and active control. Furthermore, this situation illustrates the *distinct equilibrium* case discussed in Section 4.3.

From Fig. 5.10, it is learned that fully opening all control valves is effective for the suppression of surge if $u_{t0} = 0.272$. Doing so, the operating point is moved towards the stable operating region.

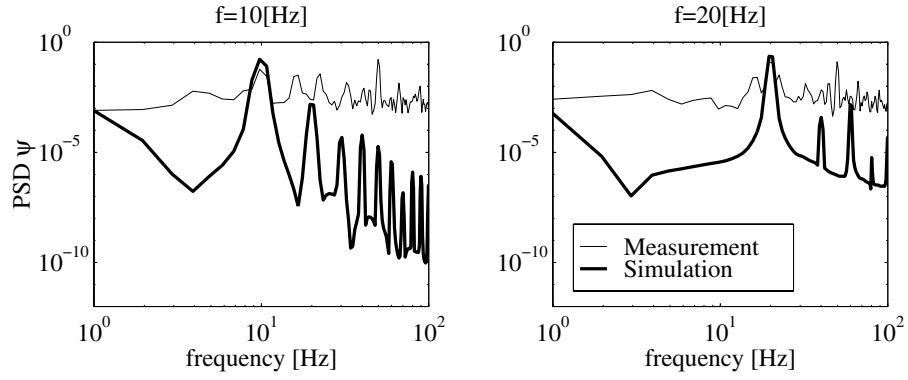


Figure 5.9: Power spectrum for compression system with valve electronics ($N = 18,000$ [rpm], $u_{t0} = 0.506$, $u_0 = 0.3$ and $A = 0.1$; *Simulation*: valve dynamics: $f_{co} = 50$ [Hz] and $\zeta = 0.6$).

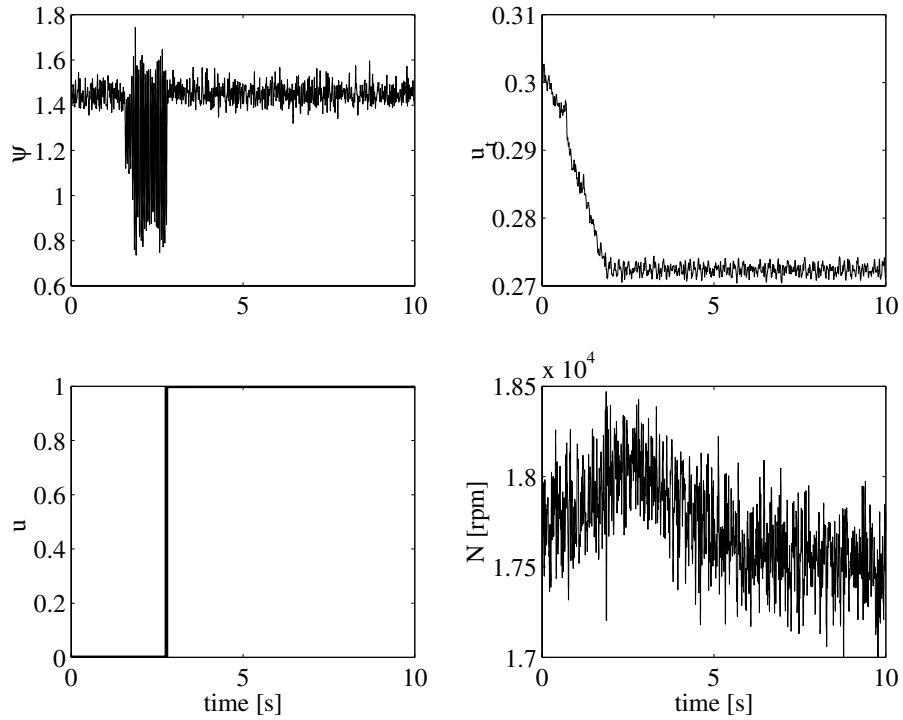


Figure 5.10: Experimental results for surge avoidance.

More precisely, the system is stabilized in an equilibrium point corresponding to $u = 1.0$. During this experiment the turbine power is kept constant. In the new equilibrium point, the system is seen to operate with approximately equal plenum pressure rise ψ and smaller rotational speed N .

5.2 One-sided surge control

Stabilization of surge is studied in the experimental set-up using the static output feedback controller, which is proposed in Section 4.2. The active surge controller is implemented using a dSPACE DS1103 controller board. This section discusses the effect of measurement noise and of the desired plenum pressure rise on control system performance. Experimental results are compared with the results of the nonlinear simulation model shown in Fig. 5.11.

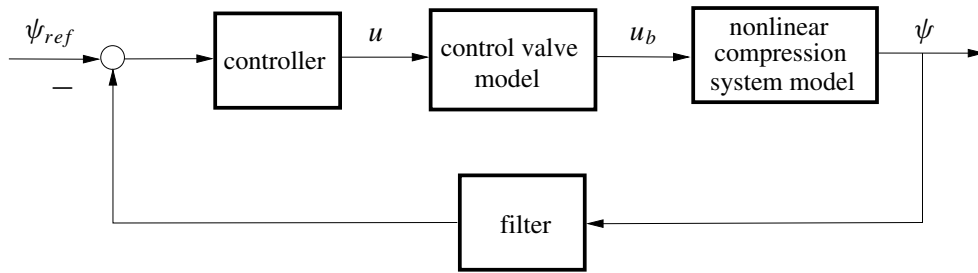


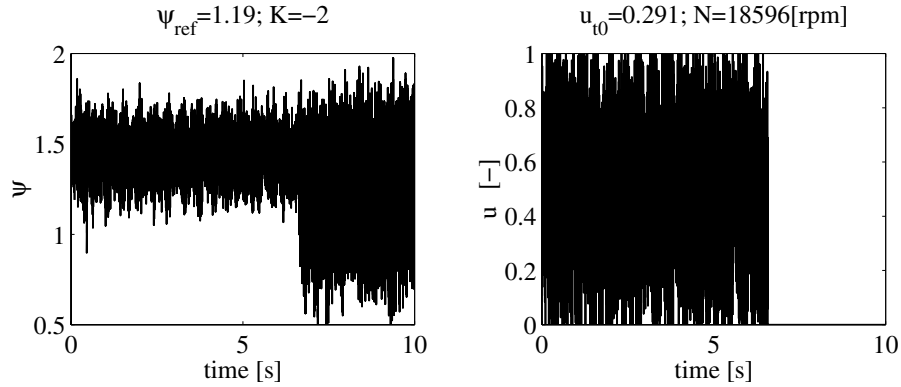
Figure 5.11: Simulation model for active surge control.

5.2.1 Effect of measurement noise

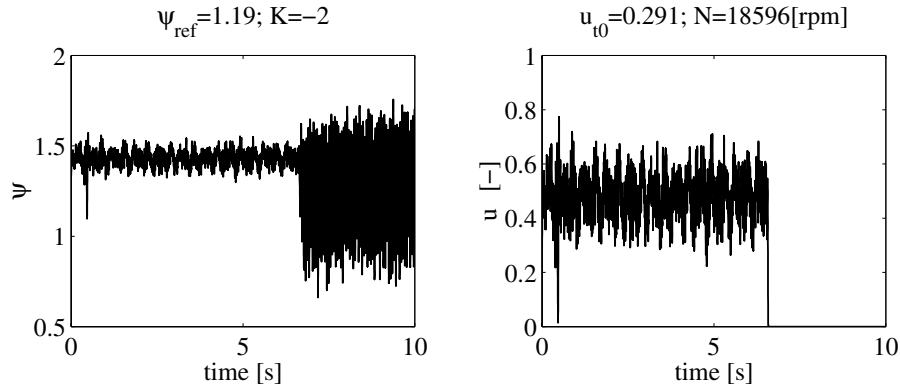
Closed-loop experiments are done for a wide range of control gains K and desired plenum pressure rises ψ_{ref} . At this point, we introduce ψ_{ref} , since the desired plenum pressure rise is not necessarily equal to the plenum pressure rise ψ_0 in the actual equilibrium point; ψ_{ref} is computed using the approximation (B.1) of the compressor characteristic, which is not accurately known for $\phi_c < \phi_{surge}$. Consequently, ψ_{ref} is likely to differ from ψ_0 .

In the experiments, the throttle is set to the desired position u_{t0} . As the turbine power is kept constant, the rotational speed N will change. If N has become constant, the controller is switched on and the closed-loop behavior is observed. For $\psi_{ref} = 1.19$ and $K = -2$, results are shown in Fig. 5.12. The system is stabilized in a distinct equilibrium point corresponding to a mean control input $\bar{u} = 0.476$. When the controller is switched off ($u = 0$) after $t = 6.6$ [s], surge is found in the compression system. During the period in which the control is active, the control valve is seen to saturate frequently (see right-hand figure of Fig. 5.12a). This is due to the noisy plenum pressure measurement. In Fig. 5.12b, the experimental data are filtered using a fourth order low-pass Butterworth filter (pass-band: 50 [Hz]) before it is plotted. This figure illustrates that the unfiltered plenum pressure signal is noisy; the equilibrium point can clearly be distinguished from surge. The measurement noise is probably caused by the applied amplifier for the measured pressure signal. Moreover, the mean control input u is large because ψ_{ref} is significantly smaller than the plenum pressure rise in the distinct equilibrium.

Simulations are run for similar operating conditions. During these simulations, the uncontrolled system is disturbed from its equilibrium (ϕ_{c0}, ψ_0) . This results in a limit cycle oscillation if $\phi_{c0} < \phi_{surge}$. Then, after 0.25 [s] the controller is activated and the controlled system behavior is observed.



(a) Unfiltered measurements.



(b) Filtered measurements.

Figure 5.12: Effect of measurement noise on controller performance.

From Fig. 5.13, it is seen that in case the effect of the control valve electronics is neglected ($H_{electr} = 1$) the system is stabilized in a distinct equilibrium point, which corresponds with $\phi_c = 2.19F$. This is in qualitative agreement with measurements, but the required control action ($\bar{u} = 0.409$) differs from the value found in the experiments: $\bar{u} = 0.476$. Inclusion of the control valve electronics in the simulation model leads to a small amplitude oscillation around the distinct equilibrium with a frequency of 30 [Hz]. This frequency is not found in the measurements. Obviously, the control valve electronics make the closed-loop unstable.

5.2.2 Effect of desired plenum pressure ψ_{ref}

As the actual nominal plenum pressure rise ψ_0 is not exactly known, the effect of ψ_{ref} on closed-loop system behavior is illustrated in Fig. 5.14. Both figures show the compressor map. Besides the compressor characteristic Ψ_c , the throttle characteristic ϕ_t and the equivalent throttle characteristic

$$\phi_{te} = [c_t u_{t0} + c_b u_b] \sqrt{\psi}$$

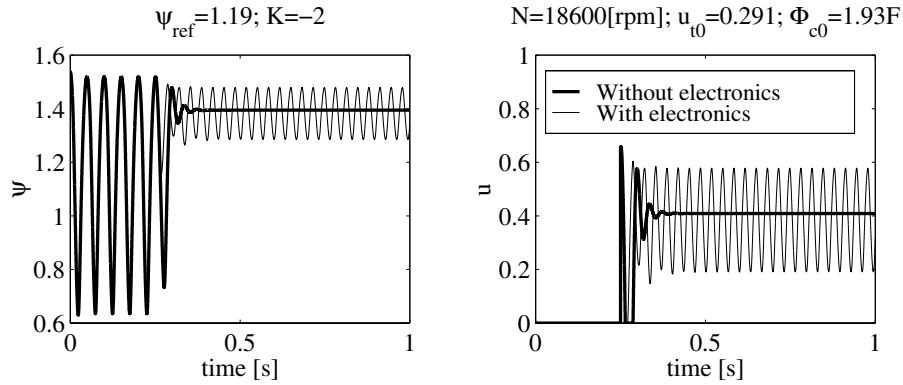


Figure 5.13: Simulation results ($c_b = 0.06c_t$, $f_{co} = 50$ [Hz], $\zeta = 0.6$).

are plotted. The dashed lines represent the throttle characteristic $\phi_t(u_{t0}, \psi)$ and the equivalent throttle characteristic for $u = 1$. The grey area indicates the region in which the one-sided controller

$$\begin{cases} u = 0 \\ u = -K(\psi - \psi_{ref}) \\ u = 1 \end{cases} \quad \text{if} \quad \begin{cases} -K(\psi - \psi_{ref}) \leq 0 \\ 0 < -K(\psi - \psi_{ref}) < 1 \\ -K(\psi - \psi_{ref}) \geq 1 \end{cases}$$

is active ($u > 0$). From Fig. 5.14a, it is concluded that the compression system has one equilibrium point for $\psi_{ref} < \psi_0$. If the desired plenum pressure rise ψ_{ref} is a very good approximation of ψ_0 and for relatively small control gains K , the system has an equilibrium point at the positively sloped part of Ψ_c . For increasing K , the slope of ϕ_{te} reduces in the region where the control valves do not saturate ($0 < u < 1$). Then, the equilibrium is located at the negatively sloped part of Ψ_c , as illustrated in Fig. 5.14a. This case is undesirable since we want to extend the stable operating region

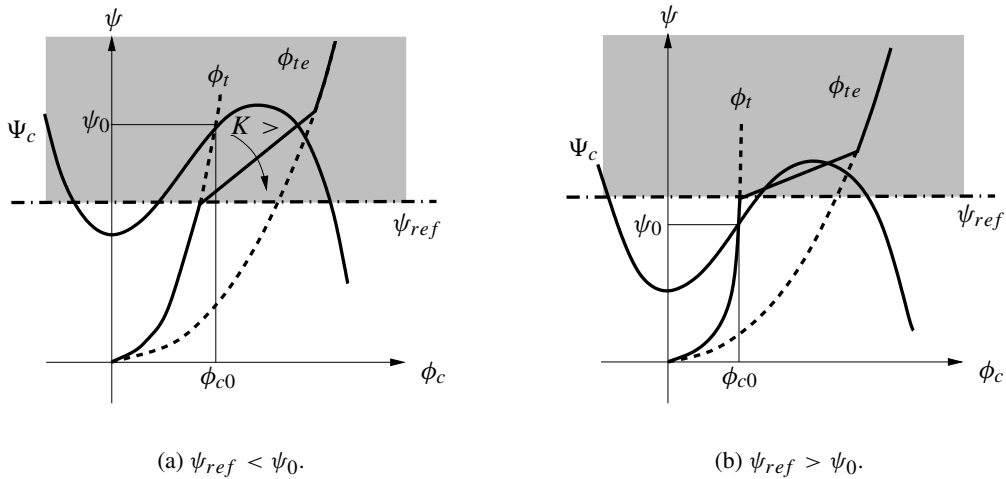


Figure 5.14: Scheme illustrating the effect of ψ_{ref} .

and to stabilize the system in an operating point with small control actions. For $\psi_{ref} > \psi_0$, two cases can be distinguished. If ψ_{ref} is larger than the compressor pressure rise $\Psi_c(\phi_c = 2F)$ at the

top of the compressor characteristic, there is no distinct equilibrium point. This can also occur for $\psi_{ref} < \Psi_c(\phi_c = 2F)$ if the control gain K is too small. However, if K is sufficiently large, two equilibrium points can be found (see Fig. 5.14b).

In summary, surge stabilization with zero stationary control valve mass flow is only feasible if the actual equilibrium point ψ_0 is exactly known. Otherwise, the system can be stabilized in a distinct equilibrium point on the positively sloped part of Ψ_c .

The effect of ψ_{ref} on system behavior is validated on the experimental set-up. In Fig. 5.15, the experimental results are shown for $\psi_{ref} = 1.36$. Contrary to the case with $\psi_{ref} = 1.19$, shown

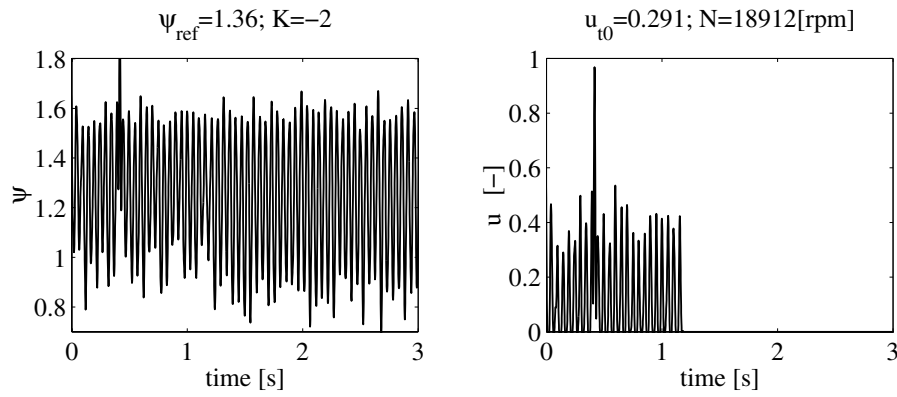


Figure 5.15: Influence of ψ_{ref} .

in Fig. 5.12, the controller is not capable to control surge; although the controller is active, large amplitude plenum pressure oscillations are found with a frequency equal to the surge frequency of the uncontrolled system: $f = 20$ [Hz]. If the controller is switched off ($u = 0$) at $t = 1.2$ [s] the amplitude of the plenum pressure oscillations only slightly increases. Note that the maximum plenum pressure rise remains unchanged.

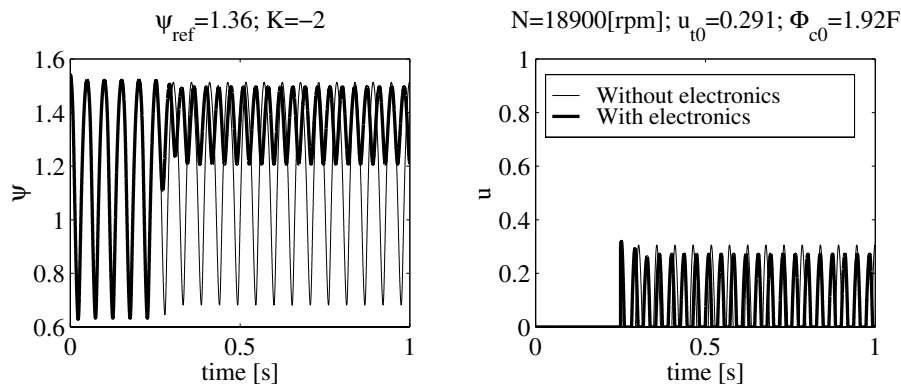


Figure 5.16: Simulation results ($c_b = 0.06c_t$, $f_{co} = 50$ [Hz], $\zeta = 0.6$, and $H_{electr} = 1$).

These experimental results are compared with simulations. If $H_{electr} = 1$, the controller is not effective (see Fig. 5.16); the amplitude and frequency of the plenum pressure oscillations ψ is only slightly changed by active control. Furthermore, the control inputs u are similar to those applied

in the actual compression system. If the effect of the control valve electronics is considered in the simulations, a small amplitude oscillation is found with a frequency of 30 [Hz]. However, this is not in agreement with experimental results.

To examine whether the system can be stabilized with small control actions, ψ_0 is determined *experimentally*; initially ψ_0 is overestimated. Then, ψ_{ref} is decreased until the plenum pressure oscill-

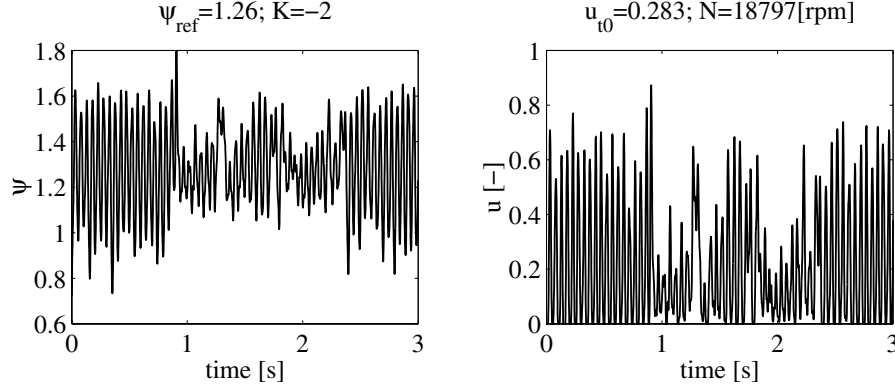


Figure 5.17: Experimental results with small control actions.

lations are suppressed and u is small. Experimental results for $u_{t0} = 0.283$ are shown in Fig. 5.17. For $\psi_{ref} = 1.26$, the amplitude of the plenum pressure oscillations is reduced during a small period of time. As seen from the upper right-hand figure, this requires relatively low control authority. However, an analysis of the power spectral density of ψ learns that during this period surge is still present in the system.

In conclusion, stabilization of surge using the bounded static output feedback controller is hampered by measurement noise and the requirement of the unknown plenum pressure rise ψ_0 . To avoid saturation of the control valves, the control gain K cannot be too large due to the noisy plenum pressure signal. Moreover, if ψ_0 is approximated inaccurately this often leads to a distinct equilibrium ($\phi_c > \phi_{surge}$) corresponding to large stationary control actions. This is undesirable since we want to extend the stable operating region and to minimize the control valve mass flow that is required for stabilization. To solve these problems, in this study a band-pass filter is applied.

5.2.3 Band-pass filter

The effect of measurement noise can be reduced by using a filter. In Willems and De Jager (2000), second order low-pass Bessel filters are applied. From this study, it is concluded that these filters introduce a phase lag, which makes the closed-loop system unstable. To compensate for this negative phase shift, a differential action is added to the proportional controller. This one-sided PD-controller is capable of suppressing the plenum pressure fluctuations, but in that case the control action is erratic.

To overcome these problems associated with measurement noise and the undesirable phase shift, the following band-pass filter is implemented:

$$H_{filter}(j\omega) = \frac{\omega_{f3}(s + \omega_{f1})}{(s + \omega_{f2})(s + \omega_{f3})}$$

with $\omega_{f1} = 2\pi \cdot 10^{-6}$ [rad/s]. This filter passes signals in a small frequency band $[\frac{\omega_{f2}}{2\pi}; \frac{\omega_{f3}}{2\pi}]$ [Hz]. This means that the average plenum pressure rise $\bar{\psi}$ is filtered out. Consequently, the controller only has

to suppress oscillations in this pass-band, so the desired plenum pressure rise is $\psi_{ref} = 0$. This is of great practical value, because in that case the actual equilibrium point need not to be known.

The effect of the pass-band on compression system behavior is experimentally investigated. For surge stabilization in the examined compression system, ω_{f2} and ω_{f3} have to be chosen such that the pass-band is around $f = 20$ [Hz]. Experiments are done for a wide range of operating conditions and values of ω_{f2} and ω_{f3} . It is seen that the system is stabilized from surge if the applied filter introduces a phase lead at the surge frequency. Stabilization with the smallest control inputs u is realized for $\omega_{f2} = 2\pi 20$ [rad/s] and $\omega_{f3} = 2\pi 70$ [rad/s]. In this case, the phase lead at the surge frequency is approximately 30 [deg]. This filter will be used for further examination of the possibilities of the proposed surge controller.

Extension of stable operating region

An important aspect of active control is the feasible extension of the stable operating region. From simulations, it is seen that the surge point mass flow can be decreased by 15% (see Section 4.3). This is validated on the experimental set-up. Similar to Eveker *et al.* (1998), first the compression system is operated at a safe distance from the surge line. Then, the controller is switched on and the system is moved to a different operating point by closing the throttle until the desired throttle position u_{t0} is reached. During this transient, the system behavior is studied. To demonstrate the effect of the surge controller, it is switched off ($u = 0$) when the system has reached the desired equilibrium point. Next, the controller is activated again to examine whether the linear controller is capable to control fully-developed surge. A typical result is shown in Fig. 5.18. From this figure, it is concluded that surge is

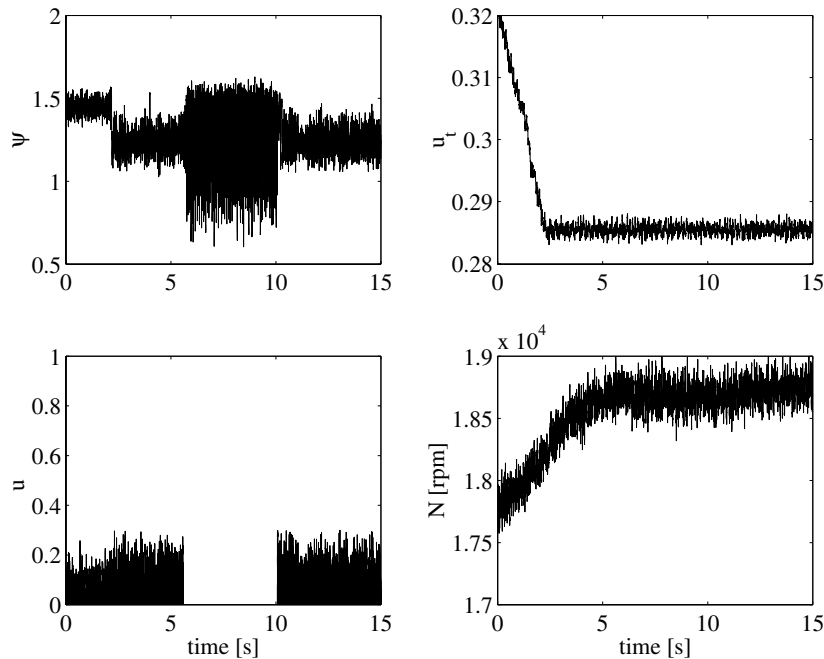


Figure 5.18: Transient with one-sided surge controller ($u_{t0} = 0.284$, $K = -2$).

suppressed by the one-sided controller; if the controller is switched off, surge oscillations are found in the system. Moreover, the mean control input to stabilize the system ($\bar{u} = 0.05$) is considerably

smaller than the control input required for surge avoidance (*i.e.*, stabilization by manually opening the control valves): $u \approx 0.3$. Note that there is a stepwise change in the plenum pressure rise ψ at $t = 2.2$ [s]. This is also found when the throttle is closed down to $u_{t0} = 0.271$, as shown in Fig. 5.19. In that case, the system remains stable if the controller is switched off. It is seen from

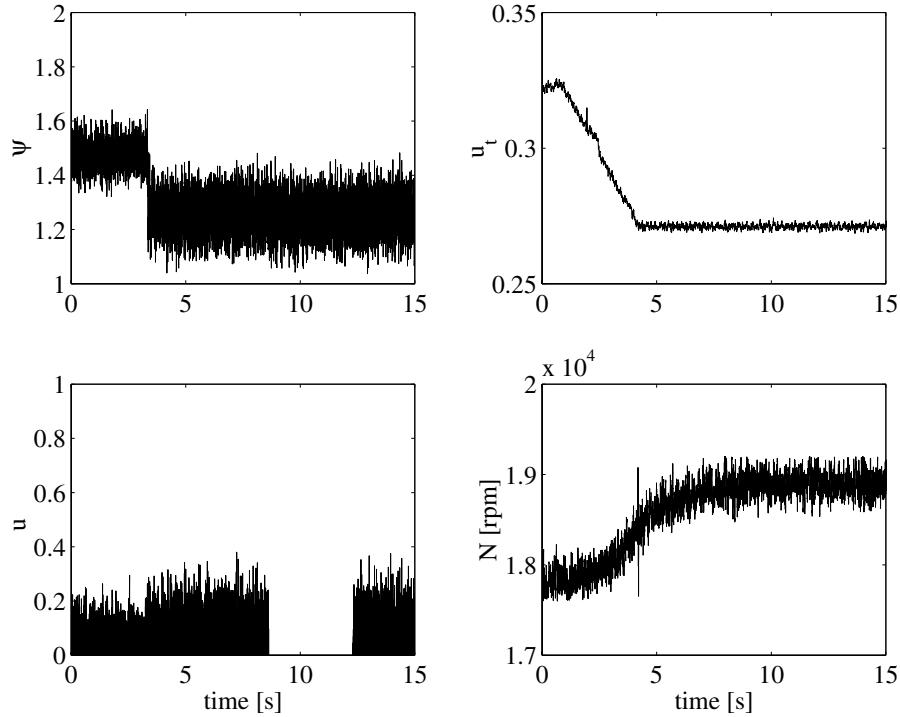


Figure 5.19: Experimental results for $u_{t0} = 0.271$ and $K = -2$.

additional experiments that surge does even not occur if the uncontrolled system is throttled further to $u_{t0} = 0.20$. Therefore, the jump in ψ is associated with *rotating stall*. As there are no pressure sensors placed around the circumference of the compressor, information about rotating stall cells is lacking. Nonetheless, analysis of the power spectral density of ψ learns that there is a peak around half of the rotor frequency: $f = 162$ [Hz] (see lower figure of Fig. 5.20). This is in line with the characteristics of rotating stall (see Section 1.2). In addition, a peak is found at 81 [Hz], which corresponds to a quarter of the rotor frequency. The peaks for 50, 150, and 250 [Hz] are probably due to grounding problems. Note that, although rotating stall is a local flow instability, it can be observed by the plenum pressure sensor which is located approximately 0.20 [m] upstream of the compressor.

In the uncontrolled case, surge is experienced if the throttle is closed, as shown in Fig. 5.21. When the plenum pressure signal is examined in more detail (see Fig. 5.22), it is seen that there is a stepwise change in ψ before surge is initiated. Next, surge is developed within 4 cycles. This path of surge initiation is not followed in all cases, as illustrated in Fig. 1.6. The controller is capable to stabilize fully-developed surge; if the controller is switched on, the system is stabilized in the same equilibrium point ($\bar{u} = 0.047$) as in Fig. 5.19. The upper figure of Fig. 5.20 shows the power spectrum for the uncontrolled case. In this figure, the surge frequency can easily be observed. Figure 5.20 clearly illustrates the effectiveness of the controller; the peak around the surge frequency is reduced considerably if the active surge controller is applied. However, rotating stall can be present, since the

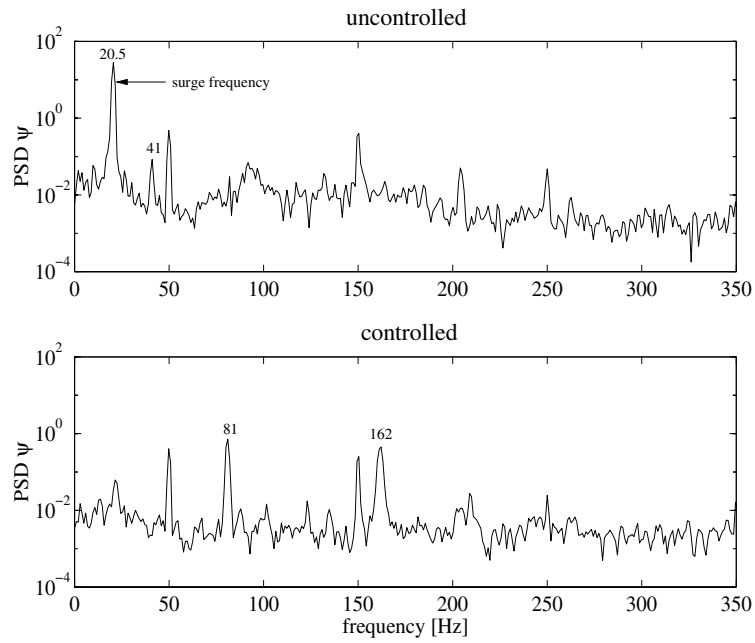


Figure 5.20: Power spectral density estimate of ψ ($f_{rotor} = 315$ [Hz]).

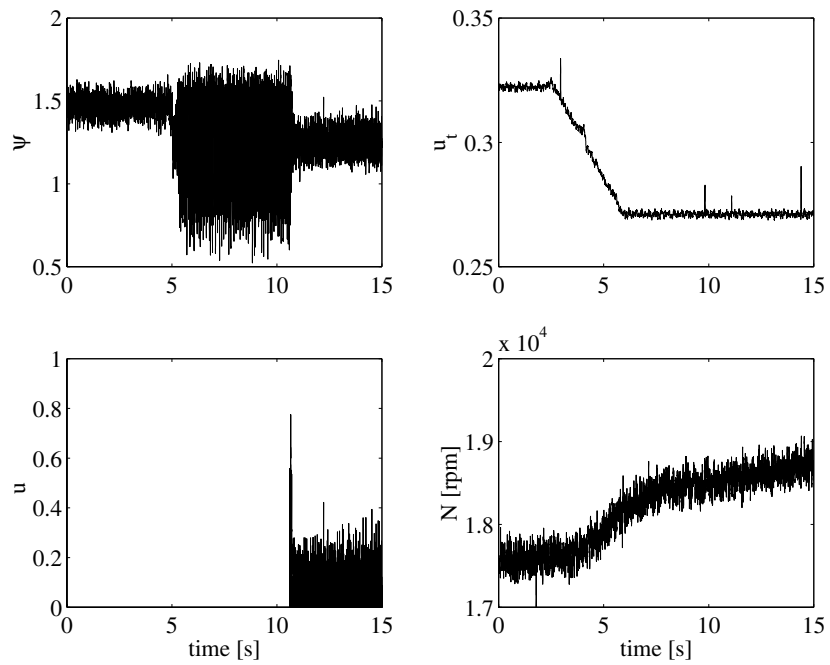


Figure 5.21: Initially uncontrolled case ($u_{t0} = 0.271$, $K = -2$).

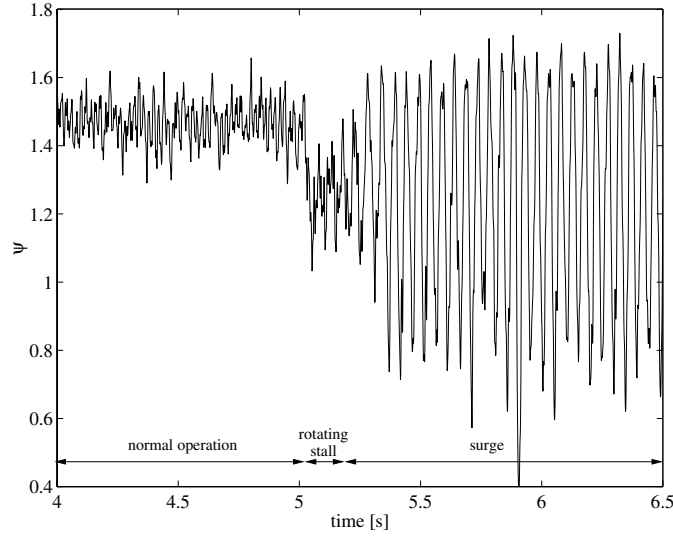


Figure 5.22: Surge initiation in detail.

controller only deals with surge. This can be overcome by using a *stall* controller as in Eveker *et al.* (1998).

In summary, the controller modifies the compression system behavior. This is illustrated in Fig. 5.23. In the *uncontrolled* compression system, surge is experienced for operating conditions associated with point B. By controlling surge, probably rotating stall is found (point C). This stabilized operating point corresponds with $u_{t0} = 0.271$ and $\bar{u} = 0.047$ in Fig. 5.21. For similar operating conditions the surge line is located at approximately $u_{t,surge} = 0.295$ (point A). Now, the realized extension of the stable region is computed as follows. We assume that, if rotating stall is not present, the system is stabilized in point B on the *unstalled* characteristic. In this unknown equilibrium point, the pressure rise is supposed to be equal to the pressure rise at the surge line: $\psi_{eq} = \psi_{surge}$. To determine the stationary bleed valve mass flow, the control valve model with the nonlinear flow curve, the valve dynamics, and valve saturation is applied to compute u_b from the measured control input u . This gives $\bar{u}_b = 0.068$ for the examined case. Then, the mass flows corresponding to the stabilized equilibrium point and to the surge line, ϕ_{eq} and ϕ_{surge} respectively, can be estimated from ($c_b = 0.06c_t$):

$$\frac{\phi_{eq}}{\phi_{surge}} = \frac{(c_t u_{t0} + c_b \bar{u}_b) \sqrt{\psi_{eq}}}{c_t u_{t,surge} \sqrt{\psi_{surge}}} = 0.93$$

This means that the surge point mass flow is reduced by 7%, but rotating stall is probably present. Although rotating stall is considered to be less harmful for the equipment than surge, it is undesirable because it degrades the performance. Consequently, for the studied compression system controllers have to be developed that deal with both rotating stall and surge.

5.3 Discussion

Active surge control is studied in a centrifugal compressor system. To stabilize surge, a bounded static output feedback controller based on plenum pressure measurements is implemented. Surge stabilization is hampered by the following practical limitations.

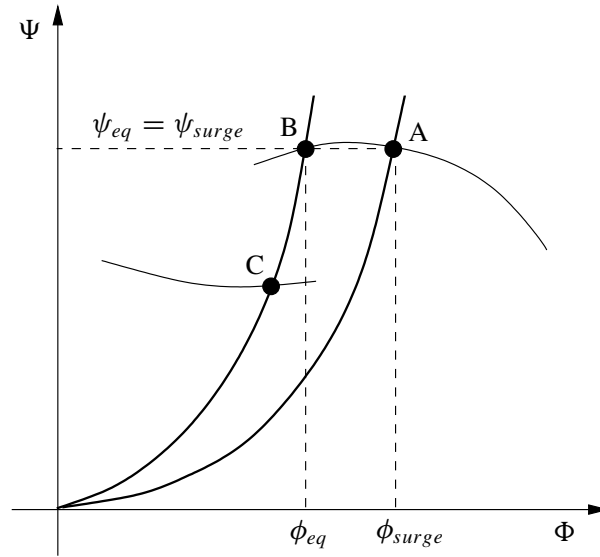


Figure 5.23: Illustration of the computed reduction in surge point mass flow.

- **Measurement noise** is seen to significantly degrade the performance of the control system; to avoid saturation of the control valves, the control gain can not be too large. Application of low-pass filters introduce a phase lag, which makes the closed-loop unstable.
- The **desired plenum pressure rise** ψ_0 is not exactly known. Consequently, the equilibrium point can not be achieved with zero stationary control valve mass flow.

These problems are overcome by applying a *band-pass filter*, which introduces a positive phase shift at the surge frequency. For this filter, the desired equilibrium point in the controller is $\psi_0 = 0$. Combination of this band-pass filter with the applied controller results in a *bounded dynamic output feedback controller*. Experiments with this nonlinear controller give promising results; the surge point mass flow is decreased by 7%. However, in that case *rotating stall* seems to be present. This has to be verified from detailed measurements of the circumferential flow variations.

To describe the compression system behavior, the Greitzer lumped parameter model is applied. This model is seen to show reasonable agreement with experiments for the frequency response measurements, but the observed nonlinearities are not captured. Inclusion of the control valve electronics in the simulation model also makes the closed-loop system unstable. This is not found in experiments. Therefore, the simulation model behavior has to be studied in more detail. The applied Greitzer model can not predict the occurrence of rotating stall. As seen in Greitzer (1976b), the stalled characteristics can be included in the approximation of the compressor characteristic Ψ_c . Then, the model can predict the pressure drop in ψ and changes in the annulus-averaged compressor flow. For the design of active stall controllers, the Moore-Greitzer model (Moore and Greitzer, 1986) can be applied. This model can describe both axial and circumferential variations of the flow.

Chapter 6

Conclusions and Suggestions for Future Research

In this thesis, the modeling and control of surge in a centrifugal compression system is investigated. The aim of this study is the development of feedback controllers that stabilize surge. Furthermore, we want to deal with the effect of sensors and actuators on control system performance. In Section 6.1, conclusions are drawn with respect to the main lines of the research. Moreover, suggestions for future research are presented in Section 6.2.

6.1 Conclusions

6.1.1 Modeling of centrifugal compressor surge

The *Greitzer lumped parameter model* has been applied in Chapter 2 to describe the behavior of the examined compression system during surge. System identification has been performed in two steps.

1. Approximations of the compressor and throttle characteristics are determined from *stationary measurements*. For mass flows smaller than the surge point mass flow, stationary compressor data is not available. In this study, cubic polynomials are used to describe the stationary behavior of the compressor also in the unstable region.
2. The Greitzer stability parameter

$$B = \frac{U_t}{2a} \sqrt{\frac{V_p}{A_c L_c}}$$

is determined from plenum pressure measurements during *fully-developed surge*. This parameter can be derived if the plenum volume V_p , the equivalent compressor duct length L_c , and the compressor duct area A_c are known. However, this is not straightforward because L_c is not exactly known. For fully-developed surge, L_c is varied such that the frequency of the measured and predicted plenum pressure oscillations show fair agreement. The applied approximation of the compressor characteristic is modified in the unstable region such that the amplitude of the measured plenum pressure oscillations is predicted properly.

Although the Greitzer model is originally developed for low pressure-ratio axial compressors, this low order model reasonably predicts the behavior of the centrifugal compression system for a broad

range of nominal throttle positions u_{t0} and rotational speeds N . The measured surge frequency is seen to decrease for increasing u_{t0} . This trend is described well by the applied model. Moreover, the model captures the nonlinearities in the system during fully-developed surge; the first higher order harmonic, which is observed in the measured plenum pressure oscillations, is predicted fairly. In the simulations, the compression system exhibits deep surge. This can not be validated from experiments, since reliable, transient mass flow measurements are not available.

6.1.2 Design of control system

The Greitzer model has been used to make an appropriate selection of sensors and actuators for surge control in the examined compression system. Based on the results of Simon *et al.* (1993) and Van de Wal *et al.* (1999) and on practical considerations, a *plenum pressure sensor* in combination with a *bleed valve* has been selected in Chapter 3. The control valve bandwidth and capacity which are required for the stabilization of surge have been specified from a stability analysis of the linearized compression system (Chapter 3) and from simulations with a nonlinear compression system model (Chapter 4), respectively.

6.1.3 Development of control strategy

A new surge control strategy has been derived in Chapter 4: *bounded static output feedback stabilization* based on plenum pressure measurements. This control strategy avoids two commonly encountered practical problems:

- Feedback is based on the easily measurable plenum pressure. Therefore, an expensive sensor to measure mass flow transients, which is proposed in, *e.g.*, Simon *et al.* (1993), is not needed.
- Control action is *one-sided*; in the stabilized operating point the valves are closed, so stationary bleed losses are avoided. This will improve the overall efficiency of the compressor system.

Stability of the constrained linearized compression system has been analyzed using the theory of *positive feedback stabilization* (Heemels and Stoorvogel, 1998). This theory is developed for non-negative control inputs and does not deal with the upper constraint on the control valve position. Hence, *local* stability can only be guaranteed. Simulations with the nonlinear compression system model show that in the examined operating region the surge point mass flow can be decreased by maximal 15% using bounded static output feedback based on plenum pressure measurements; the possible extension of the feasible operating region reduces for increasing rotational speed.

6.1.4 Realization and experiments

The proposed control strategy is successfully implemented on the examined compression system. A *band-pass filter* has been applied to overcome the practical problems associated with measurement noise and with the desired equilibrium point, which is not exactly known in the unstable region. By adding the band-pass filter to the controller, we effectively apply *bounded dynamic output feedback*. Experiments with the implemented active surge controller have generated interesting results; so far, a 7% reduction in surge point mass flow can be realized. Moreover, if surge is suppressed, *rotating stall* is probably found in the centrifugal compressor. This is of special interest, because rotating stall is only believed to be important in axial machines. In particular, little attention has been paid to rotating stall control in centrifugal compressors. To verify if stall cells are present, additional sensors could be placed around the circumference of the compressor.

6.2 Suggestions for future research

Based on the results of this research and on open problems with respect to the modeling and control of rotating stall and surge, the following directions for future research are suggested.

6.2.1 Modeling of rotating stall and surge

Profound understanding of instability onset

Various models are available in the literature for the description of rotating stall and surge. These models can describe the development of the unstable phenomena subsequent to instability onset. However, the mechanisms behind stability onset are not completely understood, especially for centrifugal compressors. Better insight in these mechanisms may allow further refinements of existing models and may provide new ideas for the stabilization of stall. A model that captures all the main features of various types of aerodynamic flow instabilities is lacking. So far, only the Moore-Greitzer model (Moore and Greitzer, 1986) and its derivatives, which are developed for axial compressors, describe the growth and decay of axial as well as circumferential perturbations. A point of interest is the application of the Moore-Greitzer model to centrifugal compressors and its prediction capability when rotating stall and surge coexist in the system. In addition, developments in the modeling of 3D flow phenomena and in the modeling of unsteady blade-row behavior will be beneficial (Gu *et al.*, 1996; Longley, 1994).

Modeling of the examined compression system

In this study, the Greitzer lumped parameter model is applied to describe surge in the examined compression system. The main problem in the applied Greitzer model is the required part of the compressor characteristic in the unstable region, which is generally not known. This problem is also observed for the other models discussed in Chapter 2. Gravdahl and Egeland (1999) propose to determine the compressor characteristic from energy considerations and compressor geometry. The practical applicability of this approach seems worth further investigations. In the companion research project *Flow models for compressor surge* performed by Corine Meuleman, the unsteady compressor behavior during periodic flow variations is currently under investigation. This research is motivated by the results in Meuleman *et al.* (1999).

Studies into the modeling of surge mainly concentrate on the description of fully-developed surge (see, *e.g.*, Hansen *et al.* (1981) or Arnulfi *et al.* (1999b)). However, surge initiation and the development of surge subsequent to instability onset is also of interest. For instance, compressor manufacturers want to approximate the location of the surge line (stability boundary) and control designers want to control small perturbations or disturbances before they grow into large perturbations or limit cycle oscillations. In the examined compression system, surge is triggered by closing the throttle valve. This results in rotational speed changes because the turbine power is kept constant. Then, similar to Fink *et al.* (1992), for the description of surge development rotational speed variations have to be included in the model. To observe the actual surge type, the system should be equipped with a mass flow sensor. Moreover, it has to be investigated whether the applied compression system model can also predict surge in high-speed centrifugal compressors, *e.g.*, in the GARRETT centrifugal compressor described in Van de Wal and Willems (1996) and Lahoye (1996). In this type of machines, pressure ratios are relatively large and compressibility effects are more important. Furthermore, rotational speed variations may affect the dynamic system behavior (Fink *et al.*, 1992).

If surge is controlled, rotating stall seems to be present in the installation. This cannot be predicted by the applied model; rotating stall can only be captured by the Greitzer model if, analogous

to Greitzer (1976b), the stalled characteristic is included in the compressor characteristic. Then, the *jump* in the plenum pressure can be predicted, but the Greitzer model only describes variations in the annulus-averaged mass flow. For the prediction of both axial and circumferential flow variations, the Moore-Greitzer model (Moore and Greitzer, 1986) is a useful starting point. This model can be used to guide the selection of sensors and actuators for stall control and the development of active stall controllers.

6.2.2 Active stall control

In this research, experiments are performed with the developed control strategy. However, it is useful to further explore its possibilities, *e.g.*, the maximal realizable reduction in surge point mass flow and results for higher rotational speeds or for a compression system which only exhibits surge. Then, attention should be paid to reduce the noise in the plenum pressure signal. Also, the problems associated with the 50, 150, and 250 [Hz] components in the measured pressure signal have to be eliminated. Furthermore, a stability analysis shows that the electronics of the applied control valves makes the closed-loop system unstable. As a result, if bounded dynamic output feedback stabilization is applied to other systems in which surge only occurs, it is recommended to select control valves which have a better dynamic performance (see, *e.g.*, MOOG (1999)).

From the results presented in Chapter 4, it is seen that the stable region of the examined compression system can be further extended if state feedback is applied. This requires information about the full state. As these measurements are not available in the installation, an observer can be applied which determines the state from the measured output. On the other hand, it is concluded from the analysis in Simon *et al.* (1993) that the region of feasible operating points can also be enlarged if the output feedback controller uses information of a static or total pressure sensor, which is placed at the compressor inlet. This has to be validated from experiments. In the literature, a theory is lacking that can deal with the effect of the experienced control constraints, $\hat{u}_b \in [0; 1]$, on system stability. The applied theory of positive feedback stabilization copes with non-negative control inputs. However, this theory cannot guarantee the local stability of the linearized compression system *with* valve dynamics for static output feedback.

Further fields worth investigating are integrated stall control, integrated speed and surge control, and the integration and implementation of active surge control strategies on existing systems. Other challenges are the modeling and control of instabilities in transonic machines (Greitzer, 1998). This situation corresponds with state-of-the-art aeroengines. In these machines, the flow is compressible and active control requires high-bandwidth actuators.

Bibliography

- Arnulfi, G., Giannattasio, P., Guisto, C., Massardo, A., Micheli, D., and Pinamonti, P. (1999a). Multistage centrifugal compressor surge analysis: Part I - Experimental investigation. *ASME J. Turbomachinery*, **121**(2), 305–311.
- Arnulfi, G., Giannattasio, P., Guisto, C., Massardo, A., Micheli, D., and Pinamonti, P. (1999b). Multistage centrifugal compressor surge analysis: Part II - Numerical simulation and dynamic control parameters evaluation. *ASME J. Turbomachinery*, **121**(2), 312–320.
- Badmus, O., Chowdhury, S., Eveker, K., Nett, C., and Rivera, C. (1993a). A simplified approach for control of rotating stall. Part 1: Theoretical development. In *Proc. of the 29th Joint Propulsion Conference*, Monterey. AIAA. Paper No. 93-2229.
- Badmus, O., Chowdhury, S., Eveker, K., Nett, C., and Rivera, C. (1993b). A simplified approach for control of rotating stall. Part 2: Experimental results. In *Proc. of the 29th Joint Propulsion Conference*, Monterey. AIAA. Paper No. 93-2234.
- Badmus, O., Eveker, K., and Nett, C. (1995a). Control-oriented high-frequency turbomachinery modeling: general 1D model development. *ASME J. Turbomachinery*, **117**(3), 320–335.
- Badmus, O., Chowdhury, S., Eveker, K., and Nett, C. (1995b). Control-oriented high-frequency turbomachinery modeling: single-stage compression system one-dimensional model. *ASME J. Turbomachinery*, **117**(1), 47–61.
- Badmus, O., Chowdhury, S., and Nett, C. (1996). Nonlinear control of surge in axial compression systems. *Automatica*, **32**(1), 59–70.
- Batson, D. (1996). Invariant coordinate systems for compressor control. ASME paper no. 96-GT-240.
- Billoud, G., Gallard, M. A., Huu, C. H., and Candel, S. (1991). Adaptive active control of instabilities. *J. Intelligent Material Systems and Structures*, **2**, 457–471.
- Bloch, H. P. (1996). *A practical guide to compressor technology*. McGraw-Hill.
- Bosgra, O. H. and Kwakernaak, H. (1995). Design methods for control systems. Notes for a course of the Dutch Institute of Systems and Control (DISC), winter term 1995-1996.
- Botros, K. (1994). Transient phenomena in compressor stations during surge. *ASME J. Engineering for Gas Turbines and Power*, **116**(1), 133–142.
- Botros, K. and Henderson, J. (1994). Developments in centrifugal compressor surge control - A technology assessment. *ASME J. Turbomachinery*, **116**(2), 240–249.
- Botros, K., Campbell, P., and Mah, D. (1991). Dynamic simulation of compressor station operation including centrifugal compressor and gas turbine. *ASME J. Engineering for Gas Turbines and Power*, **113**(2), 300–311.
- Brown, R. N. (1997). *Compressors: selection and sizing*. Gulf Publishing Company, 2nd edition.
- Buse, M., de Jongh, F., and Vial, F. (1996). Performance improvement of low volume flow centrifugal compressor stages. In *Proc. of the 6th European congress on fluid machinery for the oil, petrochemical and related industries*, volume C508/033/96, The Hague, The Netherlands.

- Camp, T. and Day, I. (1998). A study of spike and modal stall phenomena in a low-speed axial compressor. *ASME J. Turbomachinery*, **120**(3), 393–401.
- Cargill, A. and Freeman, C. (1991). High-speed compressor surge with application to active control. *ASME J. Turbomachinery*, **113**(2), 303–311.
- CCC (1997). Compressor controls, steam turbine and gas turbine turbomachinery control concepts. Notes for Honeywell & Compressor Controls Corporation (CCC) Turbomachinery Seminar, Amsterdam, The Netherlands.
- Chen, Y. and Kuo, C. (1997). Positive uncertain systems with one-sided robust control. *ASME J. Dynamic Systems, Measurement, and Control*, **119**, 675–684.
- Chen, Y. and Leitmann, G. (1987). Robustness of uncertain systems in the absence of matching assumptions. *Int. J. Control*, **45**(5), 1527–1542.
- Cohen, H., Rogers, G., and Saravanamutto, H. (1996). *Gas turbine theory*. Longman Scientific & Technical, 4rd edition.
- Cumpsty, N. (1989). *Compressor aerodynamics*. John Wiley & Sons.
- Dadd, G. and Porter, M. (1993). Surge recovery and compressor control using compressor exit Mach number measurement. *J. Aerospace Engineering*, **207**(G1), 27–35.
- Day, I. (1993a). Active suppression of rotating stall and surge in axial compressors. *ASME J. Turbomachinery*, **115**(1), 40–47.
- Day, I. (1993b). Stall inception in axial flow compressors. *ASME J. Turbomachinery*, **115**(1), 1–9.
- Day, I. (1994). Axial compressor performance during surge. *J. Propulsion and Power*, **10**(3), 329–336.
- Day, I. and Freeman, C. (1994). The unstable behavior of low and high-speed compressors. *ASME J. Turbomachinery*, **116**(2), 194–201.
- De Jager, B. (1995). Rotating stall and surge control: A survey. In *Proc. of the 34th IEEE Conference on Decision and Control*, volume 2, pages 1857–1862, New Orleans, LA.
- De Sa, D. and Maalouf, S. (1996). The operating and control philosophy of turbo-compressors. *Measurement and Control*, **29**(3), 69–72.
- DiLiberti, J.-L., van den Braembussche, R., Konya, P., and Rasmussen, S. (1996). Active control of surge in centrifugal compressors with inlet pipe resonance. ASME paper no. 96-WA/PID-1.
- Elder, R. and Gill, M. (1985). A discussion of the factors affecting surge in centrifugal compressors. *ASME J. Engineering for Gas Turbines and Power*, **107**(2), 499–507.
- Emmons, H., Paerson, C., and Grant, H. (1955). Compressor surge and stall propagation. *ASME Transactions*, **77**, 455–469.
- Epstein, A., Ffowcs Williams, J., and Greitzer, E. (1989). Active suppression of aerodynamic instabilities in turbomachines. *J. Propulsion*, **5**(2), 204–211.
- Escuret, J. and Garnier, V. (1996). Stall inception measurements in a high-speed multistage compressor. *ASME J. Turbomachinery*, **118**(4), 690–696.
- Eveker, K., Gysling, D., Nett, C., and Sharma, O. (1998). Integrated control of rotating stall and surge in high-speed multi-stage compression systems. *ASME J. Turbomachinery*, **120**(3), 440–445.
- Feulner, M., Hendricks, G., and Paduano, J. (1996). Modeling for control of rotating stall in high-speed multi-stage axial compressors. *ASME J. Turbomachinery*, **118**(1), 1–10.
- Ffowcs Williams, J. and Huang, X. (1989). Active stabilization of compressor surge. *J. Fluid Mechanics*, **204**, 245–262.
- Ffowcs Williams, J., Harper, M., and Alwright, D. (1993). Active stabilization of compressor instability and surge in a working engine. *ASME J. Turbomachinery*, **115**(1), 68–75.

- Fink, D., Cumpsty, N., and Greitzer, E. (1992). Surge dynamics in a free-spool centrifugal compressor. *ASME J. Turbomachinery*, **114**(2), 321–332.
- Freeman, C., Wilson, A., Day, I., and Swinbanks, M. (1998). Experiments in active control of stall on an aeroengine gas turbine. *ASME J. Turbomachinery*, **120**(4), 637–647.
- Garnier, V., Epstein, A., and Greitzer, E. (1991). Rotating waves as a stall inception indication in axial compressors. *ASME J. Turbomachinery*, **113**(2), 290–302.
- Goto, A. (1994). Suppression of mixed-flow pump instability and surge by the active alteration of impeller secondary flows. *ASME J. Turbomachinery*, **116**(4), 621–628.
- Gravdahl, J. T. and Egeland, O. (1997a). Compressor surge control using a close-coupled valve and backstepping. In *Proc. of the 1997 American Control Conference*, pages 982–986, Albuquerque, NM.
- Gravdahl, J. T. and Egeland, O. (1997b). A Moore-Greitzer axial compressor model with spool dynamics. In *Proc. of the 36th IEEE Conference on Decision and Control*, pages 4714–4719, San Diego, CA.
- Gravdahl, J. T. and Egeland, O. (1997c). Speed and surge control for a low order centrifugal compressor model. In *Proc. of the 1997 IEEE Int. Conference on Control Applications*, pages 344–349, Hartford, CT.
- Gravdahl, J. T. and Egeland, O. (1998). *Compressor surge and rotating stall: Modeling and control*. Springer.
- Gravdahl, J. T. and Egeland, O. (1999). Centrifugal compressor surge and speed control. *IEEE Control Systems Technology*, **7**(5), 567–579.
- Greitzer, E. (1976a). Surge and rotating stall in axial flow compressors. Part I: Theoretical compression system model. *ASME J. Engineering for Power*, **98**(2), 191–198.
- Greitzer, E. (1976b). Surge and rotating stall in axial flow compressors. Part II: Experimental results and comparison with theory. *ASME J. Engineering for Power*, **98**(2), 199–217.
- Greitzer, E. (1981). The stability of pumping systems - The 1980 Freeman scholar lecture. *ASME J. Fluids Dynamics*, **103**(2), 193–242.
- Greitzer, E. (1998). Smart engines: Case history of a multidisciplinary research program. *JSME Int. J. Series B*, **41**(1), 90–101.
- Gu, G., Banda, S., and Sparks, A. (1996). An overview of rotating stall and surge control for axial flow compressors. In *Proc. of the 35th IEEE Conference on Decision and Control*, volume 5, pages 2786–2791, Kobe, Japan.
- Gu, G., Sparks, A., and Banda, S. S. (1999). An overview of rotating stall and surge control for axial flow compressors. *IEEE Transactions on Control Systems Technology*, **7**(6), 639–647.
- Gysling, D., Dugundji, D., Greitzer, E., and Epstein, A. (1991). Dynamic control of centrifugal compressor surge using tailored structures. *ASME J. Turbomachinery*, **113**(4), 710–722.
- Hansen, K., Jørgensen, P., and Larsen, P. (1981). Experimental and theoretical study of surge in a small centrifugal compressor. *ASME J. Fluids Engineering*, **103**(3), 391–395.
- Haynes, J., Hendricks, G., and Epstein, A. (1994). Active stabilization of rotating stall in a three-stage axial compressor. *ASME J. Turbomachinery*, **116**(2), 226–239.
- Heemels, W. and Stoorvogel, A. (1998). Positive stabilizability of a linear continuous-time system. Technical Report 98I-01, Section Measurement and Control, Faculty of Electrical Engineering, Eindhoven University of Technology.
- Hendricks, G. and Gysling, D. (1994). Theoretical study of sensor-actuator schemes for rotating stall control. *J. Propulsion and Power*, **10**(1), 101–109.
- Hunziker, R. and Gyarmathy, G. (1994). The operational stability of a centrifugal compressor and its dependence on the characteristics of the subcomponents. *ASME J. Turbomachinery*, **116**(2), 250–259.
- Ishii, H. and Kashiwabara, Y. (1996). Study on surge and rotating stall in axial compressors. *JSME Int. J. Series*

- B, **39**(3), 621–631.
- Jungowski, W., Weiss, M., and Price, G. (1996). Pressure oscillations occurring in a centrifugal compressor system with and without passive and active surge control. *ASME J. Turbomachinery*, **118**(1), 29–40.
- Kämmer, N. and Rautenberg, M. (1986). A distinction between different types of stall in a centrifugal compressor stage. *ASME J. Engineering for Gas Turbines and Power*, **108**(1), 83–92.
- Khalil, H. K. (1996). *Nonlinear systems*. Prentice Hall, 2nd edition.
- Kinsler, L. R., Frey, A. R., Coppens, A. R., and Sanders, J. V. (1982). *Fundamentals of acoustics*. John Wiley & Sons, third edition.
- Kundu, P. K. (1990). *Fluid mechanics*. Academic Press Inc.
- Lahoye, M. (1996). Experimentele verificatie van de karakteristieken van een radiale uitlaatgasturbine. Technical Report WOC-WET 96.028, Fac. of Mechanical Engineering, Eindhoven University of Technology. (In Dutch).
- Lawless, P. B. and Fleeter, S. (1995). The active control of rotating stall in a low speed centrifugal compressor. In *Proc. 1995 SPIE Int. Symposium on Sensing, Actuation and Control*, volume 2494, pages 196–206, Orlando, FL.
- Liaw, D.-C. and Abed, E. H. (1992). Stability analysis and control of rotating stall. In *Proc. NOLCOS '92*, pages 88–93, Bordeaux, France. IFAC.
- Longley, J. (1994). A review of nonsteady flow models for compressor stability. *ASME J. Turbomachinery*, **116**(2), 202–215.
- Macdougall, I. and Elder, R. (1983). Simulation of centrifugal compressor transient performance for process plant applications. *ASME J. Engineering for Power*, **105**(4), 885–890.
- McCaughan, F. (1989). Application of bifurcation theory to axial flow compressor instability. *ASME J. Turbomachinery*, **111**(4), 426–433.
- McDougall, N., Cumpsty, N., and Hynes, T. (1990). Stall inception in axial compressors. *ASME J. Turbomachinery*, **112**(1), 116–125.
- Meuleman, C., Willems, F., De Lange, R., and De Jager, B. (1998). Surge in a low-speed radial compressor. ASME paper no. 98-GT-426.
- Meuleman, C., De Lange, R., and Van Steenhoven, A. (1999). Surge dynamics in a centrifugal compressor system. In *Proc of the 3rd European Conference on Turbomachinery Fluid Dynamics and Thermodynamics*, volume C557/028, pages 895–904, London, UK. IMechE.
- Montazeri-Gh, M., Alderton, D., and Elder, R. (1996). Actuator placement for active surge control in a multi-stage axial compressor. ASME paper no. 96-GT-241.
- MOOG (1999). *Servo valves: dynamic performance*. <http://www.moog.com/30-series/dynamicperformance.htm>.
- Moore, F. and Greitzer, E. (1986). A theory of post-stall transients in axial compression systems: Part I - Development of equations. *ASME J. Engineering for Gas Turbines and Power*, **108**(1), 68–78.
- Nakagawa, K., Fujiwara, M., Nishioka, T., Tanaka, S., and Kashiwabara, Y. (1994). Experimental and numerical analysis of active suppression of centrifugal compressor surge by suction-side valve control. *JSME Int. J. Series B*, **37**(4), 878–885.
- NEN3005 (1972). Het meten van het debiet van vloeistof- en gasstromen in gesloten leidingen door middel van meetschijven. Technical report, Nederlands Normalisatie Instituut. In Dutch.
- Nisenfeld, A. E. (1982). *Centrifugal compressors*. Instrument Society of America.
- Paduano, J., Valavani, L., Epstein, A., Greitzer, E., and Guenette, G. (1994). Modeling for control of rotating stall. *Automatica*, **30**(9), 1357–1373.

- Pinsley, J., Guenette, G., Epstein, A., and Greitzer, E. (1991). Active stabilization of centrifugal compressor surge. *ASME J. Turbomachinery*, **113**(4), 723–732.
- Ribi, B. and Gyarmathy, G. (1995). The behaviour of a centrifugal compressor stage during mild surge. *VDI Berichte*, (1186).
- Rodgers, C. (1991). Centrifugal compressor inlet guide vanes for increased surge margin. *ASME J. Turbomachinery*, **113**(4), 696–701.
- Simon, J. and Valavani, L. (1991). A Lyapunov based nonlinear control scheme for stabilizing a basic compression system using a close-coupled valve. In *Proc. of the 1991 American Control Conference*, volume 3, pages 2398–2406, Boston, MA.
- Simon, J., Valavani, L., Epstein, A., and Greitzer, E. (1993). Evaluation of approaches to active compressor surge stabilization. *ASME J. Turbomachinery*, **115**(1), 57–67.
- Slotine, J.-J. and Li, W. (1991). *Applied nonlinear control*. Prentice Hall.
- Smirnov, G. (1996). Stabilization by constrained controls. *SIAM J. Control and Optimization*, **34**(6), 1616–1649.
- Smith, E. and Vivian, B. (1995). *An introductory guide to valve selection*. Mechanical Engineering Publications Ltd.
- Staroselsky, N. and Nadin, L. (1979). Improved surge control for centrifugal compressors. *Chemical Engineering*, pages 175–184.
- Stenning, A. (1980). Rotating stall and surge. *ASME J. Fluids Engineering*, **102**(1), 14–20.
- Van de Wal, M. (1998). *Selection of inputs and outputs for control*. Ph.D. thesis, Fac. of Mechanical Engineering, Eindhoven University of Technology.
- Van de Wal, M. and Willems, F. (1996). Selection of actuators and sensors for compressor control. Technical Report WFW 96.155, Fac. of Mechanical Engineering, Eindhoven University of Technology.
- Van de Wal, M., Willems, F., and De Jager, B. (1997). Selection of actuators and sensors for active surge control. In *Proc. of the 1997 IEEE Int. Conference on Control Applications*, pages 121–126, Hartford, CT.
- Van de Wal, M., Willems, F., and De Jager, B. (1999). Selection of sensors and actuators for surge control. *J. Propulsion and Power*. Accepted for publication.
- Van Essen, H. (1995). Design of a laboratory gas turbine installation. Technical Report WOC-WET 95.012, Institute for Continuing Education (IVO), Fac. of Mechanical Engineering, Eindhoven University of Technology.
- Van Essen, H. (1998). *Modeling and model based control of turbomachinery*. Ph.D. thesis, Fac. of Mechanical Engineering, Eindhoven University of Technology.
- Whitehouse, R., editor (1993). *The valve and actuator users's manual*. Mechanical Engineering Publications Ltd.
- Willems, F. (1997). Modeling and control of compressor flow instabilities. Technical Report WFW 96.151, Fac. of Mechanical Engineering, Eindhoven University of Technology.
- Willems, F. (1998). Valve selection for compressor surge control. Technical Report WFW 98.042, Fac. of Mechanical Engineering, Eindhoven University of Technology.
- Willems, F. (1999). Experimental study of active surge control in a centrifugal compression system. Technical Report WFW 99.032, Fac. of Mechanical Engineering, Eindhoven University of Technology.
- Willems, F. and De Jager, B. (1998a). Active compressor surge control using a one-sided controlled bleed/recycle valve. In *Proc. of the 37th IEEE Conference on Decision and Control*, pages 2546–2551, Tampa, FL.
- Willems, F. and De Jager, B. (1998b). Modeling and control of rotating stall and surge: An overview. In *Proc.*

- of the 1998 IEEE Int. Conference on Control Applications*, pages 331–335, Trieste, Italy.
- Willems, F. and De Jager, B. (1999). Modeling and control of compressor flow instabilities. *IEEE Control Systems*, **19**(5), 8–18.
- Willems, F. and De Jager, B. (2000). One-sided control of surge in a centrifugal compressor system. In *Proc. of the ASME Turbo Expo*, Munich, Germany. Accepted for publication.
- Willems, F., Heemels, M., De Jager, B., and Stoorvogel, A. (1999). Positive feedback stabilization of compressor surge. In *Proc. of the 38th IEEE Conference on Decision and Control*, pages 3259–3264, Phoenix, AZ.
- Yeung, S. and Murray, R. M. (1997). Reduction of bleed valve rate requirements for control of rotating stall using continuous air injection. In *Proc. of the 1997 IEEE Int. Conference on Control Applications*, pages 683–690, Hartford, CT.

Appendix A

Rotating Stall

Rotating stall is a local instability phenomenon, in which one or more cells of severely stalled flow rotate around the circumference of the compressor. These cells have a constant rotational speed between 20% and 80% of the rotor speed. In this flow regime, the annulus-averaged flow is steady in time, but the mass flow has a circumferential mass deficit and has, therefore, an essentially two-dimensional distribution. In the compressor map, the occurrence of rotating stall is seen as a rapid movement from the unstalled characteristic (1) to a point on the stalled characteristic (2), as illustrated in Fig. A.1a.

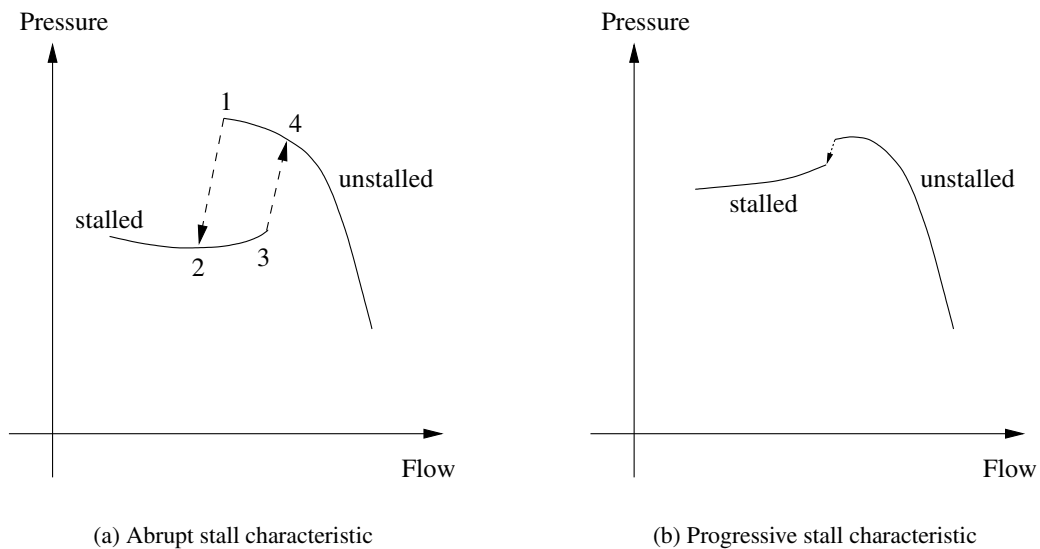


Figure A.1: Rotating stall in compressor map.

Rotating stall may be unrecoverable due to large stall/unstall hysteresis: to recover from rotating stall in point (3), in Fig. A.1a, a significantly larger mass flow is required than for rotating stall onset (1). As a result, the compressor may not restore to its unstalled condition by, for example, opening bleed valves or decreasing the rotor speed by changing the amount of injected fuel. Especially in aircraft engines, this so-called “hung” stall is undesirable since it requires a full stop and restart of the engine. This hysteresis effect is commonly met in multi-stage compressors near design speed.

Classification of rotating stall

The types of rotating stall observed in experimental set-ups can be classified as follows:

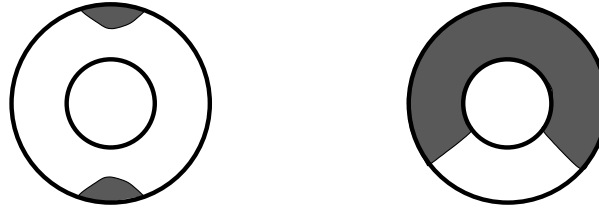


Figure A.2: Part-span stall (left) and full-span stall (right).

- **Part-span/full-span stall** referring to the size of the stalled region in terms of annulus height (Greitzer, 1981), as shown in Fig. A.2.
- **Short/long-length scale cells** describing the circumferential extent of the cell when it first forms (Day, 1993b). Analogously, low and higher order rotating stall modes or modal perturbations can be distinguished. These classifications are based on the wavelength of spatial harmonics that describes the stall pattern (Haynes *et al.*, 1994; Paduano *et al.*, 1994).

The full-span type of instability most commonly occurs in multi-stage compressors. Part-span stall is often found in single-stage compressors (Day, 1993b) and in the first stage of multi-stage, high-pressure ratio compressors during low-speed operation (Day, 1993a; Greitzer, 1981). The shape of the stalled compressor characteristic can affect the occurring type of rotating stall. According to Cumpsty (1989), full-span stall is encountered in compressors with a so-called abrupt stall compressor characteristic; this behavior, depicted in Fig. A.1a, leads to a significant drop in pressure rise and mass flow. Part-span stall is more likely to occur in compressors with a progressive stall characteristic, as shown in Fig. A.1b. However, if the compressor in part-span stall is throttled further, it may lead to full-span; the part-span cells grow radially and axially and may finally result in one cell through the whole length of the compressor. Part-span cells often rotate at close to 50% of the rotor speed whereas full-span cells usually rotate more slowly in the range 20-40%.

Spikes are seen to be a three dimensional breakdown of the flow in the rotor tip region, and are initiated by high rotor incidence angles (Camp and Day, 1998). In case a spike emerges, it rotates between 60 and 80% of the rotor speed around the annulus, as in Escuret and Garnier (1996). Within half a rotor revolution, this short-length scale perturbation quickly grows in circumferential direction and its rotational speed decreases. In addition, Camp and Day (1998) show that modal perturbations are related to a two dimensional instability in the whole compression system. These long-length scale perturbations usually rotate at a frequency less than 50% of the rotor frequency and modes of higher frequencies may occur in high-speed machines. As shown in Day (1993b), these modes are found near the top of the compressor characteristic. Note that spikes can trigger modal perturbations.

De Jager (1995) distinguishes four paths of rotating stall inception. As seen from the experimental work of McDougall *et al.* (1990) and Day (1993b) done in low-speed axial compressors, stall cells can be developed by growing smoothly out of small modal perturbations or by the abrupt formation of finite stall cells (also called spikes). In high-speed, multi-stage axial compressors, both inception paths are also found (see Garnier *et al.* (1991) and Escuret and Garnier (1996)). In addition, for high-speed multi-stage axial compressors, a blast wave emanating from the back of the machine can also

trigger rotating stall (Cargill and Freeman, 1991; Day and Freeman, 1994). In a mixed-flow pump, on the other hand, flow separation at a corner of the impeller can lead to rotating stall (Goto, 1994).

Parameters that influence rotating stall

Rotating stall is believed to be important in low-speed axial compressors (Day, 1993b; Haynes *et al.*, 1994), while surge occurs at relatively high speeds in axial as well as centrifugal compressors (Day and Freeman, 1994; Fink *et al.*, 1992; Pinsley *et al.*, 1991). Nevertheless, results have been reported of rotating stall in centrifugal compressors; Fink *et al.* (1992) and Rodgers (1991), for instance, determined impeller stall initiating deep surge in a high-speed centrifugal compressor whereas Kämmer and Rautenberg (1986) found rotating stall originating from both the impeller (for low rotational speeds) and the vaneless diffuser (for high speeds). Besides the influence of the *rotational speed*, the occurring type of instability is affected by the *plenum volume*; surge goes into rotating stall if the size of the plenum is progressively reduced (Day, 1994; Greitzer, 1976b). These effects are in accordance with the theoretical work of Greitzer (1981).

A thorough understanding of the mechanisms that lead to rotating stall is currently lacking. Emmons *et al.* (1955) postulated a mechanism that explains the propagation of rotating stall by modified incidence angles on neighbor blades due to an existing stall cell. The growth of modal perturbations into full-span rotating stall can be described by the Moore-Greitzer model (Moore and Greitzer, 1986). The initiation of rotating stall, however, is still investigated. So far, it is clear that many aspects play a role. Besides the effect of specific components, McDougall *et al.* (1990), for instance, found that compressors stall at the hub for small *tip clearances* and at the blade tip for large clearances. Although the initiation process of rotating stall is different for both cases, the end wall blockage was indicated as the most crucial factor in this study. The experimental results of Hunziker and Gyarmathy (1994) and Kämmer and Rautenberg (1986) showed the influence of the *incidence angle in the impeller and vaned diffuser*, respectively, on instability initiation. Garnier *et al.* (1991) showed that in case of *distorted inlet flow* rotating stall is initiated at smaller mass flows and the detected small “pre-stall” modal perturbations grow faster into fully developed rotating stall than in case of uniform inlet flow. Furthermore, they concluded that the *throttle rate* has a strong influence on the development of “pre-stall” perturbations. Escuret and Garnier (1996), on the contrary, found no influence of the throttle rate on the initiation process in a high-speed compressor. However, they showed the influence of *stage matching* on the axial location of rotating stall inception.

Appendix B

Experimental Set-Up

B.1 Gas turbine installation

Active surge control is investigated in the gas turbine installation shown in Fig. B.1. This installation,

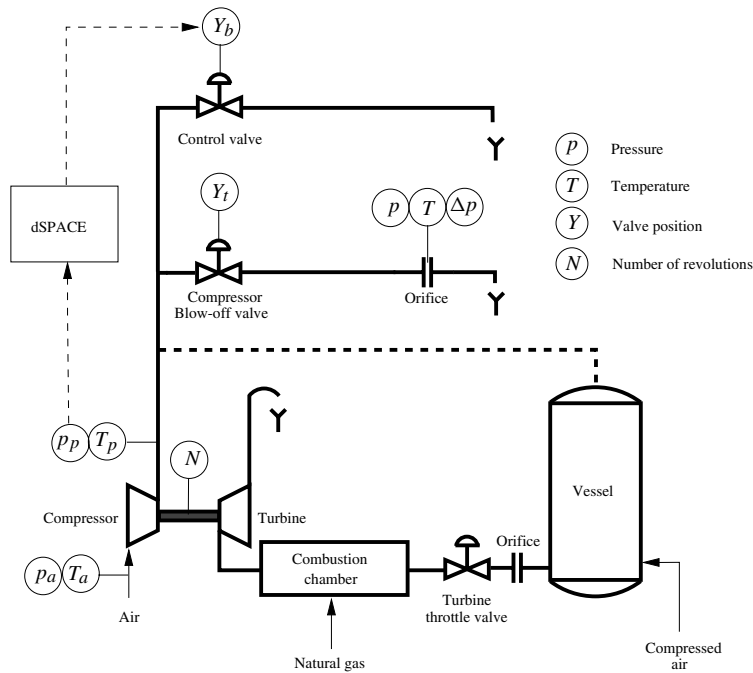


Figure B.1: Scheme of the gas turbine installation.

designed by Van Essen (1995), is built around a BBC VTR 160L turbocharger. The test turbocharger consists of a single-stage centrifugal compressor with a radial ending impeller and a diffuser with straight vanes. This compressor is mounted on the same rotational axis as the axial turbine (see Fig. B.2). Details about the geometry of the compressor are given in Table B.1.

For studies involving surge, the gas turbine installation is used in the configuration shown in Fig. B.1, with the dashed connecting line removed. Similar to Fink *et al.* (1992), the mass flows through the compressor and turbine are decoupled; the compressor pressurizes the incoming air, which is discharged via the compressor blow-off valve and the instrumented blow-off duct into the atmo-

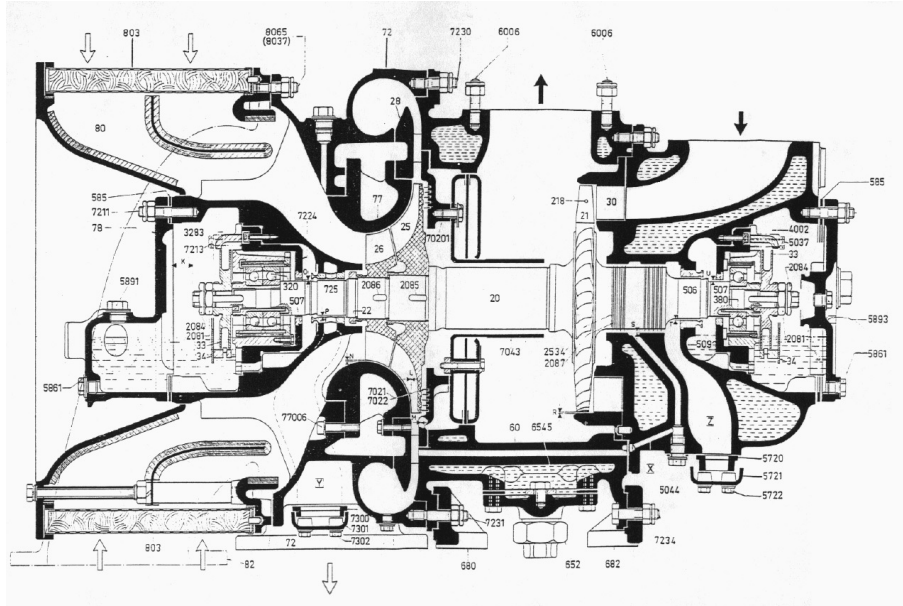


Figure B.2: Cross section of turbocharger BBC VTR 160L.

Table B.1: Parameters of the BBC compressor.

Impeller		Diffuser	
Parameter	Value	Parameter	Value
number of blades	20	number of vanes	45
inlet diameter at casing [m]	0.106	inlet diameter [m]	0.215
inlet diameter at hub [m]	0.054	outlet diameter [m]	0.258
impeller diameter [m]	0.180	vane inlet angle [deg]	28
blade inlet angle [deg]	40		

sphere. Natural gas is burned in the combustion chamber using externally supplied compressed air. The hot exhaust gasses expand over the turbine and deliver the power to drive the compressor. In this configuration, the rotational speed can be varied up to 25,000 [rpm] due to the limited mass flow rate of the externally supplied air.

For higher compressor speeds, the gas pressurized by the compressor can supplement the externally supplied compressed air, by using the dashed connecting line and closing the compressor blow-off valve. In that case, the system is run as a standard gas turbine. Because in this configuration, that includes the large vessel ($V = 2.66 \text{ [m}^3\text{]}$), surge is much more powerful and is of lower frequency, no surge measurements are possible. Otherwise damage to the machine could easily occur. Further information about the installation is given in Van Essen (1995) and Van Essen (1998).

B.2 Dimensionless component characteristics

In the applied Greitzer model, the dimensionless stationary compressor and throttle characteristics are used to describe the behavior of both components. These characteristics are approximated from available steady-state measurements.

B.2.1 Compressor characteristics

Measurements of three speed lines are shown in Fig. B.3. By scaling the pressure rise and mass flow

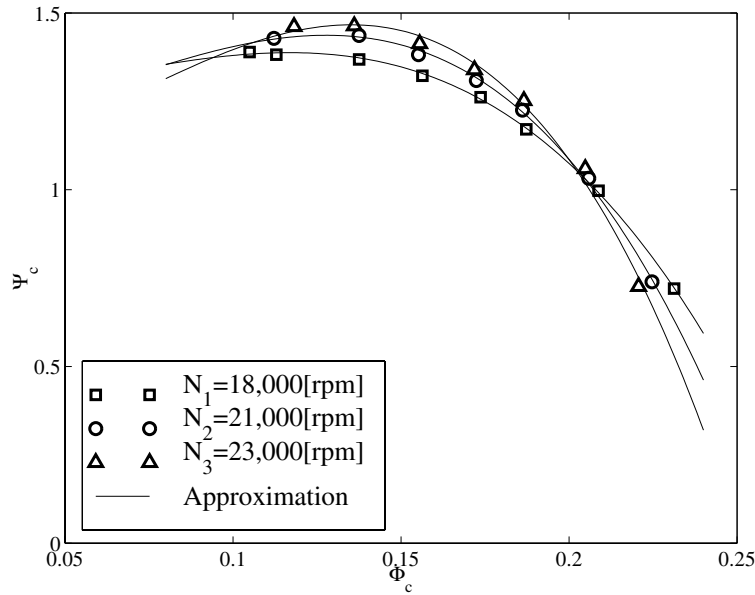


Figure B.3: Dimensionless compressor map.

with $\frac{1}{2}\rho_a U_t^2$ and $\rho_a A_c U_t$, respectively, the influence of the rotational speed on measurements is seen to be small in the examined speed range.

The compressor characteristics are approximated by a cubic approximation of $\Psi_c(\phi_c)$ (Moore and

Greitzer, 1986):

$$\Psi_c(\phi_c) = \Psi_c(0) + H \left[1 + \frac{3}{2} \left(\frac{\phi_c}{F} - 1 \right) - \frac{1}{2} \left(\frac{\phi_c}{F} - 1 \right)^3 \right] \quad (\text{B.1})$$

where $\Psi_c(0)$ is the valley point of the characteristic located at the compressor pressure rise axis, and $\phi_c = 2F$ corresponds to the dimensionless compressor mass flow at the top of the characteristic (see Fig. 2.10). In many cases, this top coincides with the surge point at each speed line. Hence, the identification problem is linear and the remaining parameters to be estimated, *i.e.*, $\Psi_c(0)$ and H , are independent. As the location of the surge line cannot be accurately determined due to *e.g.*, disturbances, in this study, a best fit of all measurements is determined in a least square sense. As a result, the identification is no longer linear in $\Psi_c(0)$, H and F . This can be easily verified if (B.1) is rewritten as:

$$\Psi_c(\phi_c, N) = c_0(N) + c_1(N)\phi_c^2 + c_2(N)\phi_c^3$$

with:

$$c_0(N) = \Psi_c(0), \quad c_1(N) = \frac{3H}{2F^2}, \quad \text{and} \quad c_2(N) = \frac{-H}{2F^3}$$

For each compressor characteristic the parameters $c_0(N)$, $c_1(N)$, and $c_2(N)$ are determined. The dependence of these parameters on rotational speed N is approximated by a quadratic polynomial in N :

$$c_0(N) = -1.0588 + 2.5979 \cdot 10^{-4}N - 7.3130 \cdot 10^{-9}N^2$$

$$c_1(N) = 223.4574 - 0.2504 \cdot 10^{-1}N + 7.9639 \cdot 10^{-7}N^2$$

$$c_2(N) = -900.9138 + 0.9750 \cdot 10^{-1}N - 3.1774 \cdot 10^{-6}N^2$$

For the measured speed lines, the result of this estimation is shown in Fig. B.3. It is concluded that in the region where compressor data is available, the compressor characteristics is approximated well.

B.2.2 Throttle characteristics

The compressor blow-off valve is an electrically powered control valve. The main specifications are listed in Table B.2. For subsonic flow conditions the compressor blow-off valve mass flow is assumed to be given by:

$$\phi_t = c_t u_t \sqrt{\psi} \quad (\text{B.2})$$

with:

$$\phi_t = \frac{\dot{m}_t}{\rho_a A_c U_t}, \quad \psi = \frac{\Delta p}{\frac{1}{2} \rho_a U_t^2}, \quad \text{and} \quad u_t = \frac{Y_t}{Y_{t,max}}$$

where $\rho_a = 1.2$ [kg/m³], $A_c = 7.9 \cdot 10^{-3}$ [m²], and Δp in [Pa]. The ratio $\frac{\phi_t}{\sqrt{\psi}}$ is determined from measurements. Figure B.4a illustrates that this ratio is linear in u_t , so c_t is supposed to be constant in the examined operating region. Measurements of ϕ_t , u_t and ψ are used to determine a best fit of

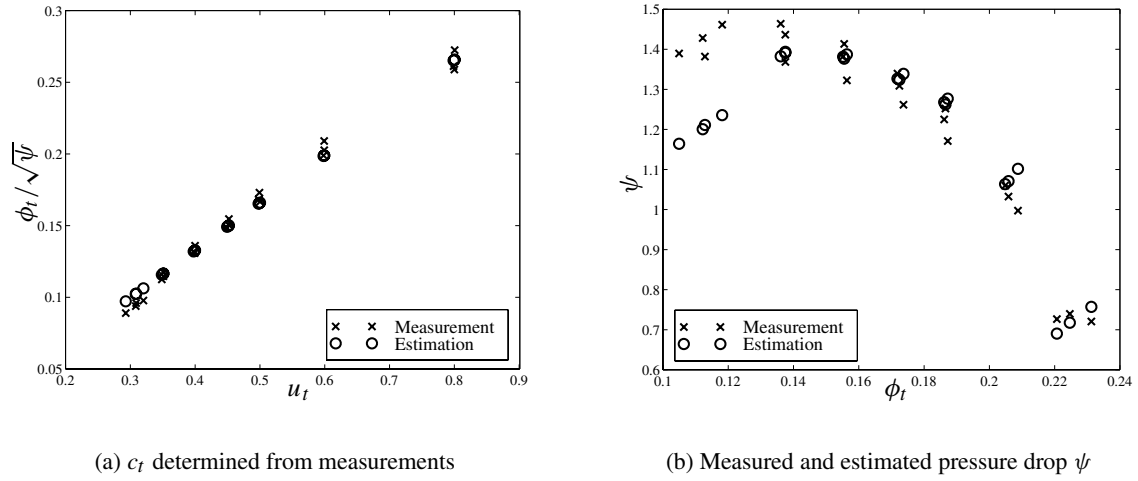


Figure B.4: Dimensionless throttle characteristic.

c_t in a least square sense: $\hat{c}_t = 0.3320$. From Fig. B.4a, it is concluded that $\frac{\phi_t}{\sqrt{\psi}}$ can accurately be described by the applied linear approximation. In addition, \hat{c}_t is used to estimate ψ :

$$\psi = \left(\frac{\phi_t}{\hat{c}_t u_t} \right)^2$$

This gives reasonable results, as shown in Fig. B.4b. However, the agreement is poor for small mass flows. These differences are due to inaccuracies in the approximation of $\frac{\phi_t}{\sqrt{\psi}}$ for small u_t , which corresponds to small ϕ_t (see Fig. B.4a).

Table B.2: Specifications for the compressor blow-off valve (ECONOSTO type Stevi-E, 12.440/CS23).

Medium	air
Flow coefficient K_v [m ³ /hr]	160
Control input [V]	0-10
Stroke [m]	0.030
Operating speed [m/min]	0.025

B.3 Measurement system

To determine the overall performance of the compressor, the installation is equipped with temperature probes and high-frequency response pressure transducers, as shown in Fig. B.1. The rotational speed of the impeller is registered by a semi-conductor pulse tachometer and two instrumented orifices are used to determine the steady turbine and blow-off mass flows. More details about mass flow measurements using an orifice are given in Section B.3.1. The angular displacements of the stem of the turbine throttle and of the compressor blow-off valve are also registered. This signal is a measure

for the opening area of the valves. As these valves have a linear flow characteristic, the mass flow through the valve is proportional to the valve position (Van Essen, 1995).

For data-acquisition, a NATIONAL INSTRUMENTS board is installed in a measurement PC. LABVIEW software controls the data storage on hard disk and real-time process monitoring on the computer screen. This system is run at 200 [Hz] sampling frequency, which is well above the expected surge frequency.

Measurements of transients into and during surge consist of data from the high-frequency response pressure probe at the compressor outlet, of the blow-off valve's rotational angle sensor, and of the rotational speed transducer.

B.3.1 Mass flow measurement

Compressor mass flow measurements are determined from the orifice located in the blow-off duct. As the orifice design is according to NEN3005 (1972), the mass flow across the orifice plate has to be determined from:

$$\dot{m} = \epsilon \alpha \frac{\pi}{4} d^2 \sqrt{2 \rho_1 \Delta p} \quad (\text{B.3})$$

The density ρ_1 follows from the relation for a perfect gas based on conditions at the orifice inlet:

$$\rho_1 = \frac{p_1}{RT_1}.$$

The meaning of the used symbols is given in Table B.3. According to NEN3005 (1972), the expansion

Table B.3: Meaning of variables.

<i>Symbol</i>	<i>Meaning</i>	<i>Unit</i>
\dot{m}	mass flow through orifice	[kg/s]
ϵ	expansion coefficient	[-]
α	flow coefficient	[-]
d	orifice diameter	[m]
ρ_1	fluid density at inlet	[kg/m ³]
p_1	pressure at inlet	[Pa]
Δp	pressure drop across orifice	[Pa]

factor ϵ is accurately described by:

$$\epsilon = 1 - (0.41 + 0.35\beta^4) \frac{\Delta p}{\kappa p_1}$$

Hence, $\epsilon = 1$ holds for incompressible fluids. For the measured Δp and p_1 values, ϵ varies between 0.9566 and 0.9939. The flow coefficient α is determined from the following empirical relation:

$$\alpha = A(\beta, D) + \frac{B(\beta, D)}{Re_D}$$

where $A(\beta, D)$ and $B(\beta, D)$ have to be determined from tables in NEN3005 (1972). The values used in (B.3) are listed in Table B.4. The Reynolds number is given by:

$$Re_D = \frac{\rho U D}{\eta} = \frac{4 \dot{m}}{\pi D \eta}$$

The influence of the Reynolds number is often neglected: $\alpha_0 \approx A(\beta, D)$. In the studied operating region, the mass flow \dot{m} is expected to vary between 0.15 and 0.5 [kg/s], so the corresponding Reynolds number is $7.7 \cdot 10^4 < Re_D < 2.6 \cdot 10^5$. As a result, variations in α due to the term with the Reynolds number are around 0.006, *i.e.*, approximately 1% of α_0 .

Table B.4: Data for mass flow computation.

Parameter	Value
Diameter orifice d [m]	$7.14 \cdot 10^{-2}$
Diameter pipe D [m]	$1.082 \cdot 10^{-1}$
Dynamic viscosity η [Ns/m ²]	$2.079 \cdot 10^{-5}$
Gas constant (for air) R [J/kg K]	287
$\beta = \frac{d}{D}$	0.6599
$\kappa = \frac{c_p}{c_v}$	1.4
$A(\beta, D)$ (20 [°C])	0.6721
$B(\beta, D)$ (20 [°C])	622.05

To determine the measurement error using this method, the following relation is given in NEN3005 (1972):

$$\frac{\sigma_{\dot{m}}}{\dot{m}} = \sqrt{\left(\frac{\sigma_{\alpha}}{\alpha}\right)^2 + \left(\frac{\sigma_{\epsilon}}{\epsilon}\right)^2 + 4\left(\frac{\beta^4}{\alpha}\right)^2 \cdot \left(\frac{\sigma_D}{D}\right)^2 + 4\left(1 + \frac{\beta^4}{\alpha}\right)^2 \cdot \left(\frac{\sigma_d}{d}\right)^2 + \frac{1}{4}\left(\frac{\sigma_{\Delta p}}{\Delta p}\right)^2 + \frac{1}{4}\left(\frac{\sigma_{\rho}}{\rho}\right)^2}$$

with $\frac{\sigma_{\alpha}}{\alpha} = 0.003$, $\frac{\sigma_D}{D} = \frac{0.05 \text{ [mm]}}{D \text{ [mm]}} = 4.6 \cdot 10^{-4}$, and $\frac{\sigma_d}{d} = \frac{0.05 \text{ [mm]}}{d \text{ [mm]}} = 7.0 \cdot 10^{-4}$. Assuming the accuracy of the sensors is 1%, $\frac{\sigma_{\Delta p}}{\Delta p} = 0.01$, $\frac{\sigma_p}{p} = 0.01$, and $\frac{\sigma_T}{T} = 0.01$. Then, $\frac{\sigma_{\rho}}{\rho}$ and $\frac{\sigma_{\epsilon}}{\epsilon}$ can be approximated by (Van Essen, 1998):

$$\frac{\sigma_{\rho}}{\rho} = \sqrt{\left(\frac{\sigma_p}{p}\right)^2 + \left(\frac{\sigma_T}{T}\right)^2} = 0.011 \quad \text{and} \quad \frac{\sigma_{\epsilon}}{\epsilon} = \sqrt{2 \left[\left(\frac{\sigma_p}{p}\right)^2 + \left(\frac{\sigma_{\Delta p}}{\Delta p}\right)^2 \right]}$$

Accordingly, we find a relative measurement error $\tau_{\dot{m}} = 2 \frac{\sigma_{\dot{m}}}{\dot{m}}$ of approximately 5% on the mass flow. If the accuracy of the applied sensors drops to 5%, $\tau_{\dot{m}}$ rises to 20%.

B.4 Surge control system

Control valves For surge stabilization in the examined compression system, ASCO proportional solenoid valves are used. The main specifications of these valves are listed in Table B.5. From the results in Section 4.3, it is seen that a control valve capacity of $c_b = 0.07c_t$ is required for active surge control. Valve manufacturers specify the control valve capacity by a so-called K_v -value (see Table B.5). To determine the required K_v -value, analogous to Willems (1998), the *instantaneous* K_v -value:

$$K_v(t) = 7.0 \sqrt{\frac{T_p}{\rho_n p_a}} \frac{\dot{m}_b(t)}{\sqrt{\Delta p(t)}}$$

Table B.5: Specifications for control valve (ASCO Type Posiflow SCE202.026V).

Medium	air
Flow coefficient $K_{v, valve}$ [m ³ /hr]	0.72
Maximal pressure difference [bar]	1.4
Control input [V]	0-10
Hysteresis [% Full scale]	< 5
Estimated response time [ms]	25-60

is computed for the most limiting case shown in Fig. 4.10. For $T_p = 340$ [K], we find: $K_{v, required} = 10.6$ [m³/hr]. Then, the number of ASCO valves needed for active surge control is given by:

$$n = \text{integer} \left\{ \frac{K_{v, required}}{K_{v, valve}} \right\}$$

As a result, 15 valves are placed in parallel on a flange, which is installed downstream of the compressor and just in front of the compressor blow-off valve. All control valves are controlled simultaneously. The valves are equipped with a control unit, which converts an input control signal (in [V]) to a coil current by means of pulse width modulation. Furthermore, this unit facilitates the adjustment of the shape of the flow curve.

Controller To implement the active surge controller on the experimental set-up, a second PC is equipped with a dSPACE DS1103 PPC controller board. This board consists of a IBM Power PC 604e with 400 [MHz] and has 2 [MByte] local SRAM. It is programmable using MATLAB/SIMULINK block diagrams and allows rapid control prototyping. Furthermore, a large number of I/O interfaces are offered (16×16 bits ADC, 4×12 bits ADC, 8×14 bits DAC, and 32 digital I/O). Application of this board guarantees real-time implementation of the controller. It is also used for data-acquisition. In that case, a subset (plenum pressure, rotational speed, and blow-off valve and control valve positions) of the available data is gathered at 1 [kHz] sampling frequency. These measurements are used to study rotating stall.

Pressure transducer To measure the plenum pressure oscillations during surge a DATA INSTRUMENTS high-frequency response pressure transducer, which is located at approximately 0.20 [m] from the compressor outlet, is used. For the maximal allowable relative pressure, 3.45 [bar], this strain gauge transducer gives an output signal of 100 [mV] (see Table B.6). This means that in the

Table B.6: Specifications for DATA INSTRUMENTS pressure transducer (Model AB, Option 7HP).

Range [bar g]	3.45
Span of output signal [mV]	100
Operating temperature [°C]	-54 to 93
Accuracy [% span]	± 0.5

region of interest this output signal is of the order of 10 [mV]. To obtain a reasonable resolution, the measured plenum pressure signal is pre-amplified ($100\times$) before this signal is processed on the dSPACE controller board.

Appendix C

Lumped Parameter Modeling

C.1 Helmholtz resonator

The Helmholtz resonator shown in Fig. C.1 is an example of a lumped acoustic element (Kinsler *et al.*, 1982); the kinetic energy of the fluid is associated with the motion in the small opening whereas the potential energy is related to the compression in the volume. This system consists of a closed volume

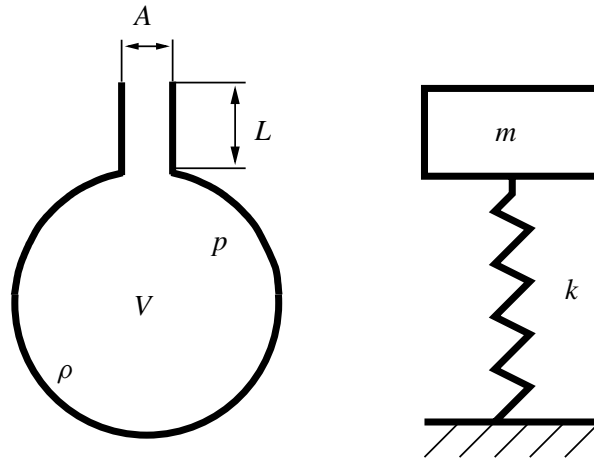


Figure C.1: A Helmholtz resonator and its mechanical analogue.

V with a rigid wall and a small *neck* of area A and of length L connecting it to a much larger space, or to a duct. If the wavelength of the pressure oscillations is much larger than the length L , the gas in the neck can be assumed to be incompressible. For a perfect gas under adiabatic conditions, the absolute pressure is related to the volume of the gas inside the *cavity* by:

$$p = \rho RT \quad \text{and} \quad pV^\gamma = \text{constant}$$

The continuity equation for this volume is given by:

$$Vd\rho + \rho dV = m_{in} \tag{C.1}$$

with m_{in} the amount of mass transported into the closed volume V . We assume that changes in ρ and p are related by isentropic relations, so the following relation can be derived:

$$d\rho = \frac{\rho}{\gamma p} dp \quad (C.2)$$

As a result, (C.1) can be written as:

$$\frac{V\rho}{\gamma p} dp + \rho dV = m_{in} \quad (C.3)$$

If gravitation and viscous effects are neglected, the one-dimensional momentum equation for the gas in the neck is given by:

$$\rho \frac{\partial u}{\partial t} + \rho u \frac{\partial u}{\partial x} = -\frac{\partial p}{\partial x} \quad (C.4)$$

with the axial velocity u of the gas and

$$\frac{\partial u}{\partial x} = 0,$$

since the flow in the neck is assumed to be incompressible. In addition, using $u = \frac{d\xi}{dt}$ and integrating (C.4) over the volume of the neck, this leads to:

$$\rho \frac{d^2 \xi}{dt^2} = -\frac{dp}{L} \quad (C.5)$$

where ξ is the displacement of the gas in the neck. Substitution of the speed of sound for a perfect gas, $a = \sqrt{\gamma RT}$, and of $dV = -\xi A$ in (C.3) finally yields:

$$\rho L \frac{V}{a^2} \frac{d^2 \xi}{dt^2} + \rho A \xi = -m_{in} \quad (C.6)$$

This can be interpreted as a mass-spring system excited by a force $F(t)$, as illustrated in Fig. C.1:

$$m \frac{d^2 x}{dt^2} + kx = F(t)$$

with mass m , stiffness k , and resonance frequency $\omega_0 = \sqrt{\frac{k}{m}}$. For the studied resonator, the resonance frequency is called the Helmholtz frequency:

$$\omega_H = a \sqrt{\frac{A}{VL}}$$

Hence, the frequency of oscillation depends on the volume V and the geometry of the neck, and not on their shape (Emmons *et al.*, 1955; Kinsler *et al.*, 1982).

C.2 Greitzer lumped parameter model

Emmons *et al.* (1955) showed that oscillations associated with surge can be captured by a model similar to the Helmholtz resonator model discussed in the previous section. This linearized model is

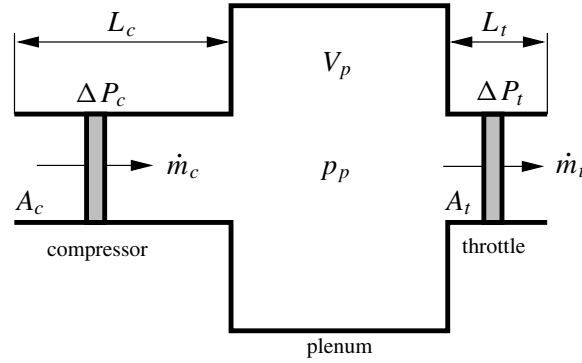


Figure C.2: Greitzer lumped parameter model.

further developed by Greitzer (1976a) to study the nonlinear behavior of systems with low pressure-ratio axial compressors.

The Greitzer model is illustrated in Fig. C.2. Two large volumes, *i.e.*, the atmosphere and the plenum, are connected to each other by a duct, in which the compressor works. If the length of the interconnecting duct is small compared to the wavelength of the pressure oscillations, the gas in the duct can be assumed to be incompressible. As a result, compressibility effects are associated with the compression in the plenum while inertia effects are lumped on the acceleration of the gas in the compressor duct. The compressor and its ducting are replaced by an *actuator disk* and a straight pipe of length L_c . The actuator disk theory assumes that a blade row can be represented by a small plane across which the mass flow is continuous, but pressure changes can be discontinuous. The geometry of the compressor duct is chosen such that a given mass flow change leads to the same pressure difference in the actual duct and in the model. A similar approach is used to model the throttle behavior.

The derivation of the lumped parameter model is based on the following major assumptions:

1. One-dimensional incompressible flow in the ducts.
2. Isentropic compression process in the plenum.
3. In the plenum, velocity is negligible and pressure is uniformly distributed.
4. Quasi-steady compressor and throttle behavior.
5. Influence of rotor speed variations is small.
6. System's overall temperature ratio is near unity.

C.2.1 Conservation equations

To describe the one-dimensional flow of the gas in the ducts and in the plenum, principles of conservation of mass, momentum, and energy are applied. If gravitation and viscous effects are neglected, this leads to the following conservation equations (see, *e.g.*, Kundu (1990)):

$$\frac{\partial \rho}{\partial t} + u \frac{\partial \rho}{\partial x} + \rho \frac{\partial u}{\partial x} = 0 \quad (\text{C.7})$$

$$\rho \frac{\partial u}{\partial t} + \rho u \frac{\partial u}{\partial x} = -\frac{\partial p}{\partial x} \quad (\text{C.8})$$

$$\rho \frac{\partial h}{\partial t} + \rho u \frac{\partial h}{\partial x} = \frac{\partial p}{\partial t} + u \frac{\partial p}{\partial x} - \frac{\partial q}{\partial x} \quad (\text{C.9})$$

In addition, relations for a perfect gas are applied:

$$p = \rho R T \quad (\text{C.10})$$

$$h = c_p T \quad (\text{C.11})$$

The meaning of the variables used in the conservation equations is listed in Table C.1.

Table C.1: Meaning of the applied variables.

Variable	Meaning
A	flow through area [m ²]
c_p	heat capacity at constant pressure [kJ/kg K]
c_v	heat capacity at constant volume [kJ/kg K]
h	enthalpy [kJ/kg]
L	length of control volume [m]
q	power flux [W/m ²]
Q	power $Q = qA$ [W]
R	specific gas constant [kJ/kg K]
s	specific entropy [kJ/kg K]
T	absolute temperature [K]
u	axial gas velocity [m/s]
V	control volume [m ³]
x	axial displacement [m]
ρ	density [kg/m ³]
γ	isentropic coefficient $\gamma = \frac{c_p}{c_v}$

Compressor and throttle ducts In the ducts, temperature effects are neglected, so the energy equation (C.9) is not required. Furthermore, the flow in the ducts is assumed to be incompressible. This seems reasonable because the model describes systems with low inlet Mach numbers and with pressure rises that are small compared to the ambient pressure. Moreover, the oscillations associated with surge are supposed to have small frequencies, so the wavelength of the pressure oscillations is large compared to the length of the ducts. Application of the one-dimensional momentum equation to the incompressible flow in the ducts gives:

$$\rho \frac{\partial u}{\partial t} = -\frac{\partial p}{\partial x} \quad (\text{C.12})$$

Integrated over the compressor duct volume this equation becomes:

$$\frac{L_c}{A_c} \frac{d\dot{m}_c}{dt} = p_a - p_p + \Delta P_c \quad (\text{C.13})$$

where $\dot{m}_c = \rho A_c u$. Note that the integration of $\frac{\partial p}{\partial x}$ gives $\frac{p_p - p_a}{L_c}$. Greitzer (1976a) incorporated the effect of the compressor as a *forcing term* ΔP_c . Analogously, the flow in the throttle duct can be described by:

$$\frac{L_t}{A_t} \frac{d\dot{m}_t}{dt} = p_p - p_a - \Delta P_t \quad (\text{C.14})$$

The behavior of the compressor and throttle is described by algebraic equations:

$$\Delta P_c = f_1(\dot{m}_c, N, T_c) \quad (\text{C.15})$$

$$\Delta P_t = f_2(\dot{m}_t, Y_t, T_t) \quad (\text{C.16})$$

These flow- Δp relationships are often available from the manufacturer.

Plenum In the plenum, the velocity of the gas is negligible and $\frac{\partial p}{\partial x} = 0$. Consequently, the mass and energy conservation equations are only needed to describe the compression process in the plenum:

$$\frac{\partial \rho}{\partial t} + u \frac{\partial \rho}{\partial x} + \rho \frac{\partial u}{\partial x} = 0 \quad (\text{C.17})$$

$$\rho c_p \frac{\partial T}{\partial t} + \rho c_p u \frac{\partial T}{\partial x} = \frac{\partial p}{\partial t} + u \frac{\partial p}{\partial x} - \frac{\partial q}{\partial x} \quad (\text{C.18})$$

Integrated over the plenum volume, the continuity equation is given by:

$$V_p \frac{d\rho}{dt} = \dot{m}_c - \dot{m}_t \quad (\text{C.19})$$

Recall that the pressure and temperature are homogeneous within the plenum, so the conditions at the outlet are taken equal to those inside the plenum. Pressure rises in the compressor duct are accounted for by (C.13). In the Greitzer lumped parameter model, the compressor exit pressure and temperature are equal to the plenum pressure and temperature. As a result, the terms $\frac{\partial p}{\partial x}$ and $\frac{\partial T}{\partial x}$ in (C.18) are omitted. Moreover, assuming the process in the plenum to be adiabatic ($\frac{\partial q}{\partial x} = 0$), the energy equation for the plenum can be written as:

$$\rho c_p \frac{\partial T}{\partial t} = \frac{\partial p}{\partial t} \quad (\text{C.20})$$

From the equation of state:

$$T ds = dh - \frac{1}{\rho} dp,$$

it can easily be verified that (C.20) is associated with the isentropic compression of a perfect gas. In that case, the following relation also holds:

$$\frac{d\rho_p}{dt} = \frac{\rho_p}{\gamma p_p} \frac{dp_p}{dt} \quad (\text{C.21})$$

and (C.19) can be rewritten as:

$$\frac{V_p \rho_p}{\gamma p_p} \frac{dp_p}{dt} = \dot{m}_c - \dot{m}_t \quad (\text{C.22})$$

If the overall pressure and temperature ratios are near unity, $\frac{\rho_p}{p_p}$ can be replaced by $\frac{\rho_a}{p_a}$. Then, to solve (C.22) no extra equation of state is required that describes the relation between ρ_p and p_p , and the speed of sound $a = \sqrt{\gamma R T_a}$ can be based on ambient temperature.

Dynamic compressor behavior To describe the compressor behavior during rotating stall transients, Greitzer (1976a) applied a first order linear system:

$$\tau \frac{d\Delta P_c}{dt} = \Delta P_{c,ss} - \Delta P_c \quad (\text{C.23})$$

with the measured steady compressor characteristic $\Delta P_{c,ss}$ and the time constant τ associated with the circumferential development of a stall cell (in number of rotor revolutions N_τ):

$$\tau = \frac{2\pi R_t N_\tau}{U_t}$$

However, Hansen *et al.* (1981) used (C.23) to *match* simulation results with experimental data. In that case, dynamic compressor phenomena are all lumped on (C.23), so it has no physical meaning.

C.2.2 Dimensionless equations of motion

In the Greitzer model, the equations are normalized in the following manner: mass flows are scaled with $\rho_a A_c U_t$, pressure with $\frac{1}{2}\rho_a U_t^2$, and time with the Helmholtz frequency ω_H :

$$\omega_H = a \sqrt{\frac{A_c}{V_p L_c}}$$

where $a = \sqrt{\gamma R T_a}$ is the speed of sound corresponding to ambient conditions.

Compressor and throttle duct Scaling of the one-dimensional momentum equation of the compressor and throttle duct gives, respectively:

$$\frac{d\phi_c}{d\tilde{t}} = B[\Psi_c - \psi] \quad (\text{C.24})$$

$$\frac{d\phi_t}{d\tilde{t}} = \frac{B}{G}[\psi - \Psi_t] \quad (\text{C.25})$$

where the dimensionless mass flows and pressure differences are denoted as ϕ and Ψ , $\tilde{t} = t\omega_H$ is the dimensionless time, and the parameters B and G are defined as:

$$B = \frac{U_t}{2\omega_H L_c} \quad \text{and} \quad G = \frac{L_t A_c}{L_c A_t}$$

Plenum Analogous to Fink *et al.* (1992), $\frac{\rho_p}{p_p}$ is used in (C.22) for the derivation of the dimensionless mass balance of the plenum. This leads to:

$$B \frac{d\psi}{d\tilde{t}} = \frac{T_p}{T_a} [\phi_c - \phi_t] \quad (\text{C.26})$$

Note that Greitzer (1976a) studies compression systems in which $\frac{\rho_p}{p_p}$ can be replaced by $\frac{\rho_a}{p_a}$, so $T_p = T_a$.

Dynamic compressor behavior It can easily be verified that scaling of (C.23) results in:

$$\frac{d\Psi_c}{d\tilde{t}} = \frac{1}{\tilde{\tau}} [\Psi_{c,ss} - \Psi_c] \quad (\text{C.27})$$

Samenvatting

Het operationele werkgebied van axiaal en centrifugaal compressoren wordt voor kleine massastromen begrensd door het optreden van twee stromingsinstabiliteiten: *rotating stall* en *surge*. Deze instabiliteiten beperken de prestatie en efficiëntie van het systeem, en nog belangrijker, ze kunnen tot schade aan de machine leiden. De instabiliteiten kunnen worden voorkomen door gebruik te maken van een “actieve” regeling. In dat geval wordt door terugkoppeling van stromingsperturbaties de dynamica van het compressor systeem zodanig gewijzigd dat dit leidt tot uitbreiding van het stabiele operationele gebied. Een vergroot werkgebied is tevens voordelig voor de prestatie van het systeem.

Dit proefschrift beschrijft de toepassing van *active surge control* op een experimentele opstelling met een centrifugaal compressor. Het gedrag van het compressor systeem tijdens surge is beschreven met het *Greitzer lumped parameter model*. Dit model is geïdentificeerd en experimenteel gevalideerd. Het Greitzer model blijkt in staat om de gemeten fenomenen in een breed werkgebied te beschrijven, en is als uitgangspunt genomen voor het ontwerp van een surge regeling voor het onderzochte systeem.

Systematische methoden voor de selectie van sensoren en actuatoren laten zien dat een *plenum* druk-opnemer en een afblaasklep geschikt zijn voor het gebruik in een surge regeling. Het Greitzer model is uitgebreid met een klepmodel om de invloed van de dynamica van de afblaasklep op het systeemgedrag mee te nemen. Aan de hand van simulaties met dit niet-lineaire model zijn de benodigde bandbreedte en capaciteit van de afblaasklep bepaald voor de “actieve” regeling van surge in de bestudeerde opstelling.

Voor de stabilisatie van surge is een nieuwe regelstrategie ontwikkeld: *one-sided control*. Bij deze strategie is de afblaasklep in het gewenste evenwichtspunt gesloten. One-sided refereert naar het feit dat de klep alleen geopend kan worden om het systeem in dit werkpunt te stabiliseren. Indien verstoringen en meetruis afwezig zijn, wordt het systeem in het gestabiliseerde evenwichtspunt bedreven zonder het gecomprimeerde gas af te blazen. Deze aanpak verbetert de efficiëntie van het compressor systeem in vergelijking met strategieën die in het gewenste werkpunt continu gas afblazen of recycleren. Simulaties met het uitgebreide Greitzer model laten zien dat surge gestabiliseerd kan worden met een proportionele uitgangsterugkoppeling gebaseerd op plenum drukmetingen. Voor de stabiliteitsanalyse van het gelineariseerde compressor systeem met begrenzingen op de kleppositie is gebruik gemaakt van de theorie van *positive feedback stabilization*.

Het ontwikkelde regelsysteem is geïmplementeerd op het experimentele compressor systeem. Om praktische problemen met betrekking tot meetruis en het onbekende, werkelijke, evenwichtspunt op te lossen is een band-pass filter toegepast. Combinatie van dit filter met de proportionele uitgangsterugkoppeling resulteert in een dynamische uitgangsterugkoppeling. Experimenten met het regelsysteem laten zien dat surge gestabiliseerd wordt en de massastroom waarbij surge optreedt met 7% gereduceerd kan worden. Echter, in het geval dat surge onderdrukt wordt treedt waarschijnlijk rotating stall op in het systeem.

Dankwoord

Graag wil ik iedereen bedanken die een bijdrage heeft geleverd aan het tot stand komen van dit proefschrift, met name de volgende personen.

In de eerste plaats, gaat mijn dank uit naar Jan Kok en Bram de Jager voor de vrijheid die ze me gegeven hebben en voor de talrijke gedachtenwisselingen en suggesties die in belangrijke mate aan het resultaat van dit onderzoek hebben bijgedragen. Jullie enthousiasme en stimulerende begeleiding heb ik zeer gewaardeerd.

De overige leden van het Compressor Surge Project (Corine Meuleman, Harm van Essen, Rick de Lange en Anton van Steenhoven) dank ik voor de ondersteuning en adviezen bij de experimenten, de waardevolle discussies en de prettige werksfeer. Het was een boeiende ervaring om onderdeel van dit multi-disciplinaire team uit te maken. Niels Olthuis, Rens Kodde, Karel Koekkoek, Frits van Veghel, Frank Seegers, Peter Ewalts en Lambert van der Schoot ben ik erkentelijk voor de technische ondersteuning in het laboratorium.

Verder wil ik Maurice Heemels en Anton Stoorvogel noemen voor de plezierige samenwerking die heeft geresulteerd in een belangrijke theoretische bijdrage (zie hoofdstuk 4), en Harold Mehagnoul en Stephan Hermans voor de bijdrage in de vorm van hun stages.

Tevens ben ik de leden van de klankbord-commissie (prof.ir. van Buijtenen (TU Delft), prof.dr.ir. Jonker (Universiteit Twente), ir. Smeulders (TNO-TPD) en ir. Vial (Demag Delaval)) dankbaar voor hun belangstelling en voor hun vragen en adviezen die het project mede richting hebben gegeven.

Belangrijk voor mij waren verder de contacten met (ex-)kamergenoten (Jan Vissers, Hans Muijderman, Marc van de Wal, Bert van Beek, Olaf van der Sluis (*LaTeX-helpdesk extraordinary*), Liviu Raulea en Edo Aneke) en met vrienden, die zorgden voor plezier en de noodzakelijke afwisseling van het dagelijks werk. In het bijzonder, wil ik het “relativerend instituut” Seize Bouteilles noemen.

Tenslotte dank ik mijn ouders voor hun steun en de mogelijkheden die ze me altijd hebben geboden en bewonder ik Anke voor haar begrip en het doorstaan van mijn verschillende gemoedstoestanden gedurende het schrijven van dit proefschrift. Anke, na deze hectische periode kunnen we samen verder aan onze toekomst “bouwen”.

Frank Willems.
Eindhoven, 9 april 2000.

Curriculum Vitae

- 13 juni 1971** Geboren te Heerlen.
- 1983-1989** Atheneum- β , College Sancta Maria, Kerkrade.
- 1989-1995** Ingenieurs-opleiding aan de Technische Universiteit Eindhoven, Faculteit Werktuigbouwkunde. Het afstudeerproject *Mean value modelling of spark ignition engines for control purposes* is uitgevoerd bij de sectie Systems & Control in samenwerking met GENTEC b.v. te Son en Breugel.
- 1995-2000** Werkzaam als assistent in opleiding (AiO-4) aan de Technische Universiteit Eindhoven, Faculteit Werktuigbouwkunde, sectie Systems & Control. Gedurende deze periode is onderzoek verricht in het kader van het project *Flow stabilization by active control of turbo machinery*. Dit onderzoek maakt deel uit van het Compressor Surge Project.
- juni 2000-** Wetenschappelijk medewerker, TNO Wegtransportmiddelen, afdeling Verbrandingsmotoren.